Damping behaviour of plant-fibre composite materials

Marie Joo Le Guen

Department of Mechanical Engineering

University of Canterbury

Biopolymer Network

A thesis submitted in partial fulfillment of the requirements for the Degree of

Doctor of Philosophy

2014

Abstract

The vibration damping property of plant fibres composites is of practical interest for commercial applications of biobased and eco-composites. Damping behaviour has been observed by experimentation and exploited in the marketing of sporting equipment but the origins of this behaviour have so far been only based on conjectures.

In this thesis, the damping capacity of plant fibre composites was attributed to their chemical composition and the reversible interactions enabled by the breaking and reforming of hydrogen bonds under stress.

The approach to explaining the mechanisms started with the characterisation of different plant fibre types to search for correlations between their physical and chemical structure. The investigation continued with quantifying the effect of hydrogen bonding compounds such as water, glycerol and polyglycerol on the damping coefficient of fibres and reinforced composites.

The results of the polyol impregnation indicated that applying a pretreatment enhanced the vibration damping performance of flax reinforced composites, validating the hypothesis of the essential role played by hydrogen bonds in the fibres.

The improvement in the damping coefficient of the composites was shown to be to the detriment of their stiffness. The compromised between the two properties was investigated in the final part of this thesis by using hybrid flax-carbon fibre reinforced composites.

Deputy Vice-Chancellor's Office
Postgraduate Office

UNIVERSITY OF CANTERBURY
Te Whare Wānanga o Waitaha
CHRISTCHURCH NEW ZEALAND

Co-Authorship Form

This form is to accompany the submission of any thesis that contains research reported in co-authored work that has been published, accepted for publication, or submitted for publication. A copy of this form should be included for each co-authored work that is included in the thesis. Completed forms should be included at the front (after the thesis abstract) of each copy of the thesis submitted for examination and library deposit.

Please indicate the chapter/section/pages of this thesis that are extracted from co-authored work and provide details of the publication or submission from the extract comes:

*A journal publication entitled "*Tailoring the vibration damping behaviour of flax fibre-reinforced epoxy composite laminates via polyol additions" *was accepted to Composite Part A (20/07/14). The publication was entirely based on the findings of Chapter 5 (Utilisation of polyol compounds to improve vibration damping of plant fibre composites).*

Please detail the nature and extent (%) of contribution by the candidate:

The candidate contributed to around 90% in the design and the completion of the experimental work. The redaction of the manuscript was carried out by the student and then edited by the supervisors.

Certification by Co-authors:

If there is more than one co-author then a single co-author can sign on behalf of all

The undersigned certifys that:

- The above statement correctly reflects the nature and extent of the PhD candidate's contribution to this co-authored work
- In cases where the candidate was the lead author of the co-authored work he or she wrote the text

Name: *Dr Mark Staiger* Signature:  Date: *23/07/14*

Acknowledgements

The study was carried out between 2011 to 2014 at the University of Canterbury in the mechanical engineering department (Christchurch) and Scion in the chemicals and biopolymers group (Rotorua). Part of the experimental research was undertaken at the Australian Synchrotron in Melbourne.

The project was financially supported by the Biopolymer Network Ltd under the New Zealand Ministry of Business, Innovation and Employment contract number BPLY0801. Two travel grants were provided by the Royal society of New Zealand (Young microscopist award) and the Ministry of Business, Innovation and Employment (International Relationships Fund) to attend and present some research at the 26^{th} NZ microscopy conference (Christchurch) and the 19^{th} International conference on composite materials & value chain for natural fibres workshop (Montreal).

The research was supervised by Dr Mark Staiger (University of Canterbury), Dr Roger Newman (Scion) and Dr Alan Fernyhough (Scion). I want to thank my supervisors for their time, effort and constant encouragements. In addition, I would like to thank BPN CEO Ms Sarah Heine for her support in plant fibre composites research. I also want to express my gratitude to Dr Grant Emms for sharing his knowledge in acoustic testing, Ms Sunita Jeram for her help in chemical analysis, Dr Nigel Kirby for setting up the X-ray experiments, Dr Ibrar Hussain for his time and interest in my research.

Coming to the every day support, I really want to thank, my very dear partner Dr Stefan Hill and my friends, Ms Gaelle Guyader and Mr Damien Even. I also want to thank Dr Jean-Philippe Garancher

for his help in mechanics and introduction to the type setting program Latex. To my French and Kiwi families, my old and new friends, my colleagues, I want to say, thank you very much for your genuine compassion, kind understanding and comforting emails, chats, beers, coffees and horse rides.

In memory of Dr Roger H. Newman,
for his kindness, support and wealth of knowledge (*some of which unfortunately never got published*)

Contents

List of Figures

List of Tables

Nomenclature

Q	quality factor
W	work in Newton meter or joule
Δ	logarithm decrement
ϵ	strain
η	damping coefficient
λ	wavelength
η	damping coefficient
θ	incident angle
δ	phase angle
ψ	specific damping capacity or SDC
σ	strength
ζ	damping ratio
CFM	confocal microscopy

CP cross-polarisation

$DMTA\ or\ DMA$ dynamic mechanical thermal analysis

EMC equilibrated moisture content

$FESEM$ field emission scanning electron microscopy

$HWHM$ half width at half maximum

CI confidence interval

IR infra-red

MAS magic angle spinning

MFA microfibril angle

$NFRP$ natural fibre-reinforced polymers

NMR nuclear magnetic resonance

odg oven dried gram

PCA principal component analysis

RH relative humidity

$ROHM$ rule of hybrid mixtures

ROM rule of mixtures

$SAXS$ small angle x-ray scattering

$SDOF$ single degree of freedom

T_g glass transition temperature

tex unit of textile measurement which is a linear mass density defined as grams per kilometre

TTS time temperature superposition

UD unidirectional

$WAXS$ wide angle x-ray scattering

Chapter 1

Introduction

The use of natural cellulosic fibres as reinforcement for polymer composite materials has become popular over the last decades and a vast amount of research has been undertaken to characterise them, assess their limitations and identify their potential fields of application [Wambua et al., 2003, Bos, 2004, Müssig, 2010]. They present some key advantages over man-made fibres including reduced occupational health issues in manufacturing, lower environmental impact, lower costs and good specific mechanical properties [Saheb and Jog, 1999, Summerscales et al., 2010].

More recently natural fibre has shown promise in composite structures that requires energy absorbing materials [Kumar et al., 2014]. They display improved vibration damping compared to carbon or glass fibres and comparable mechanical properties when they are hybridised (*e.g.* carbon with flax) [Gomina, 2012]. Commercial outcomes have exploited this property in their marketing strategy such as Museeuw and Schwimm bikes, Artengo racquets and Xboards snowboards. New composite manufacturers have emerged around environmentally friendly but yet structural products and presented vibration damping as one of their key feature (e.g. Lineo, Namateco ®, Dragonkraft ®, BComp ®).

Fundamental research studies have demonstrated improvement in the area of acoustics [Buksnowitz et al., 2010], impact [Meredith et al., 2012], fatigue [Newman et al., 2012, Hughes et al., 2007] and vibrations [Ghosh et al., 2010, Duc et al., 2014]. However, little is known about how plant fibres dissipate energy.

Hence, the aim of this research was to develop fundamental knowledge about

the physical mechanisms involved in energy dissipation of plant fibres used for composite reinforcement.

1.1 Hypothesis

Plant fibres can be considered as composites of cellulose micro-fibrils reinforcing a polysaccharide matrix. The chemical structure and composition govern the mechanical properties of plant fibres [Müssig, 2010, p 29]. In composite science, the individual properties of each component, their structure and their interfaces are important to determine the overall properties of the composite. In plant fibres, the reinforcement, e.g. the microfibrils of cellulose, is known to be the most important parameter influencing the strength and stiffness properties [Müssig, 2010, p 29]. However, in terms of vibration damping, the non-cellulosic matrix and the interface between the cellulose and matrix are believed to be of greatest importance, as in the case in composite science [Berthelot et al., 2008].

This thesis argued that the reversible dynamic hydrogen bonding between the cellulose microfibrils and the non-cellulosic matrix provides the greatest contribution to energy dissipation during vibration damping by plant fibres, but that other factors such as the cellulose microfibril angle must be considered when interpreting data for energy dissipation under quasi-static conditions.

By understanding the underpinning science behind these characteristics, this research study will assist in the design of more efficient composites tailored for specific energy absorption applications. It will contribute to improving the processes and post-treatments of natural fibres for composite applications. Ultimately, it may help to overcome some of the shortfall of plant fibres and facilitate the uptake of plant fibres as man-made fibre replacements by the composite industry.

1.2 Scope and objectives

The difficulty lied in the possibility of simultaneous combinations of different damping mechanisms such as viscoelasticity, presence of voids or defects or chem-

ical interactions. Separating the different contributions was necessary and was done by investigating plant fibres alone, then by studying them embedded in a polymer matrix as a composite structure. Therefore, the scope of the thesis was concentrated initially on the characterisation of some selected plant fibres and secondly, on composites reinforced with plant fibres. Even though it was certainly considered important in composite design, the science of damping in terms of optimising the composite architectures was not covered in this thesis.

The objectives of this research were to:

- Describe and identify the damping mechanisms involved during elastic and plastic deformations of plant fibres;
- Determine if there are relationships between the damping property and physical/chemical composition of the fibres;
- Investigate the conditions that influence the magnitude of damping in plant fibres;
- Investigate potential treatment to improve the damping property of plant fibre composite applicable for the composite industry.

The final stage of the project was to manufacture composites that illustrated vibration damping improvement.

1.3 Outline of the manuscript

Chapter 1 provides the hypothesis of the study, the drivers, scope, objectives and outline of the thesis.

Chapter 2 presents the background and literature review relevant to the study. Definitions and methods of tests are reviewed and the chosen experimental methodology is presented.

Chapter 3 focuses on the characterisation of selected plant fibres in terms of morphology, chemical and mechanical properties. Insight into the energy absorption with regards to toughness and damping coefficient are also discussed in relation to the cellulose structure, chemical composition and water content .

Chapter 4 utilises the findings of Chapter 3 by testing compounds that have a similar effect as water while being non volatile in order to maintain the improved damping property of the fibres as observed when being hydrated.

Chapter 5 is the investigation of a novel pre-treatment with the aim of improving vibration damping in plant fibres composites by impregnated the reinforcement with hydrogen bonding polyols.

Chapter 6 investigates the trade-off compromise between stiffness and damping of carbon-flax hybrid composites.

Chapter 7 presents the conclusions and potential areas of future work.

Chapter 2

Background

2.1 Introduction

In this Chapter, the discussion starts by defining several parameters used to measure energy absorption and the methodologies to characterise it. The published data on plant fibre composite for energy absorption applications is then summarised and the different damping mechanisms proposed by researchers are reviewed.

Subsequently, a brief overview of plant fibres in their natural and extracted state is presented. The similarities between plant fibres and composite structures are then discussed. The main factors that contribute to energy absorption in man-made composites are used by analogy to identify the features in plant fibres that potentially have similar effect.

2.2 Measure of energy absorption

Energy loss or dissipation is an irreversible process that occurs in a system when the mechanical work of the output energy is less than that input into the system. In mechanics, the capacity of a material to store energy is quantified by the area under a force-displacement curve. When a material is tested up to failure, the area represents its toughness and is generally measured in joules per cubic metre. When a material is tested in cyclic deformation (e.g. fatigue test), during one

cycle of oscillation, if the area under the loading force-displacement curve W_t is greater than the unloading curve W_f, the difference ΔW represents the quantity of dissipated energy by the material. The ratio of dissipated to stored energy per cycle (ψ) is defined as the specific damping capacity of a material (Equation 2.1) and is graphically represented by a hysteresis loop (Figure 2.1).

$$\psi = \frac{\Delta W}{W_t} \tag{2.1}$$

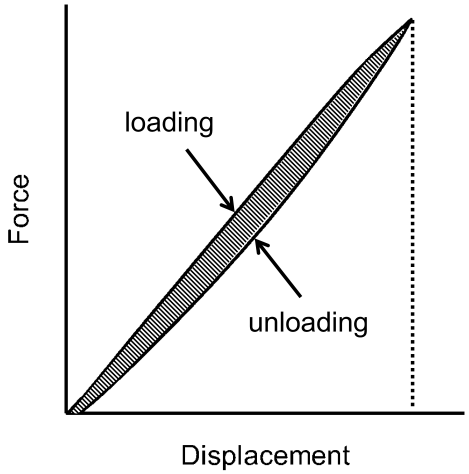

Figure 2.1: Hysteresis loop representing the specific damping capacity

The specific damping capacity (SDC) is dependant on the stress level and the strain rate imposed [Handcock, 1975]. SDC provides information on the behaviour of materials under cyclic stress over extended period of time such as in fatigue tests [Towo and Ansell, 2008].

Measuring energy absorption in composite structures covers a wide range of tests that depends on stress levels and strain rates (e.g. impacts, fatigue, vibrations). Typical tests at high stress levels and high strain rate (e.g. ballistics) provide information on impact resistance, fracture propagation and the capacity of the material to disperse energy [Meredith et al., 2012].

Energy loss at low strain and high frequency is the regime of vibration damping. Vibrations are displacement oscillations around an equilibrium position. Their damping can not be measured directly but instead is calculated from the response characteristics of selected vibrating systems. A vibrating system can be studied by using the equation of motion of a mass-spring-damper model illustrated in Figure 2.2 for a single degree of freedom (Additional details on the equation of motion is provided in Appendix A).

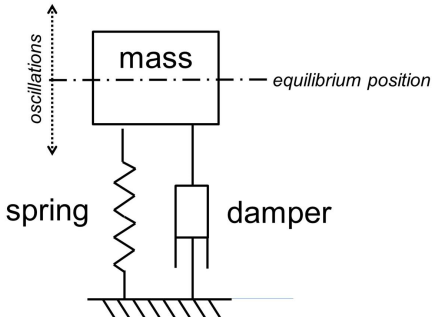

Figure 2.2: Mass-spring-damper model for system with a single degree of freedom.

The steady state response of a SDOF system, excited by a single excitation or harmonic force of constant amplitude, provides damping information through the observation of characteristics such as the bandwidth of the frequency response, amplitude of response at resonance, Nyquist plots, hysteresis loops and dynamic stiffness [Nashif et al., 1985].

The resonance method (single excitation) is non-destructive (ASTM E1875-13, E1876-09) and is particularly attractive for large specimens (ranging up to meters to tens of meters long) [ASTM E1875-13, ASTM E1876-09]. The damping value is determined by observing the evolution over time of oscillations created by a mechanical impulse and corresponds to the energy dissipated that reduces the amplitude of a displacement. It can be quantified by using either the logarithm of the ratio of two successive amplitudes of oscillation called the decrement logarithmic (Δ), or using the half-power bandwidth method that provides the damping coefficient (η) of the material (Appendix A). A typical set-up for a resonance test is presented in Figure 2.3 where the specimen is struck and the amplitude of the oscillations is recorded over time. The sensor is generally an accelerometer but

depending on the size of the specimen and mass of the accelerometer, the damping can be overestimated. An alternative to accelerometers are non-contact sensors such as microphones and laser vibrometers [Berthelot and Sefrani, 2004].

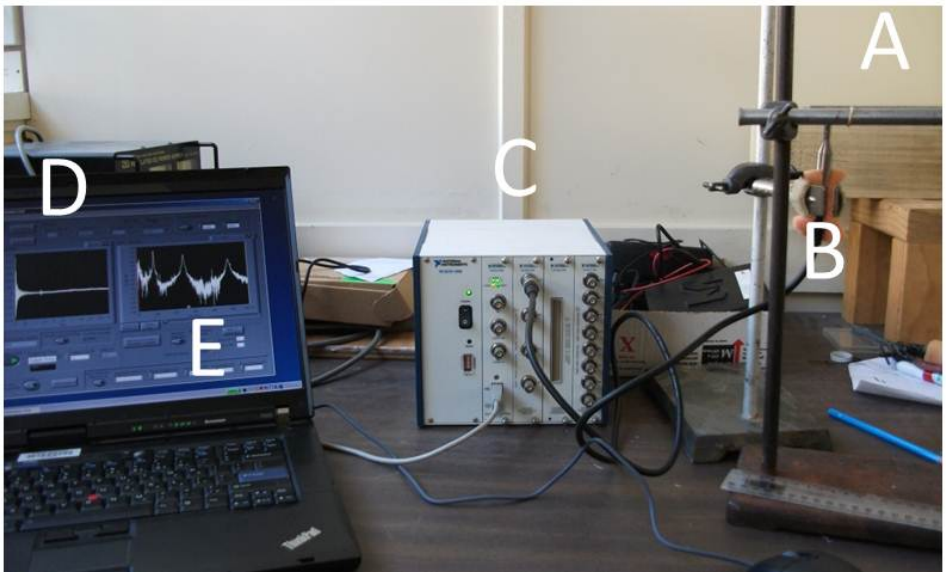

Figure 2.3: Resonance set up, A: specimen, B: sensor, C: amplifier, D: oscillation decay in time domain, E: Fourier transform of the oscillations decay in the frequency domain.

When the system is subjected to a forced oscillation within the linear viscoelastic range of the material, the damping coefficient is equal to the tangent of the phase difference between the strain oscillation and its stress response (tan δ). Tan δ can be measured using a dynamic mechanical thermal analysis (DMTA or DMA) instrument in flexural, tensile, compression and shear mode (Figure 2.4). The response to the deformation can be monitored as a function of temperature or time/frequency. The main drawback of the DMTA is the size of the specimen that are typically around $50 \times 5 \times 3$ mm^3 and the properties observed may not always be representative of larger specimen. Thus, combining resonant and DMTA methods is relevant to the study of vibration damping in small to medium size specimens (tens to hundreds of millimetres).

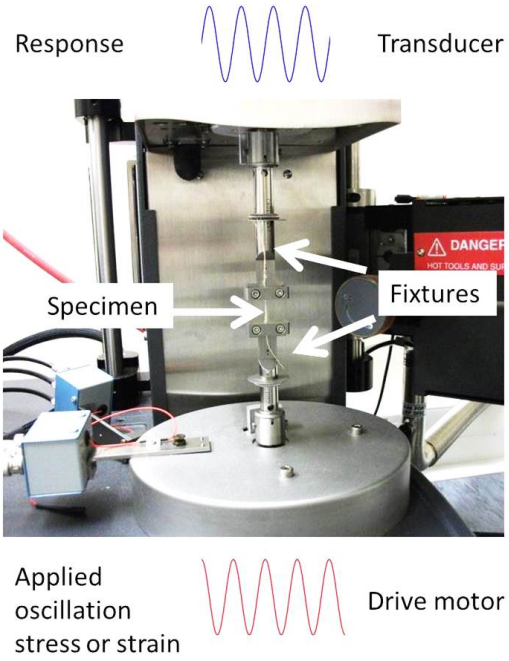

Figure 2.4: DMTA instrument in tensile mode.

The relation between stress (ϵ) and strain (σ) is given by:

$$\sigma = \sigma_0 sin(\omega t + \delta) \tag{2.2a}$$

$$\epsilon = \epsilon_0 sin(\omega t) \tag{2.2b}$$

where σ_0 and ϵ_0 are initial amplitude of stress and strain, w is the angular frequency and δ is the phase angle. Equation 2.2a can be re-written as Equation 2.3:

$$\sigma = \sigma_0 sin(\omega t) cos\delta + \sigma_0 cos(\omega t) sin\delta \tag{2.3}$$

The dynamic modulus can then be defined by a complex number (Equation 2.3):

$$E^* = \frac{\sigma}{\epsilon} = E' + iE'' \tag{2.4}$$

where

$$E' = \frac{\sigma_0}{\epsilon_0} cos(\delta) \tag{2.5a}$$

$$E'' = \frac{\sigma_0}{\epsilon_0} sin(\delta) \tag{2.5b}$$

$$tan(\delta) = \frac{E''}{E'} \tag{2.5c}$$

E' is defined as the storage modulus and is associated with the ability of the material to store potential energy, E'' is the loss modulus and is associated with the ability of the material to dissipate energy. $tan\delta$ is associated with the damping capacity of the material.

For low levels of damping ($\eta < 0.1$) within the linear region of the viscoelastic material, the different damping parameters are linked by Equation 2.6 [Kinra, 1992].

$$\eta = \frac{\psi}{2\pi} = \frac{\Delta W}{2\pi W_t} = \frac{\Delta}{\pi} = tan\delta = \frac{1}{Q} \tag{2.6}$$

where η is the damping coefficient, ψ is the specific damping capacity, Δ is the logarithm decrement, δ is the phase angle which represents the time lag between the applied strain and its stress response and Q is the quality factor. In this study, the parameter used the most often is the damping or loss coefficient, η which is defined as the amount of energy dissipated over one radian of a cycle and expressed relative to the total energy stored.

2.3 Plant fibre composite for energy damping applications

2.3.1 Energy absorption in plant fibre composites

Plant fibres have lower ultimate mechanical properties than man-made fibres such as glass or carbon [Summerscales et al., 2010, Nunna et al., 2012]. However, they have shown promise in structural applications where they can meet standard regulations [Shah et al., 2013, Shah, 2013], and in energy absorption applications where they were shown to match man-made fibres composites. Meredith et al. reported that non-woven mat hemp performed as well as carbon fabric during high speed impacts. The specific energy absorption of hemp epoxy and carbon epoxy composites were 54.3 and 55.7 Jg^{-1} respectively [Meredith et al., 2012]. However the results were somewhat ambiguous since the fibre volume fraction of the carbon was not reported and the authors stated that fibre volume fraction influences energy absorption properties. Furthermore, other studies have reported results questioning the use of plant fibres as composites reinforcement in energy absorption applications. Hughes et al. found that the fracture toughness of jute and hemp composites was 3 time lower than glass chopped strand mat composites [Hughes et al., 2002]. His findings were supported later by Shahzad who also reported lower impact damage tolerance when comparing chopped strand mat and hemp composite at similar fibre fraction [Shahzad, 2011].

However, there is a general consensus on the benefits of using plant fibres in the vibration damping area. Indeed, Gomina reported a 20% in reduction of vibration by replacing a portion of the carbon fibre in a bicycle frame with flax fibre [Gomina, 2012] and Lineo claim on their website that the Artengo flax tennis/squash racquet absorbs 25% more vibration than a traditional racquet. Yet surprisingly, only a few recent publications present experimental results quantifying the increase in vibration damping of plant fibre composites compared to man-made fibre composites [Ghosh et al., 2010, Vanwalleghem, 2010, Duc et al., 2014]. The University of Gent has worked on the characterisation of flax-carbon fibre hybrid composites and their effect on vibration damping of a bicycle frame [Ghosh et al., 2010, Vanwalleghem, 2010]. They claimed that flax fibre improved

vibration damping compared to carbon and steel, however no quantitative comparison was provided. Duc et al. recently measured damping values 3 to 5 time higher for flax epoxy composites compared to carbon and glass-fibre reinforced composites using dynamic mechanical analysis [Duc et al., 2014].

2.3.2 Hypothetical energy absorption mechanisms of plant fibres

The most obvious reason for the increase in damping is the lower stiffness of plant fibre composites compared to glass and carbon fibre composites. Damping and stiffness are antagonist properties and improving one is often to the detriment of the other one [Haddad and Feng, 2003, Chung, 2003]. Martone et al. found that micromechanical hybridisation using elastane fibres (Lycra®) commingled with carbon fibre increased damping absorption by 82% but also decreased the elastic modulus by 37% [Martone et al., 2011].

Furthermore, the differences in the hydrophilicity of plant fibre and the polymer matrix tend to generate weak interfaces that act as energy sinks [Duigou et al., 2014]. Compatibilising fibres and matrix increases strength and stiffness due to improved stress transfer, but simultaneously decreases damping by decreasing interfacial shear deformation [Dhakal et al., 2007, Yan, 2012].

At high deformation, the energy absorption properties of a plant fibre composite are dependent on the fibre tensile strength. Gassan compared the specific damping capacity (SDC) (Equation 2.1) of flax and jute composites in their plastic region [Gassan, 2002]. The higher SDC of flax was attributed to its higher cellulose content compared to jute.

Several authors attributed the energy absorption of the composites to the microfibril angle (MFA) of the reinforcing fibres. The MFA refers to the angle between the direction of the cellulose microfibrils and the axial direction of the fibre cell. Pavithran et al. reported that the work to failure of UD sisal composites was more than twice the value for coir composites [Pavithran et al., 1987]. He attributed the low toughness of coir-fibre composites compared with sisal-fibre composites to the high deformation of the coir fibres, leading to failure of the matrix, followed by crack propagation at the fibre-matrix interface and fibre pull out. An optimal

fibre MFA in the range of 15° to 20° was concluded depending on the elongation to failure of the resin matrix [Pavithran et al., 1987]. Idicula et al. found that sisal composite performed better in terms of impact strength than banana fibre composites due to their difference in MFAs (20° for sisal and 10° for banana fibres) [Idicula et al., 2005].

Liang et al. associated high damping with low density, comparing flax and glass fibres in fatigue tests [Liang et al., 2012].

Hughes found that unidirectional flax fibres exhibit non-linear behaviour that was attributed to the presence of kink bands in the flax fibres [Hughes, 2012]. The kink bands were proposed to act as energy sinks, concentrating stresses and causing unidirectional (UD) fibres to behave as separate segments of fibres aligned in the same direction rather than continuous reinforcement.

Vanwalleghem attributed the damping properties of flax fibre to the weak interactions between the cellulose and hemicellulose chains [Vanwalleghem, 2010]. Although the author did not elaborate further on this statement, the idea was reasonable in view of the wood Velcro® theory [Keckes et al., 2003, Kretschmann, 2003].

2.3.3 Damping in composite materials

The detailed structure of plant fibres is still not known precisely due to the presence of different intermingling components (i.e. lignin, hemicellulose, cellulose). However, a plant fibre can be thought of as a composite of cellulose reinforcing a polysaccharide and lignin matrix [Shah, 2013]. In order to study damping in plant fibres, it is useful to consider the contributing factors to damping generally observed in composite science.

Energy absorption in composite structures is achieved by mechanisms that occur within the polymer matrix, the reinforcing fibres and through other features such as voids, fillers and fibre-matrix interface. These contributions involves reversible (viscoelasticity) and irreversible (fracture, plasticity, interfacial debonding) mechanisms [Chandra et al., 1999]. The contribution of each mechanism depends on the intrinsic properties of the components, their interactions and the type of deformation they undergo.

At low deformation such as vibrations, the viscoelasticity of the matrix has a large influence on the damping properties of a composite especially if the matrix is deformed above its glass transition temperature (T_g). The more flexible the back bone of the matrix, the higher the damping. Pothan et al. approximated the damping coefficient of a composite to the sole contribution of the matrix using dynamic mechanical thermal analysis methods (Equation 2.7) [Pothan et al., 2003].

$$tan\ \delta_{composite} = tan\ \delta_{matrix}(1 - V_f) \tag{2.7}$$

where V_f is the fibre volume fraction of the composite.

In some cases, Equation 2.7 is too reductive as it ignores the contribution of the fibres and fibre-matrix interface. The damping contribution of the reinforcing fibres is generally lower than the matrix, however some fibres significantly contribute to damping through viscoelastic mechanisms such as aramid and elastane fibres [Hoa and Ouellette, 1984, Chandra et al., 1999, Martone et al., 2011]. Also, energy dissipation via shear forces at fibre-matrix interface can contribute significantly to structural damping of composite materials. A common method of manufacturing composites is to embed additional layers of viscoelastic material within the composite laminate. The shear stresses that arise from such constrained layers is converted into heat that increases damping [Chung, 2003]. Shear stresses are influenced by the structure of the reinforcement (i.e. woven, knitted, unidirectional), laminate configuration [Kamal, 2010, Muralidhar et al., 2012] and aspect ratio of the fibres [Kamal, 2010, Gassan, 2002, Suarez et al., 1986].

At high deformation rates, the capacity of a composite to dissipate energy is governed by the strength of the fibres and the type of reinforcing structure [Wambua et al., 2003, Shah et al., 2012a]. Harris reported a toughness optimum when the reinforcing fibres were 10° off-axis for steel fibre-polymethyl methacrylate and glass fibre-polyester composites [Harris, 1999]. Later, Berthelot studied the influence of the fibre orientation in UD composite comparing aramid and glass fibre. Maximum damping occurred when the fibres were off-axis by 30° for the aramid fibres and 60° for the glass fibres [Berthelot and Sefrani, 2004].

Since plant fibres can be thought of as composite structures, the parameters

influencing energy absorption include: the matrix (polysaccharides and lignin composition), shear stress arising from the fibre-matrix interface (cellulose and non-cellulosic matrix), and structure of the reinforcement (microfibril angle, fibre cells, kink bands and fibre geometry). Plant fibres exhibit major differences in chemical and physical properties depending on their origin [Müssig, 2010, pp 303-304]. The following section provides a general overview of plant fibres and their main differences according to published literature.

2.4 The physiochemical properties of plant fibres

2.4.1 Plant fibre types

Extensive literature is available on the characterisation of non-wood plant fibres [Müssig, 2010]. Hence, this section will focus on the fibres that are used in the experimental work of this study when literature data was available. The selected plant fibres can be classified according to their origin in the body of the plant: bast, leaf, seed/mesocarp. The bast fibres correspond to the fibres located around the stem of dicotyledonous plants such as European flax (*Linum usitatissimum*), hemp (*Cannabis sativa*) and ramie (*Boehmeria nivea*). The fibres are arranged in bundles glued to each other in the cuticle by pectin and calcium ions [Jauneau et al., 1997].

The leaf fibres are extracted from monocotyledonous plants such as sisal (*Agave sisalana*), harakeke (*Phormium tenax*) or abacca fibres (*Musa textilis*).

The last major class of plant fibres used as composite reinforcement includes the seed trichomes produced by cotton (*Gossypium spp*) or kapok (*Ceiba pentandra*) plants. The strength and stiffness of seed trichomes are generally lower than the other types of fibres. The mesocarp fibres are also classified as seed fibres, an example being the coir fibre extracted from the husk of the coconut. Coir fibres are known to contain a high level of lignin compared to the other fibres making them resistant to salt water [Müssig, 2010, p 207].

2.4.2 Chemical composition

Plant fibres are mainly composed of cellulose, hemicellulose, pectin, lignin, wax and ash (Table 2.1). The proportion of these components differs depending on their types, species, growth conditions and stage, or location in the plant [Morvan et al., 2003], [Müssig, 2010, p 32].

Cellulose is a linear polysaccharide that is semi-crystalline, existing as one of several polymorphs (I_α, I_β, II, III_I, III_{II}, IV_I, IV_{II}). Its repeating unit or cellobiose is produced by the condensation of two glucose molecules linked by a β (1-4) bond (Figure 2.5).

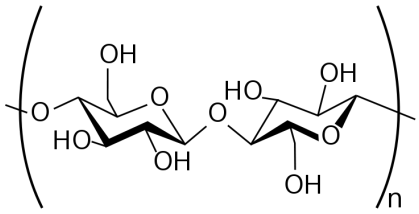

Figure 2.5: Cellulose unit

The cellulose microfibrils are thousands of nanometres in length and 5 to 50 nm in diameter and form the primary and secondary cell wall layers of plant fibres [Bos, 2004]. They can agglomerate in highly crystalline regions due to presence of hydrogen bonding between the hydroxyl groups but may also exist in the amorphous state [Kabir et al., 2012]. The mechanical properties of the fibres can change dramatically depending on the cellulose amount present in the fibre cell wall and MFA (Figure 2.6) [Müssig, 2010, Kraessig, 1987].

Hemicellulose is a general term used to describe amorphous branched polysaccharides composed of monomers of glucose, galactose, mannose, xylose arabinose and galacturonic acid [Scheller and Ulvskov, 2010]. Within these combinations of monomers, subtypes can be grouped into categories based on their hydration affinity. Low hydration polysaccharides, such as arabinoxylans, xyloglucans, are structural components of the fibre cell and stabilise the cell wall along with cellulose and lignin. Other hemicellulose such as galactoglucomannans, glucomannans, galactomannans and β-glucans tend to be more hydrated and have fewer ester

Table 2.1: Typical chemical composition of selected plant fibres in wt. %.

Fibre	Cellulose	Hemicellulose	Lignin	Pectin	Extractive	Sources
European flax	71.2	18.2	2.2	2.0	4.3	[Müssig, 2010, p 303]
Ramie	68-85	3-17	0.5-1	1.9-2.1	5.5-6.4	[Müssig, 2010, p 303]
Jute	61.5	20.0	12.0	0.2	1.2	[Wang et al., 2009]
Sisal	73.1	13.3	11.0	0.9	1.3	[Müssig, 2010, p 304]
Harakeke	45.1	30.0	11.2	0.7	2.2	[Richter et al., 2011]
Coir	35.6	15.4	32.7	5.1	3.0	[Mwaikambo and Ansell, 2002]

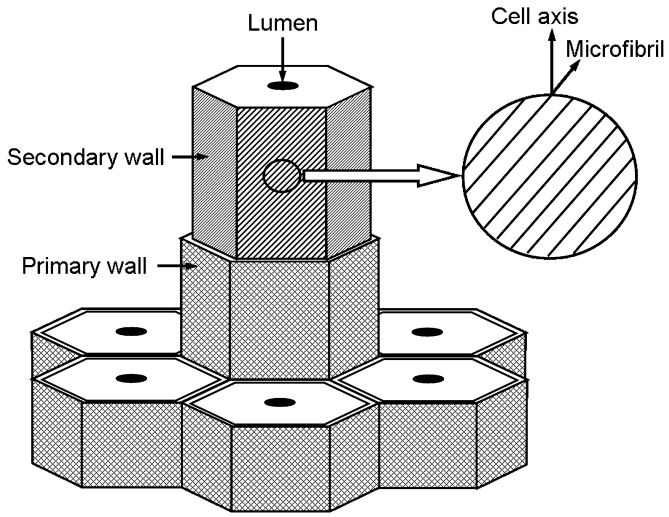

Figure 2.6: Representation of the microfibril angle in cell wall. Courtesy of Dr Roger Newman [Newman, 2008]

side groups. They are used primarily as extra cellular energy and water storage, especially in seeds [Dumitriu, 2005]. Structural hemicellulose vary in chemical composition across plant species and plant maturation stage. It is believed that hemicellulose types are location specific. The closer they are to the cellulose microfibrils, the more of the glucommannans are present and the more complex the hemicellulose [Akerholm, 2001]. Hemicellulose is reported to interact with cellulose via hydrogen bonds and Van de Waals forces, while its interaction with lignin occurs via covalent bonding with the ester and ether linkages of the xylan side groups [Dumitriu, 2005].

Pectin consists of polysacharides of mainly galacturonic acid. They form a complex network cemented by calcium cations. Pectin plays an important role along with hemicellulose to cement the fibre cells to one another [Jauneau et al., 1997, Morvan et al., 2003].

Lignin is composed of an amorphous 3D network of aromatic compounds. It mainly consists of *p*-coumaryl alcohol, coniferyl alcohol, and sinapyl alcohol [Freudenberg, 1959]. Lignin is a stiff, water resistant barrier and is generally the last component to biodegrade [Scott and Stead, 1994].

Waxes, minerals (silica, calcium, potassium), ash are also constituent of plant

fibres to a lesser proportion. Waxes are lipids that mainly appear on the outside of the plant acting as a protective layer against external attack such as micro-organisms or insects [Müssig, 2010, p 20].

2.4.3 Mechanical properties

Plant fibres exhibit large variations in their mechanical properties [Müssig, 2010, p 32]. The utilisation of the fibres *in vivo* provides an insight into their performance as a potential reinforcement for composites [Newman, 2008]. Fibres that reinforce stems tend to require high elastic moduli and strength, fibres that reinforce leaves require toughness and flexibility, and fibres formed as seed hairs require little in the way of mechanical performance [Newman, 2008]. High elastic moduli and strength found in bast fibres such as flax and ramie have been correlated to their high content of cellulose and low values of the microfibril angle [Gassan, 2002].

The terminology used to define "fibre" can be ambiguous. Generally, the term fibre is used to describe a single fibre cell while a fibre bundle consists of fibre cells that may consists of hundreds of cells. Table 2.2 summarises the tensile properties for bast, leaf and mesocarp plant fibre bundle as they are typically used in composite reinforcement. There is a lot of scatter in the values of mechanical properties of plant fibres reported in the literature. The variability of the properties arises from differences in growth conditions and extraction processes of the fibres [Baley, 2004, Bos, 2004]. Another reason for the large scatter in mechanical properties is due to the approximations made regarding the cross-sectional area of the fibres. Generally, the strength and stiffness are calculated using the cross-sectional area based on the assumption that the fibres are perfect cylinders. However the geometry of the fibres can vary from hexagonal to flat ribbon shape. The lumen and fibre porosity is also approximated due to the difficulty of measuring these parameters accurately. Indeed, Baley found that there was a decrease in stiffness with an increase in the diameter of flax fibres due to an under estimation of the lumen size [Baley, 2002]. Similar observations are reported by De Rosa 2010 on the tensile strength of harakeke fibre bundles [De Rosa et al., 2010].

Table 2.2: Tensile properties of selected plant fibres.

Fibre	Stiffness (GPa)	Ultimate strength (MPa)	Ultimate strain (%)	References
European flax	27.6	345-1035	6-11	[Bledzki and Gassan, 1999]
Ramie	32	627	2.7	[Nam and Netravali, 2006]
Jute	38-41	306-258	0.6-1	[Fidelis et al., 2013]
Raffia	28-36	148-660	2	[Elenga et al., 2009]
Harakeke	26.2	465-770	16	[Richter et al., 2011]
Sisal	20	349-619	1.7-4.5	[Fidelis et al., 2013]
Windmill palm	1.3	114	39.5	[Zhai et al., 2013]
Coir	4-6	153	30-49	[Müssig, 2010, p 301]

2.4.4 Morphology of plant fibres

The fibre cell is composed of a primary and secondary wall as described in the Section 2.4.2 (Figure 2.6). The primary wall is generally thinner than the secondary wall and mainly consist of pectins that add stiffness to the fibre cell. The secondary wall takes up the largest proportion of the fibre cell, consisting of several layers that have S or Z helicoidal arrangements of cellulose micro-fibrils [Müssig, 2010, p 27]. Fibre bundles in bast-fibre plant are generally small bundles of a few fibre cells. In contrast, the leaf and mesocarp fibre bundles tend to consist of hundreds of fibre cells (Figure 2.7).

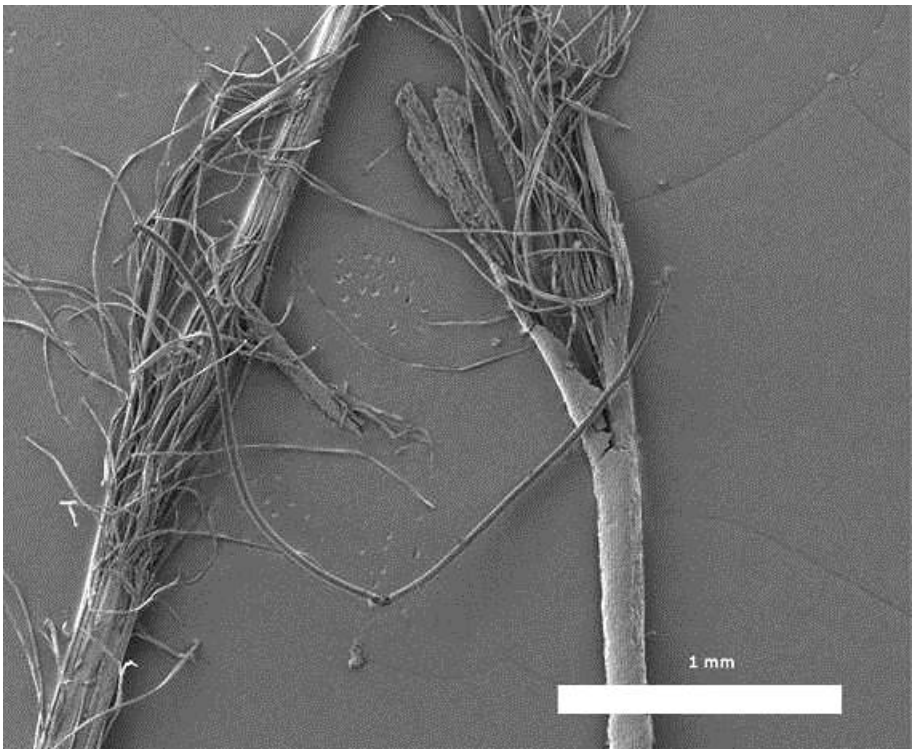

Figure 2.7: Field emission scanning electron microscopy of two harakeke fibre bundles showing hundreds of fibre cells, magnification $\times 30$.

The morphology of plant fibre cells differ dramatically from one type to another. In the seed fibres, the cells tends to be curlier compared to bast fibres while leaf fibres tend to be more ribbon-like (Figure 2.8).

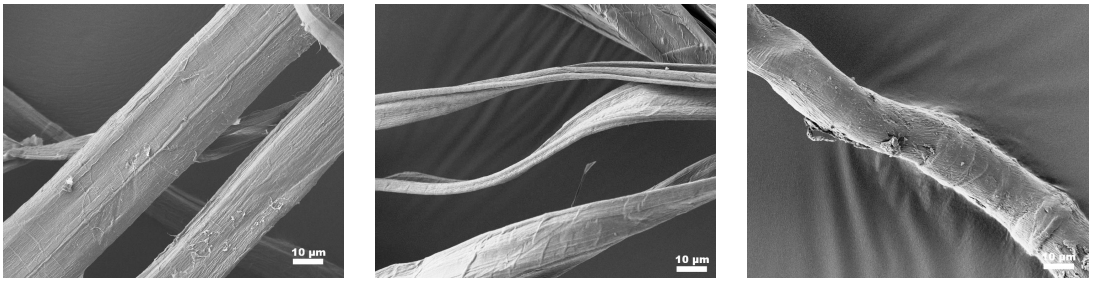

(a) (b) (c)

Figure 2.8: Field emission scanning electron microscopy of individual fibre cells, magnification ×1000, for (a) hemp, (b) agave and (c) linseed.

The aspect ratio of the fibre is another important parameter especially when considered for composite reinforcement, generally the higher the better in terms of strength and stiffness. The highest aspect ratio was reported for ramie fibre [Müssig, 2010, p 26]. European flax fibres have dimensions in the range of 5-76 μm in diameter and 4-77 mm in length [Baley, 2004]. This average length can be reduced by the presence of defects that includes kink bands, microcompression and dislocations. These defects are created during the growth of the plant but mainly occur due to the method of extraction [Bos, 2004]. They are locations where the orientation of the cellulose microfibrils deviate from the axial direction of the fibre cell (Figure 2.9) and the cellulose crystal structure is less ordered [Bos, 2004, Baley, 2004]. Although no correlation has been observed between the number of kink bands and mechanical behaviour of European flax fibres, kink bands are known to be the location where failure initiates [Baley, 2004]. Thygensen et al. observed kink bands in hemp fibres *in-situ* during tensile testing using microscopy [Thygesen et al., 2007]. Kink bands were shown to fully straighten at 50% of the maximum stress (830 mN) and 4% strain. However, they reappeared when the load was removed, exhibiting a viscoelastic behaviour [Thygesen et al., 2007].

The porosity created by the lumen has an influence on the scatter of the mechanical properties found in literature (Section 2.4.3). The lumen size of the fibre cell varies depending on the plant type and its maturation stage [Müssig, 2010, p 25]. However, depending on whether the lumens are collapsed or not, the estimation of the mechanical properties can be erroneous (Figure 2.10) [Madsen, 2003].

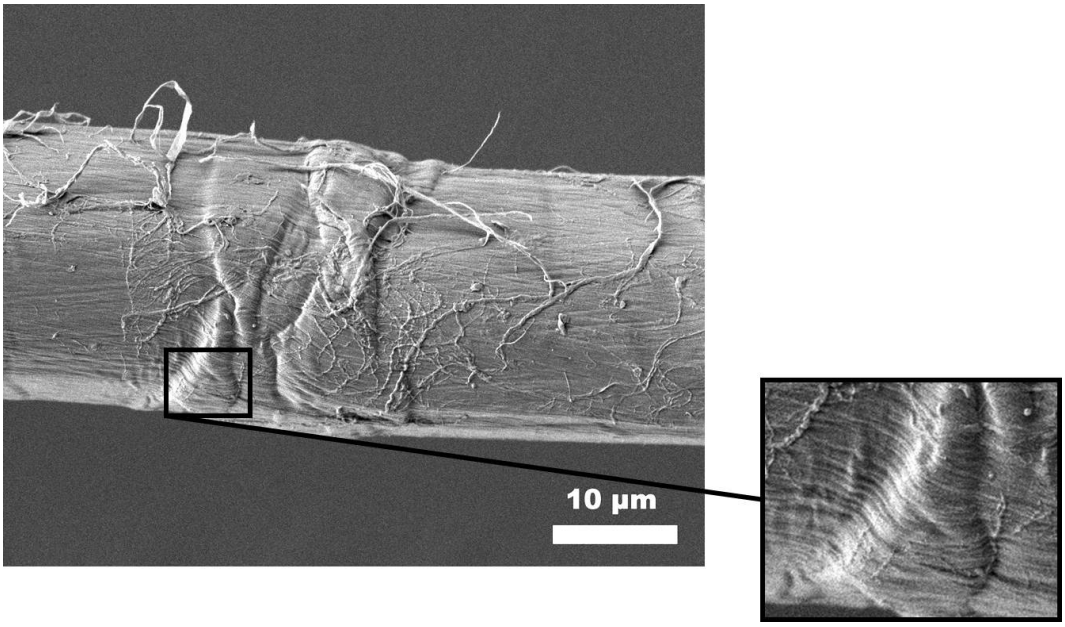

Figure 2.9: Field emission scanning electron microscopy of a kink band in European flax, magnification ×2000.

Most of the studies on plant fibres report the value of their mechanical properties using average of the fibre cross section assuming a cylinder shape [Müssig, 2010, p 285]. Figure 2.10 shows a flax fibre in (x,y) and (x,z) planes, highlighting the potential risk of wrongly estimating the cross section using microscopic images.

However, when the lumens remain open, their presence can influence the composite mechanical properties. If they are free of resin, they contribute to the void content and thus possibly improve damping. Alternatively, if they are filled with resin or polymer, their presence can improve the mechanical properties of the composite by allowing a larger surface contact between the fibres and the resin (Figure 2.11).

2.5 Discussion

A review of the literature has shown that the parameters that contribute to energy absorption in plant fibre composites included: chemical composition, MFA, fibre defects, loss of stiffness and chemical interactions such as hydrogen bond-

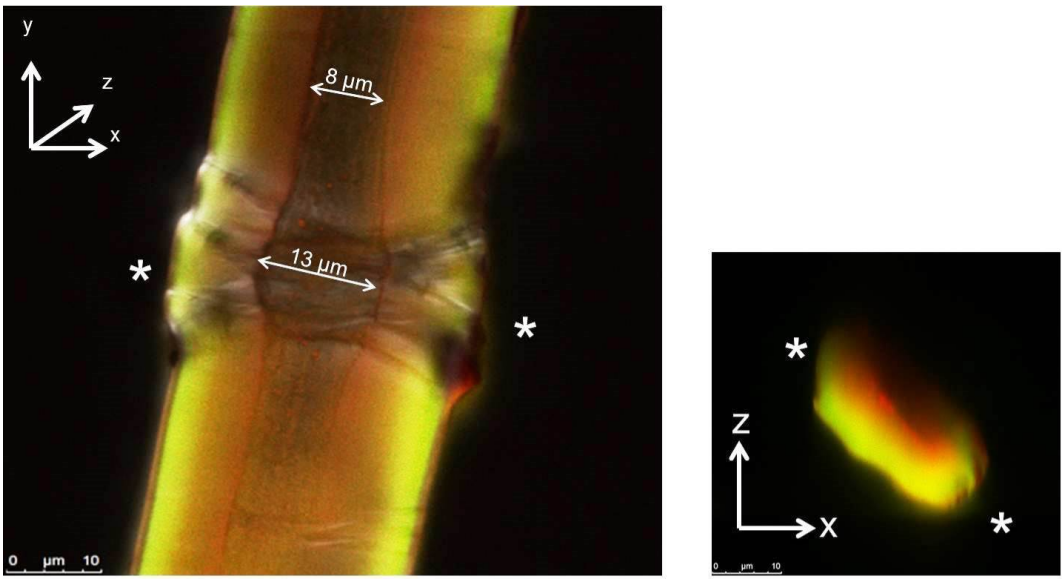

Figure 2.10: Polarised light micrograph of a kink band in European flax. On the (xy) plane (right micrograph) the lumen seems larger within the kink band rather than in the rest of the fibre and represents around 1/3 of the volume of the fibre, yet when observing in the (xz) plane (left micrograph), the lumen proves to be collapsed.

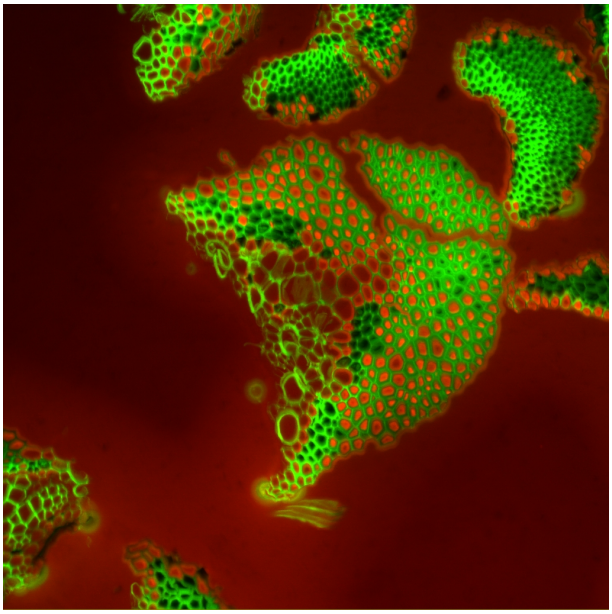

Figure 2.11: Confocal micrograph of a harakeke composite cross section. The red colour indicates presence of resin in some fibre lumen, the black colour indicates void in lumen.

ing. The approach undertaken to identify the importance of each factor started by comparing the fibres to man-made composite structure .

The cellulose microfibrils are the reinforcing structure of the fibre cell that contribute to its strength [Gassan and Bledzki, 1999]. The microfibrils are embedded in a mixture of hemicellulose, pectin, lignin that can be described as the matrix [Shah et al., 2012b]. A major contributor to damping in composite structures, is the viscoelasticity of the resin especially if the matrix is below its glass transition temperature. In the case of plant fibres, the chemical composition varies drastically depending on the type of fibre considered [Müssig, 2010, p 303-304]. Vibration damping could likely be improved by selecting plant fibres according to their chemical composition. However, the influence of the chemical composition of plant fibres on their damping capacity has not yet been investigated.

The cellulose microfibrils are wound around the cell wall at various angles depending on the plant. Thus, fibres with a large MFA may be more appropriate as reinforcement for a composite with higher vibration damping property as it was

found in composite material reinforced with off-axis fibres [Berthelot and Sefrani, 2004]. Hence, leaf or seed fibres may be more advantageous than bast fibres in this regards. Pavithran et al. demonstrated that fibres with a MFA between 15° to 20° were the most appropriate for reinforcing composites used in impact resistance applications. Although, only four fibre types were tested: sisal, pineapple, banana and coir fibres with MFA ranging from 12° to 45° [Pavithran et al., 1987]. No fibres with MFA $\leq$12° were tested, limiting their conclusions to only comparing leaf and mesocarp fibres.

The dissipation of energy due to shear stress at the fibre-matrix interface is another contributor to damping in composites. In plant fibres, the cohesion between the cellulose and matrix is achieved via hydrogen bonding which also makes their mechanical properties susceptible to moisture levels and chemicals that can interfere with hydrogen bonding. Studies on the mechanical properties of wood have shown that the damping property of wood varies with moisture and hydrogen bonding compounds [Ebrahimzadeh and Bertilsson, 1998, Entwistle, 2005]. Similarly, plant fibres mechanical properties vary with moisture [Placet et al., 2012]. However no results on the influence of moisture on the damping property of non-wood cellulosic plant fibre have yet been presented.

Kink bands or microcompressions in fibres can also lead to energy dissipation as they act as energy sinks [Hughes et al., 2002, Newman et al., 2012] and exhibit reversible visco-elastic behaviour [Thygesen et al., 2007]. This behaviour could be thought of as acting like a damper within the fibre itself and dissipating energy via viscoelastic mechanisms.

Finally, stiffness and damping are generally antagonist properties and increasing damping could be to the detriment of stiffness [Lakes, 2002]. The trade-off between these two mechanical properties is necessary as an increase in damping that lead to a dramatic decrease of stiffness would not be of interest in structural composite materials.

This thesis proposed to fill some of the information shortfall and investigate the factors identified in Chapter 2 as potential contributors to damping in non-wood cellulosic fibres and their composites.

Chapter 3 focused on the characterisation of a range of plant fibres (bast, leaf, mesocarp) and attempted to isolate the different contributions of the factors men-

tioned above. The chemical and physical properties were studied and correlations were investigated between the chemical composition, variation of MFA and measures of energy absorption.

Chapter 3

Deformation mechanisms for energy absorption in non-wood plant fibres

3.1 Introduction

Chapter 2 defined some key parameters and methods to measure energy absorption and vibration damping in composite structures. It also reviewed the factors that potentially influence the plant fibres damping property and identified MFA and chemical composition as important factors. In the present chapter, the effet of MFA and chemical composition were studied on the toughness and vibration damping properties of some selected plant fibres.

As mentioned in Chapter 2, plant fibres used in composite reinforcement originate from various types of plants. Consequently, they have significantly different physical and chemical characteristics. Previous studies have focused on the correlation between the tensile strength, stiffness and strain of plant fibres and their associated MFA [Chakravarty and Hearle, 1967], [Müssig, 2010, p 29]. Models for calculating the elastic moduli of plant fibres showed decreased stiffness with increased microfibril angle [Gassan et al., 2001]. Large microfibril angle has also been associated with large deformation, resulting in high values of work to failure [Chakravarty and Hearle, 1967, McLaughlin and Tait, 1980]. Satyanarayana et

al. reported the values of MFA of different plant fibres along with their tensile stress-strain properties showing that generally the higher the MFA, the higher the toughness [Satyanarayana et al., 1982]. Mukherjee and Pavithran presented similar findings with a toughness of 3200 MN m^{-2} for coir fibre (MFA of 45°) and 1250 MN m^{-2} for sisal fibre (MFA of 20°) [Mukherjee, 1986, Pavithran et al., 1987]. The toughness of wood was studied for samples where the MFA varied between 5° to 50° [Reiterer et al., 2001]. An optimal toughnes was observed for MFA of 27°. Chauhan et al. reported the highest damping coefficient in wood with a MFA of 30° [Chauhan, 2006]. A previous study on wood indicated a power law variation between the damping coefficient and MFA, and showed that wood with MFA around 45° had a damping coefficient 50% higher that wood with a MFA of 15°[Bremaud, 2012]. Similarly to wood, it was expected that high MFA fibres would present an advantage in vibration damping applications and that potentially, an optimal MFA value could be observed [Bremaud, 2012]. However, no data was available to compare the damping behaviour of different non-wood cellulosic fibres.

Another major contributing factor to mechanical property variation was the chemical composition of the fibres or the "matrix" as analogous to composite structures (Chapter 2). In fatigue cycles above the elastic region, Gassan attributed the higher specific damping capacity of flax composite compared to jute to either higher a cellulose content or lower lignin content [Gassan and Bledzki, 1999]. In wood, Chauhan attributed energy absorption to MFA but also to the dissipation of shear stresses that arise between hemicellulose and lignin [Chauhan, 2006] while Entwistle et al. attributed damping to the hemicellulose content during elastic deformations at high frequency [Entwistle, 2005].

As mentioned in Chapter 2, the matrix contribution to damping in composite structure is the greatest when tested above its T_g. Since the T_g of hemicellulose is reported to be around room temperature while that of lignin is around 75 °C, the hypothesis that damping in plant fibres was influenced by their hemicellulose content is strengthened [Entwistle, 2005, Dumitriu, 2005].

The experimental work presented in this chapter begins with the chemical and mechanical characterisation of some selected plant fibres. Different fibre types were selected for their known variation in MFA and chemical composition (bast,

leaf, mesocarp) (Section 2.4.2). The mechanical properties were described as Newton per tex similarly to the textile industry and to avoid the errors caused by the approximation of the fibres as perfect cylinders [Charlet et al., 2009]. The carbohydrate composition was determined by hydrolysis and anion-exchange liquid chromatography [Pettersen, 1991]. The MFA was determined by Synchrotron based X-ray diffraction. Attention was paid to technical harakeke fibres where the MFA was known to vary within the plant itself [Richter et al., 2011]. The fibres were then tested in tensile mode to measure the stiffness, tenacity, toughness and damping coefficient using DMA. The correlation between variables were then studied by principal components analysis.

3.1.1 MFA characterisation using X-ray diffraction

MFA can be determined using different techniques which differentiate themselves by looking at the individual fibre cell (microscopy) or looking at the average value of several fibre cells (X-ray diffraction) [Donaldson, 2008]. X-ray diffraction is an accurate method to determine the MFA of cellulosic fibres [Cave, 1997]. Especially, when using a Synchrotron light source, where data is collected within seconds with a resolution that is not achievable using conventional X-ray sources [Hill, 2010].

X-rays are a form of electromagnetic radiation with a wavelength range of 0.01 nm to 10 nm, enabling the detection of structures at the molecular level. When the wavelength (λ) is of the same order of magnitude as the distance between atoms, X-ray diffraction occurs due to an interference phenomenon. A synchrotron light source is produced by accelerating electrons through a linear particle accelerator and a booster ring. The high energy electrons are then injected into a storage ring and emit electromagnetic radiation. When an electron is hit by an X-ray beam, it vibrates and releases the vibration energy by radiation. If the structure of atoms is organised as it is in crystals, the X-ray radiation scattered by each atom of the crystal causes diffraction (Figure 3.1). For a parallel set of atomic planes with a given d-spacing between the planes, constructive interference of the incident electromagnetic waves occurs when Bragg's law is satisfied (Equation 3.1)

to create a diffraction pattern.

$$n\lambda = 2d \sin\theta \tag{3.1}$$

where θ is the angle between the incident wave and the crystal planes, λ is the incident wavelength and d is the spacing between planes.

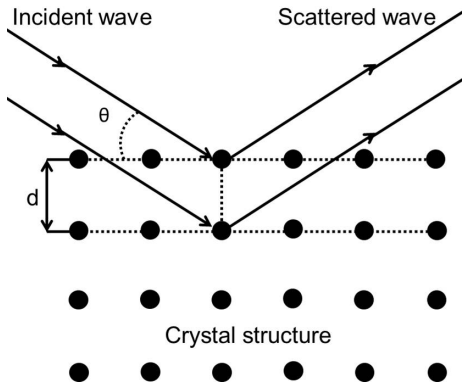

Figure 3.1: Constructive interference occur when Bragg's equation is satisfied (Equation 3.1).

The microfibril angle (or μ) can be determined by X-ray diffraction due to the crystal structure of the cellulose microfibrils. Microfibril angle is determined by measuring the half-width at half maximum height (w) of the peak due to the cellulose (200) reflection in the azimuthal plots [Sugiyama et al., 1991, Kölln et al., 2005, Diddens et al., 2008, Newman, 2008].

Figure 3.2 presents a diffraction pattern of a ramie fibre where the (200) reflection is shown, while Figure 3.3 presents the integration of the (200) reflection as a function of the azimuthal angle. The diffraction due to the (200) planes is measured within the scattering angle plots of the counts measured at an angle range of $2\theta = 11.32°$ and $12.84°$ against the azimuthal angle (ϕ) at the chosen wavelength of the X-ray. The analysis of the diffraction pattern is carried out by specialised image analysis software. The integration procedure of the (200) reflection consists firstly of masking off the areas not included in the analysis. Then the software converts the image into a plot of pixel intensity as a function of distance from the originating beam. The plot which relates to CCD pixel location, scattering

angle and spacing between crystal planes, is then expressed in terms of intensity (Figure 3.3).

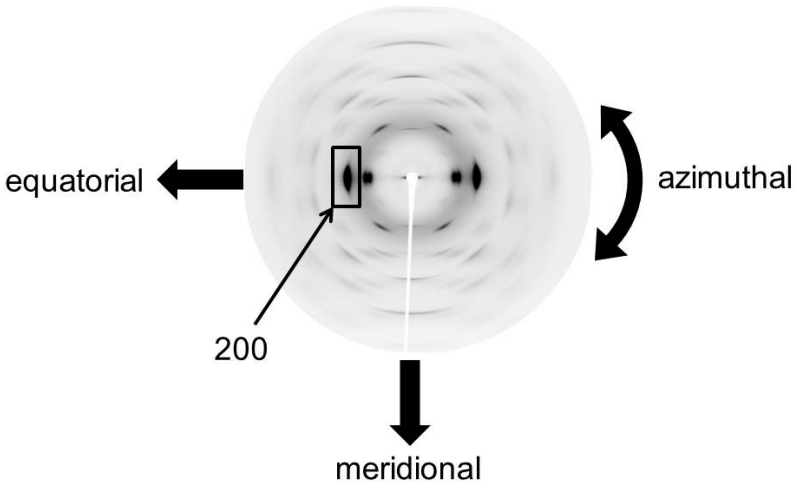

Figure 3.2: An example of a typical diffraction pattern for a ramie fibre showing the (200) reflection.

The reasoning behind the use of w as an approximate measure of μ is outlined below. Azimuthal plots on cellulosic fibres sometimes show double maxima [Martinschitz et al., 2008]. The distance between the two maxima is approximately equal to 2μ [Sisson, 1935]. However, the values of μ are usually so small that the two maxima cannot be resolved [Müller et al., 2006]. In such cases, the value of μ is sometimes calculated from the second moment S^2 around the peak maximum in an azimuthal plot, using an approximate relationship [Evans, 1999]:

$$S^2 \approx 0.5\mu^2 + \sigma^2 sec\mu \tag{3.2}$$

where σ is the standard deviation of μ for the collection of fibre cells exposed to the beam. If $\mu \ll 1$ radian, as in the case of most plant fibres, then $sec\mu \approx 1$. Cave found that $\sigma \approx \mu/3$ for wood [Cave, 1997]. If the peak profile can be

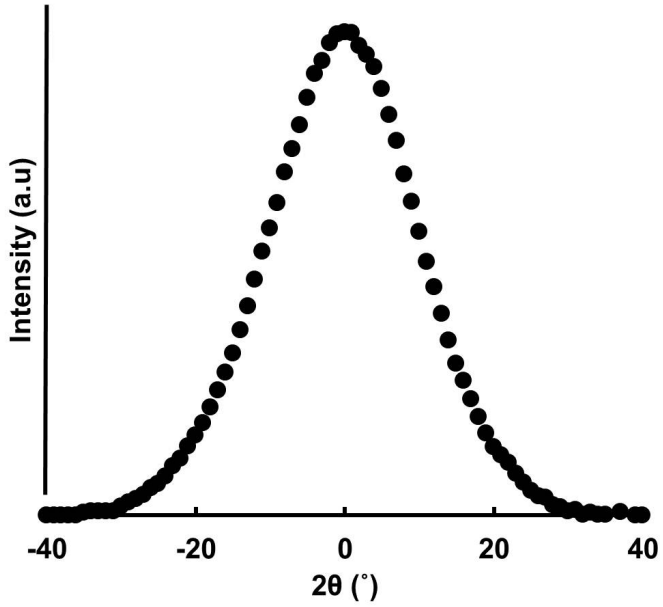

Figure 3.3: Intensity plot of the (200) reflection in the azimuthal direction after image processing of the diffraction pattern (Figure 3.2).

approximated as a Gaussian shape, then the half-width at half maximum height is given by $w = 1.177S$. Combining these approximations yields $w \approx 0.92\mu$. Thus, the half-width at half maximum height is approximately equal to the mean value of the microfibril angle.

3.2 Experimental procedures

3.2.1 Materials

Fibres were purchased and/or harvested from garden centre plants in Rotorua, New Zealand (38.1378 South, 176.2514 East). European flax fibres and slivers (*Linum usitatissimum*) were imported from Tongling Worldbest Linen and Ramie Textile Co. Ltd by Ag Research. The flax fibres were field retted, scutched and hackled into textile grade slivers. No additional information was provided concerning the origins or the processing of the ramie fibres. Jute fabric (*Corchorus*) was purchased from a fabric retailer (Spotlight), sisal (*Agave sisalana*) twine from Donaghys and

loose mesocarp coir fibres (*Cocos nucifera*) from Horticom (using two suppliers and labelled coir 1 and 2). European flax and coir fibre bundles were used as received. Fibre bundles of jute were obtained from the weft and wrap part of a plain weave fabric and sisal fibres were extracted from the twine. In both cases, the fibre bundles were straightened in water to remove the waviness caused by the weave or the twine, dried and equilibrated at room temperature.

Windmill palm fibres (*Trachycarpus fortunei*) were gathered from the sheath of the leaves of a palm tree growing in Rotorua. Nikau fibres (*Rhopalostylis sapida*) were harvested from the stipe of a leaf from a garden in Rotorua and extracted by hand. Raffia fibres (*Raphia textilis*) were obtained as place mats imported from Uganda by Trade Aid in Rotorua. The place mat contained dried leaves which were soaked in water prior to extracting the fibres by hand. Harakeke fibre bundles (*Phormium tenax*) were collected from a garden in Rotorua and were hand-extracted from mature leaves harvested in July 2012. The extraction process yielded fibre bundles up to 1.2 m in length that were transversely sectioned for X-ray diffraction, damping coefficient and toughness characterisation to study the properties variation along the whole length as presented in Figure 3.4. Additional fibres were extracted from the top, middle and bottom of leaves in July 2013 for mechanical test replicates and chemical analysis. Details of the extraction process as well as photographs of the different extracted fibre types are provided in Appendix B.

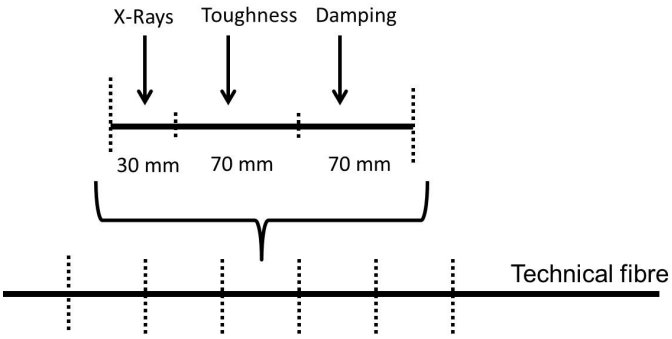

Figure 3.4: Sectioning of a 1200 mm long harakeke fibre bundles for X-ray, toughness and damping experiments to study the variation of properties along the fibre length.

All fibre specimens were weighed using a Mettler AT261 Delta range scale ((Metler Toledo,Switzerland) at five decimal precision to calculate the linear mass in tex after conditioning at least 48 h at 23 °C and 50% relative humidity. The EMC was measured on equivalent fibres that were left for a week to condition at 23 °C 50% RH weighed and then dried to 105 °C until constant weight (1 h) and re-weighed in a glass jar.

3.2.2 MFA determination using X-Ray diffraction

Wide-angle X-ray scattering (WAXS) patterns were collected on the SAXS/WAXS beamline at the Australian Synchrotron (Melbourne, Victoria). The radiation wavelength was 0.8266 Å. Diffraction patterns were collected with a two-dimensional MAR-165 CCD detector (Rayonix LLC, Evanston, IL, USA), located 120.714 mm from the specimen. The beam size was approximately 150 μm in diameter and the detector pixel size was 79 μm $\times$ 79 μm. 15 scans of 1 second exposure at different positions were recorded and the results were averaged on 5 fibres. Data was processed using Australian Synchrotron software Scatterbrain Version 1.235. Raffia, nikau and windmill were not characterised by X-ray diffraction as they were not available at the time of the experiments. Literature values were used when possible to compare them with the other fibres.

3.2.3 Chemical composition

The chemical composition of the fibres was carried out by hydrolysis and anion-exchange liquid chromatography on a Dionex ICS 3000. 2 g of fibres were pre-ground to 40 mesh through a Wiley mill. Ground samples (including routine mature pine for quality control) were extracted with dicholoromethane in a Soxhlet apparatus (Tecator Soxtec System Model HT 1043) using a boiling time of 1 h and a rinsing time of 1 h. The total lignin content was determined in duplicate as the sum of Klason plus acid-soluble lignins following Tappi standard T222 om-88 1988 and Tappi standard UM-250 1991. In the cases of the nikau and windmill palm, the analysis was scaled down to analyse 0.25 g fibre sample due to the limited amount available. Monomeric sugars in the filtrates from Klason lignin determinations were analysed in duplicate by ion chromatography [Pettersen, 1991]. The results were

expressed as anhydrosugar units. Lignin and carbohydrate results were validated when the duplicates were within 2% of each other and sample total sugar and lignin values within the range 90-100%.

3.2.4 Tensile properties

Quasi-static tensile test were performed on a RSA-G2 DMTA instrument (TA instruments) in axial mode using a 35 N load cell. The cross-head speed was 2 μm s^{-1}. The speed of the testing was chosen to prevent abrupt failure caused by clamping artefacts and to compare with published papers [Placet et al., 2014]. The gage length was 10 mm and load-displacement curves were recorded, providing values of tenacity in Newton per tex and strain to failure in percent. A pre-load of 0.1 N was applied to the fibres prior to beginning the test. The elastic modulus values were taken from the initial slope of the load-strain curve from 0 to 0.1% strain. The toughness values were derived from the tenacity-strain curves by numerical integration of the area under the curve. 20 to 30 fibre bundles per type were tested with the exception of the full length harakeke fibre bundles where only one fibre per segment was available (Figure 3.4).

3.2.5 Damping property

Segments of fibre bundle from 70 to 100 mm were tested in frequency sweep tensile mode on a RSA-G2 DMTA instrument (TA instruments). The gage length was 10 mm during the loading of the specimens. Displacement was recorded to with four decimal precision during the test. Consecutive frequency sweeps from 0.1 to 100 Hz were performed at 0.05% strain on each specimen with a pre-load of 0.1 N. The method development is presented in Appendix C. Tan δ and oscillating stresses were measured at 1 Hz and averaged over the 10^{th} and 20^{th} cycles. At low levels of damping, tan δ is considered equal to the damping coefficient (η) (Section 2.2, Equation 2.6). The storage modulus was calculated according to Equation 3.3.

$$E' = \frac{F}{LM\ \epsilon} \tag{3.3}$$

where E' the storage modulus in N/tex, F the oscillating force in N, LM the linear mass in tex and ϵ is the strain amplitude.

3.2.6 Optical microscopy

A stereo microscope Leica MZ12.5 was used to characterise the morphology of the fibre bundles. The fibres were attached to microscope slides and photos were taken with a video camera Leica DC 100 fitted to the microscope. The images were processed using DC 200 digital imaging system.

3.2.7 Principal component analysis

Principal component analysis (PCA) is a statistical procedure used to identify patterns in data. It expresses the data in such a way as to highlight similarity and differences in variables. It uses an orthogonal transformation to convert a set of data of possibly correlated variables into a set of values of linearly uncorrelated variables called principal components. PCA is an efficient tool to assess relationship between variables and reduce the dimensionality of a data set by separating the influencing and non-influencing variables. The PCA was performed on average value of 10 variables using a correlation matrix. The variables were: cellulose, lignin, hemicellulose content, MFA, tenacity, stiffness, strain, toughness, damping and water content at 50% RH. The PCA was interpreted using R version 3.1.0 (R Development Core Team), and R studio version 0.98.945 (RStudio, Inc.).

3.3 Results and discussion

3.3.1 Carbohydrate and lignin composition of the plant fibres

The percentage content of cellulose, hemicellulose and lignin were within the expected range (Chapter 2, Section 2.4.2), with the exception of the cellulose content of jute fibres that was lower than previously reported (Table 3.1). The chemical analysis could not differentiate the pectin content from the other soluble components. Pectin content in plant fibres is generally minor compared to cellulose,

hemicellulose and lignin [Müssig, 2010, p 303-304]. However, there was up to 23.3% of "other" components (waxes, minerals, pectin) in the fibres which was higher than expected and potentially due to losses during the extraction (Table 3.1).

Table 3.1: Chemical composition of plant fibres (wt. %)

	Cellulose	Hemicellulose	Lignin (Klason)	Others
Pinus radiata	44.1	19.81	27.6	7.9
European flax	72.6	8.7	3.2	14.7
Ramie	96.0	0.5	0.36	3.1
Jute	46.2	12.5	15.4	23.3
Raffia	46.4	20.4	11.5	15.8
Harakeke	49.2	21.2	6.8	18.7
Sisal	45.3	20.4	15.1	15.5
Nikau	46.4	20.4	17.7	18.7
Windmill	36.2	17.8	35.6	18.6
Coir 1	32.9	25.2	35.0	5.5
Coir 2	34.1	20.9	33.6	9.6

Differences in the cellulose to lignin ratio were observed for the harakeke fibres sampled at three different locations in the leaf (Table 3.2). The fibres extracted at bottom of the leaf were richer in lignin than the top part of the leaf. Richter et al. studied the entire harakeke leaf using raman imaging and reported that higher lignin content was present in the fibres at the very bottom of the leaf than at the top. It was assumed that the purpose of the lignin was to provide extra stiffness at the base of the plant to support the whole leaf [Richter et al., 2011].

The hemicellulose types were differentiated by their chemical structure and potential mobility, and interactions with lignin and cellulose [Koshijima, 2003, Newman, 2005]. Xylan was associated with fibres containing high level of lignin, while mannan was associated with fibre containing higher levels of cellulose which was consistent with literature (Table 3.3) [Akerholm, 2001]. Table 3.4 presents the carbohydrate composition of the harakeke fibre as a function of the location

Table 3.2: Chemical composition of harakeke fibres sampled from different locations within the leaf (wt. %).

	Cellulose	Hemicellulose	Lignin (Klason)	Others
Top	59.0	22.0	5.1	10.0
Middle	57.5	22.4	5.7	10.1
Bottom	55.6	22.6	7.6	9.53

in the leaf. In contrast to the lignin content, the sugar composition did not vary with the exception of the mannan content. As discussed, mannan was associated with cellulose, and a decrease in the cellulose content also likely correlated with a decrease in mannan [Akerholm, 2001]. No correlation was observed between the variation of lignin and xylan content.

Table 3.3: Hemicellulose composition of various plant fibres (wt. %).

	Arabinan	Galactan	Xylan	Mannan
Pinus radiata	1.37	2.87	4.71	10.86
European Flax	0.12	3.85	0.57	4.15
Ramie	< 0.01	0.50	< 0.01	< 0.01
Jute	0.02	0.32	11.88	0.32
Raffia	1.78	0.55	20.10	0.57
Harakeke	0.42	0.56	20.55	0.86
Sisal	0.19	0.48	19.70	< 0.01
Nikau	0.70	0.29	19.37	< 0.01
Windmill	0.77	0.30	16.78	< 0.01
Coir 1	0.64	0.19	24.37	< 0.01
Coir 2	0.69	0.22	19.97	< 0.01

Table 3.4: Hemicellulose composition of harakeke fibres from different locations within the leaf (wt. %).

	Arabinan	Galactan	Xylan	Mannan
Top	0.46	0.55	20.70	0.86
Middle	0.42	0.56	20.55	0.86
Bottom	0.46	0.61	20.39	0.55

3.3.2 Morphological aspect of fibre bundles

The single fibre cells of the the European flax, jute, harakeke and sisal fibre bundles were visualised by optical microscopy in reflected light (Figures 3.5). Bright streaks were observed in the European flax, ramie and sisal fibres that indicated of the presence of kink bands. A hypothesis was built around the role of kink bands on the damping properties of the plant fibres although no correlation was made between the presence of theses defects and the damping response of the fibres (Appendix F). Most of the fibres exhibited rough surfaces that corresponded to the residual plant tissue following the extraction of the fibres with the exception of windmill palm fibres that did not require extraction but still exhibited rough surface (Figure 3.5 (g)). The windmill palm fibres originate from the stipe of the leaf and were separated from each other when the surrounding tissue disintegrated as the fibre bundles matured and lignified around the trunk of the palm tree (Appendix B, Figure B.5 (a)) [Zhai et al., 2013]. The coir fibres presented a smooth surface, requiring no extraction procedure. In general, the fibre bundles of bast plants had the smallest diameter, as illustrated by comparing European flax and ramie to the other fibre bundles (Figure 3.5).

3.3.3 MFA variation in various plant fibres and within a harakeke fibre bundle

The MFA determined by X-ray diffraction were consistent with literature with the exception of the ramie fibres which was lower that previously reported (Table 3.5) [Müssig, 2010, p 30-31]. There was a variation in the MFA depending on the fibre

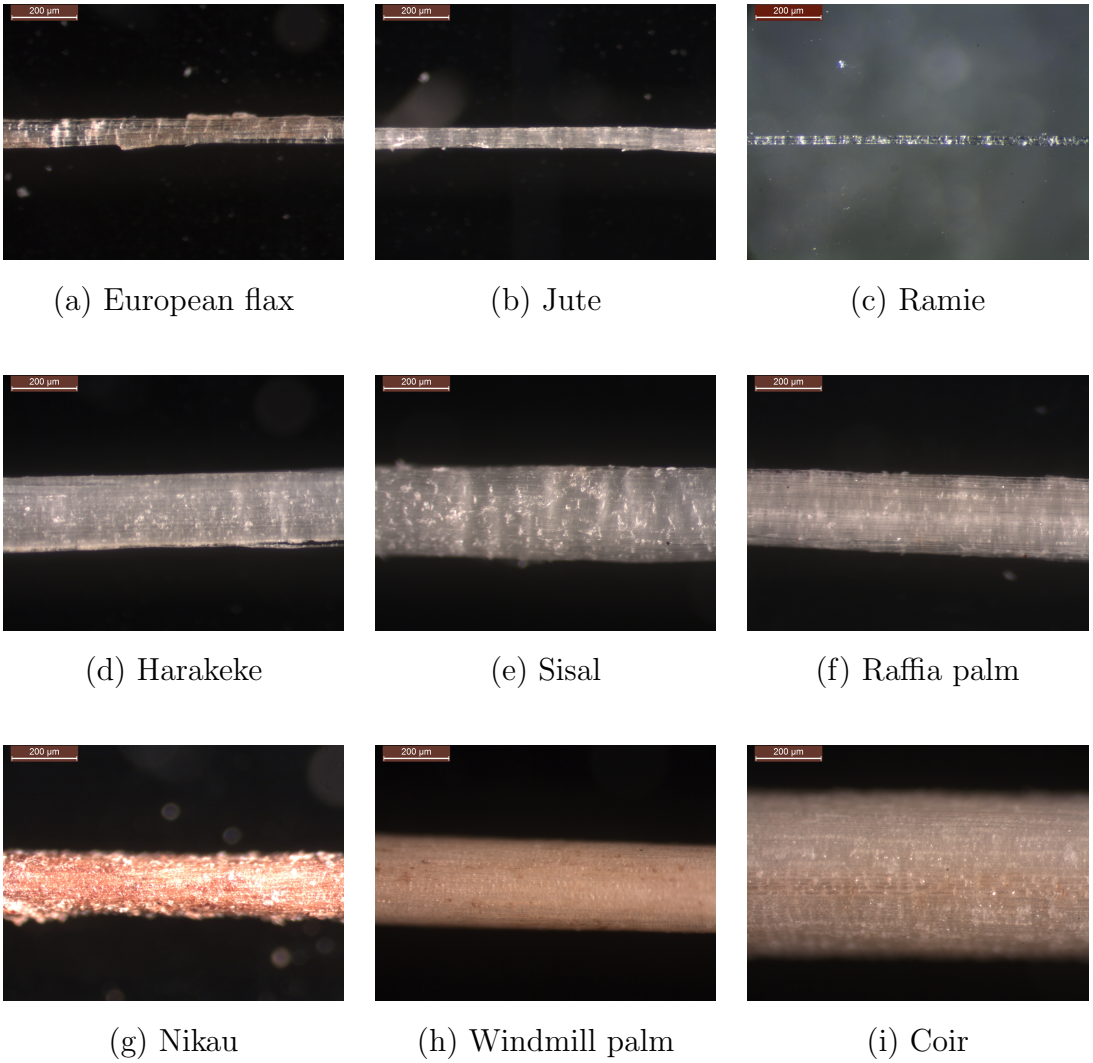

(a) European flax (b) Jute (c) Ramie

(d) Harakeke (e) Sisal (f) Raffia palm

(g) Nikau (h) Windmill palm (i) Coir

Figure 3.5: Reflected light micrographs of the selected plant fibres, magnification ×10)

.

types: 4-10° for bast fibres, 10-20° for leaf fibres, and >20° for mesocarp fibres. The MFA values of 39.5° for windmill fibres was used from literature while the MFA of nikau and raffia could not be found and therefore were not present in the graphical representations plotted as a function of MFAs [Zhai et al., 2013].

The MFA was found to vary from 10.7° to 16.7° linearly from the bottom to the top of a whole harakeke technical fibre measuring 1200 mm in length (Figure 3.6). The higher in the plant, the higher the MFA. Similarly, Richter calculated that the MFA of harakeke schlerenchyma fibres varied from 4° to 16° from the bottom to the top part of the leaf using a model based on Raman spectroscopy experiments. He proposed a correlation with the lignin content and the MFA, showing a high level of lignin was present at the base of the leaf in connection with a low MFA (Table 3.2) [Richter et al., 2011].

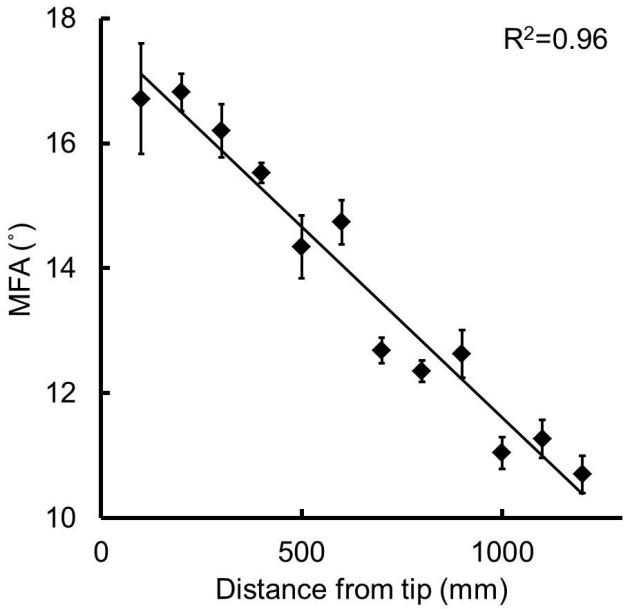

Figure 3.6: MFA variation in a 1200 mm long harakeke technical fibre. The black line represents a linear fit.

Table 3.5: MFA of the selected plant fibres. The value in brackets represents 1 standard deviation.

	Type	Litt MFA (°)	Expt MFA (°)	References
European flax	Bast	4.4	4.5 (0.1)	[Müller et al., 1998]
Ramie	Bast	7.5-8	4.2 (0.1)	[Bledzki and Gassan, 1999]
Jute	Bast	8	6.6 (0.1)	[Bledzki and Gassan, 1999]
Raffia	Leaf	NA	NA	
Harakeke	Leaf	16	11.4 (0.3)	[Richter et al., 2011]
Sisal	Leaf	20	15.2 (0.2)	[Pavithran et al., 1987] [Munawar et al., 2007]
Nikau	Leaf/stipe	NA	NA	
Windmill palm	Leaf/stipe	37.8	NA	[Zhai et al., 2013]
Coir 1	Mesocarp	45	46.8 (0.8)	[Martinschitz et al., 2008]
Coir 2	Mesocarp	45	NA	[Martinschitz et al., 2008]

3.3.4 Tensile properties of plant fibres

The elastic moduli was in the same order of magnitude for the European flax, ramie, Jute and raffia fibres (Table 3.6). European flax fibres displayed the highest ultimate stress and coir fibres the highest strain and toughness which is consistent with published literature [Müssig, 2010, p 301]. In terms of intermediate properties, harakeke fibres exhibited the highest combined performances in ultimate stress, strain and elastic modulus.

The tensile properties of harakeke fibres extracted from the tip and mid sections of the leaf were similar however, as trends, the fibres extracted from the lower part were stiffer but not as strong or tough as the fibres from the other sections (Table 3.7). These findings were supported by observations from Richter et al. on the high lignin content present at the bottom part of harakeke leaves [Richter et al., 2011]. When considering the function of the fibres within the leaf, the bottom part of the plant requires greater stiffness than the top to support the rest of the leaves.

The stress-strain behaviour of plant fibres was divided into 3 categories. Quasi-linear behaviour was typical of fibres with a MFA less than 10° (Figure 3.7). Bi-phasic behaviour without a distinctive yield point occurred for fibres where the MFA lay between 10° to 20° (Figure 3.8). Bi-phasic behaviour with a distinctive yield point and large plastic deformation occurred for MFA above 20° (Figure 3.9).

The European flax fibres exhibited a non-linear stress-strain behaviour between 0 to 0.5% of strain (Figure 3.7). Non-linear behaviour at low strain was observed before in single hemp fibres by Placet et al. who attributed it to the re-orientation of the amorphous cellulose and shear strain-induced crystallisation [Placet et al., 2014]. Due to the fact that none of the other fibres displayed this behaviour, the origin of the deviation from linear behaviour remained uncertain.

The difference between the stress-strain profile of the fibres was partially attributed to the straightening of the cellulose microfibrils leading to a decrease of the MFA as observed *in-situ* by combining mechanical and chemical characterisation methods (X-ray diffraction, Raman, and FTIR) [Köhler and Spatz, 2002, Keckes et al., 2003, Martinschitz et al., 2008, Gierlinger et al., 2006].

During tensile testing, the force resultant on the cellulose microfibrils is depen-

Table 3.6: Tensile properties for each fibre type. The value in brackets is the 95% confidence interval.

	Ultimate stress (N/tex)	Ultimate strain (%)	E-modulus (N/tex)	Toughness (N/tex)
European flax	0.52	1.89	20.8	0.0051
	(0.08)	(0.21)	(3.7)	(0.0014)
Ramie	0.31	1.84	26.8	0.0057
	(0.07)	(0.16)	(4.4)	(0.0008)
Jute	0.39	1.53	24.6	0.0032
	(0.09)	(0.21)	(5.6)	(0.0009)
Raffia	0.36	1.87	20.8	0.0036
	(0.04)	(0.12)	(1.9)	(0.0005)
Harakeke	0.48	2.77	17.2	0.0095
	(0.07)	(0.31)	(2.5)	(0.0024)
Sisal	0.40	2.65	18.7	0.0058
	(0.05)	0.30	(3.0)	(0.0012)
Nikau	0.23	7.04	9.3	0.0102
	(0.02)	(1.00)	(0.69)	(0.0017)
Windmill palm	0.12	17.94	4.0	0.0154
	(0.01)	(2.71)	(0.2)	(0.0029)
Coir 1	0.12	24.44	3.8	0.0210
	(0.02)	(4.21)	(0.6)	(0.0051)
Coir 2	0.14	38.50	3.1	0.0365
	(0.02)	(5.48)	(0.3)	(0.0069)

Table 3.7: Tensile properties of the harakeke fibres extracted from the tip, middle, and bottom of the leaves. The value in brackets is the 95% confidence interval.

	Ultimate stress (N/tex)	Ultimate strain (%)	E-modulus (N/tex)	Toughness N/tex)
Top	0.49	3.66	17.0	0.0099
	(0.06)	(0.24)	(2.7)	(0.0014)
Middle	0.48	3.47	17.2	0.0095
	(0.10)	(0.38)	(2.5)	(0.0024)
Bottom	0.37	3.02	18.7	0.0071
	(0.10)	(0.32)	(2.0)	(0.0015)

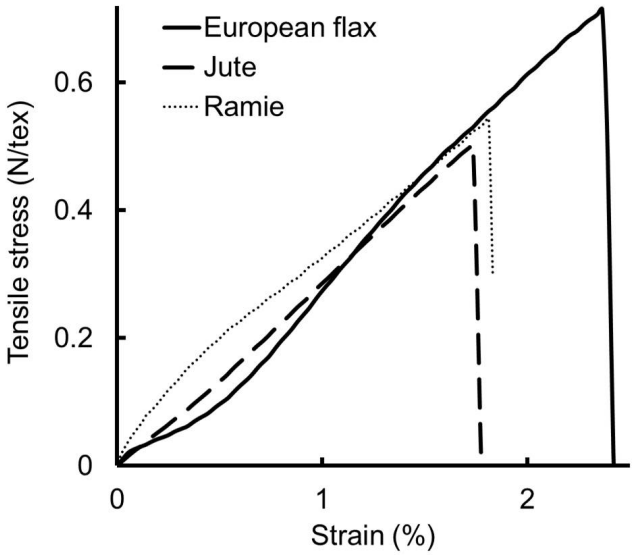

Figure 3.7: Typical stress-strain curves for fibres with a MFA less than 10°.

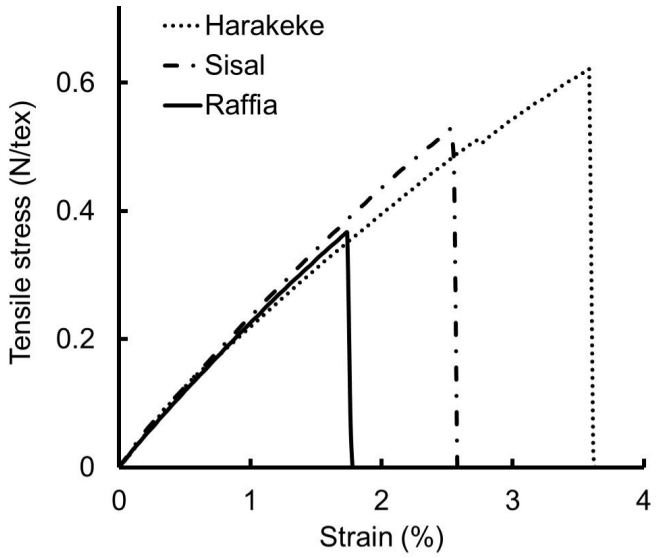

Figure 3.8: Typical stress-strain curves for fibres with MFA between 10° to 20°.

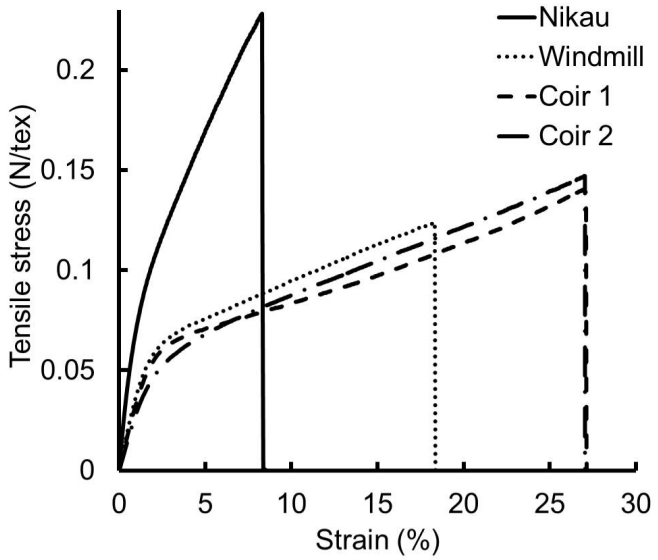

Figure 3.9: Typical stress-strain curves for fibres with MFA above 20°.

dent on the cosine of the MFA (μ_0). The larger μ_0, the less the cellulose microfibrils contribute to the stiffness at the beginning of the test explaining the low stiffness of mesocarp fibres compared to bast fibres (Table 3.6).

In the case of bast fibres, the microfibrils realignment was minimal due to their initial low MFA [Kölln et al., 2005]. Hence, the stress-strain deformation was quasi-linear (Figure 3.10 (a)). In the case of leaf fibres, μ_0 was between 10° to 20°. The microfibrils reoriented during the test, causing enough shear stresses in the hemicellulose/lignin matrix to provoke a gradual transition from elastic to plastic deformation (Figure 3.10 (b)). When μ_0 was greater than 20° (Figure 3.10 (c)), the beginning of the stress-strain curve was matrix dominated as the hemicellulose/lignin carried the initial load. Past the yield point, the load gradually transferred to the cellulose microfibrils exhibiting a second linear behaviour. Martinschitz et al. measured the MFA of coir fibre *in-situ* during tensile testing up to failure. Coir fibres were found to exhibit a bi-linear deformation while the MFA decreased linearly with strain [Martinschitz et al., 2008]. The yield point was the point where the shear stresses due to the microfibrils realignment caused plastic flow of the hemicellulose/lignin matrix.

In terms of fracture, coir and windmill fibres failed abruptly after a long plastic deformation. Coir fibre had a smooth fracture surface after tensile testing where all the cells broke in the same plane. In contrast, harakeke, sisal or European flax fibres failed independently and consecutively causing them to slide past each others, resulting in extensive defibrillation (Figure 3.11).

3.3.5 Damping coefficient of plant fibres

The damping coefficient ($\tan \delta$) of the plant fibres was measured between 0.0125 to 0.0198 (Table 3.8). Berthelot et al. measured by acoustics damping coefficients of 0.012 for glass fibres, 0.0062 for carbon fibres and 0.0165 for aramid fibres. Berthelot's results showed that the plant fibres have a significant advantage in damping applications compared to glass and carbon fibres [Berthelot and Sefrani, 2007]. Basu reported a damping coefficient of ∼0.05 at 0.5% strain for cotton fibres using DMTA [Basu, 2012]. Differences in the damping coefficient between the fibre types were observed however no obvious trend emerged with MFA, chemical

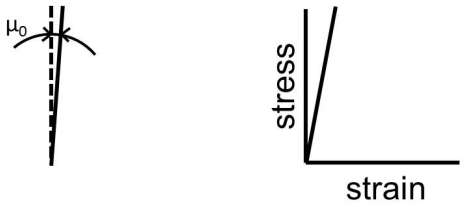

(a) μ_0 below 5°

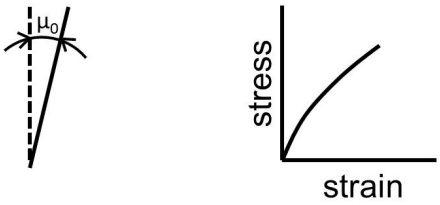

(b) μ_0 between 5° to 20°

(c) μ_0 above 20°

Figure 3.10: Difference of stress-strain behaviour caused by the realignment of μ_0 for (a) low, (b) intermediate, and (c) high.

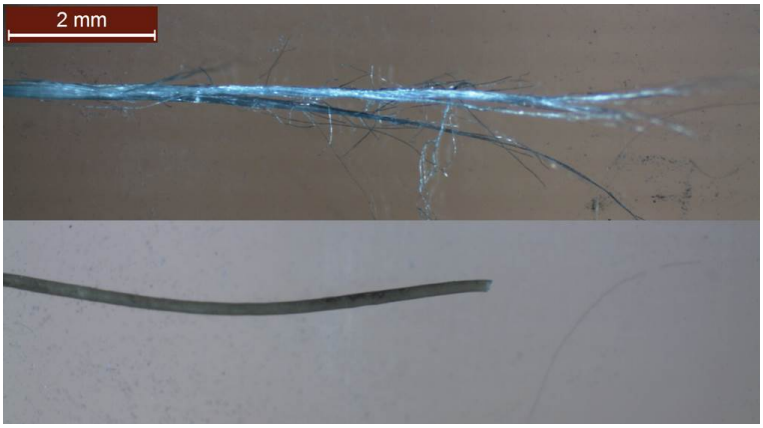

Figure 3.11: Transmitted light micrographs of fractured fibres after tensile test (top) harakeke and (bottom) coir.

composition or type of hemicellulose.

As mentioned previously the damping coefficient could be influenced by several variables (chemical composition, MFA). These variables were correlated to each other with a multivariate analysis presented in the next section.

3.3.6 Determination of the correlation between variables using PCA

The calculation of the Pearson correlation coefficients between all variables suggested that the chemical components had high degree of correlation with the mechanical properties (e.g. toughness and strain or cellulose and lignin) (Appendix D, Figure D.1). Principal components analysis was limited to the first two components as they accounted for 89% of the variance (Table D.2 and Figure D.2).

A bi-plot of the data in the space of the first two principal components was produced with the fibres (scores) and the variables (loadings) (Figure 3.12).

All variables were important for describing the variation as none were located close to (0;0). Also some variables were clustered together and were considered similar. The analysis could therefore be separated into 3 groups:

- Group 1: MFA, lignin, strain and toughness.

Table 3.8: Damping coefficient and moisture content. The value in brackets is the 95% confidence interval.

	Damping coefficient	Moisture content (%)
European flax	0.0140 (0.0018)	10.6
Ramie	0.0142 (0.0020)	10.2
Jute	0.0128 (0.0010)	9.4
Raffia	0.0125 (0.0022)	10.1
Harakeke	0.0176 (0.0027)	10.2
Sisal	0.0198 (0.0023)	9.5
Nikau	0.0144 (0.0008)	11.0
Windmill palm	0.0194 (0.0018)	10.2
Coir 1	0.0180 (0.0012)	9.6
Coir 2	0.0165 (0.0026)	8.1

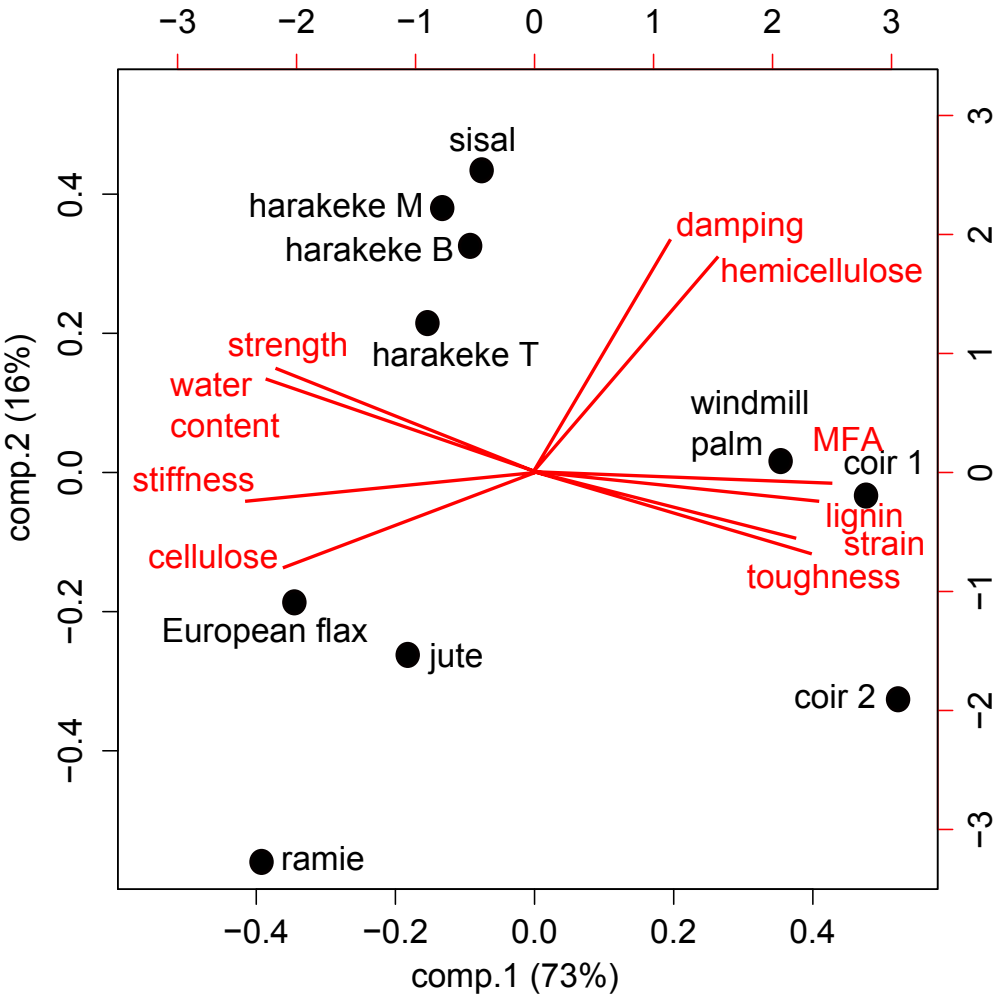

Figure 3.12: Bi-plot of the variables (loading and scores) using principal component 1 and 2.

- Group 2: hemicellulose and damping.

- Group 3: cellulose, stiffness, water content and tenacity.

Group 1 and 3 were oppositely related. This observation indicated that when the variables from group 1 (MFA, lignin, strain, toughness) were high, the variables from Group 3 were low. The variables from Group 2 (damping and hemicellulose) were different from Group 1 and 3.

High tenacity was correlated with cellulose content and low lignin content. This behaviour was analogous with conventional composite theory based on strengthening a polymer matrix with high strength reinforcing fibres.

Salmen examined the modulus of the various components of wood fibre in dry conditions and wet condition. The modulus of cellulose and lignin did not change with moisture content while hemicellulose decreased from 2000 to 20 MPa, leading to an overall decrease in the mechanical properties of the wood fibres [Salmen, 2004]. However, in this study, water content was not associated with damping which indicated that the source of damping was not directly linked to the motion of the water molecules but the plasticising of the hemicellulose.

Jarvis hypothesised that the cellulose chains at the surface of a microfibril are loosely packed compared to the cellulose within the crystal, enabling more hydrogen bonding between the cellulose and the hemicellulose or water. It was believed that a small amount of hemicellulose was present between the cellulose microfibrils enabling access for a limited amount of water [Jarvis, 2005]. His observations were aligned with the correlation between water and cellulose content.

In terms of energy absorption variables, high toughness was strongly related to high MFA (Group 1) and high damping strongly related to hemicellulose (Group 2). The following sections investigated in more detail the relationship between toughness and MFA, and damping coefficient with hemicellulose. No correlation was found between the linear density (tex) and damping coefficient (results not shown here).

3.3.7 Toughness as a function of the MFA: bilinear approximation

The stress-strain curves of plant fibres can exhibit quasi-linear deformation (e.g. flax, ramie) or a plastic deformation with a more or less distinct yield point (e.g. coir) depending on their MFA (μ) [Kulkarni et al., 1981, Baley, 2002, Munawar et al., 2007]. In this work, the stress-strain curves of the fibres were approximated to a bi-linear behaviour (Figure 3.13) where the change in MFA below the yield point was considered insignificant compared to that in the plastic range. This allowed a relationship between toughness and variation in MFA to be established across a wide strain range.

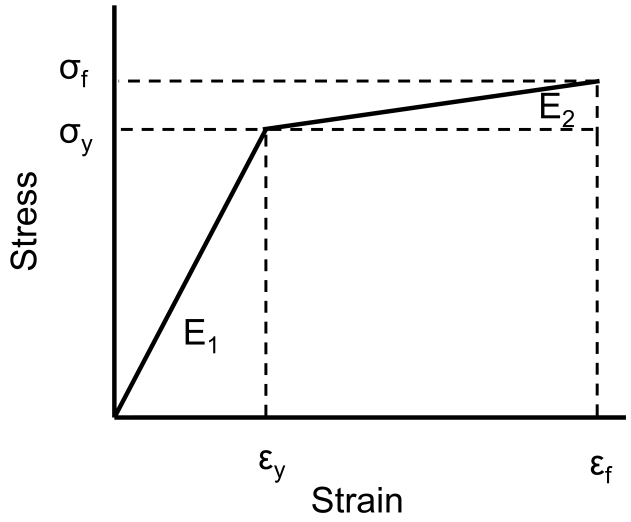

F

Figure 3.13: Bilinear representation of the stress-strain behaviour of a plant fibre. E_1 and E_2 are the moduli before and after the yield point respectively, σ_y, ϵ_y and σ_f, ϵ_f are the stress and strain at yield and failure point.

The maximum stress can be determined by using Equations 3.4:

$$\sigma(\epsilon) = \begin{cases} \sigma = E\epsilon & \text{if } \sigma < \sigma_y \\ \sigma_y = E\epsilon_y & \text{if } \sigma = \sigma_y \\ \sigma = \sigma_y + E_2(\epsilon - \sigma_y/E_1) & \text{if } \sigma > \sigma_y \end{cases} \tag{3.4}$$

where E_1 is the elastic modulus of the fibre, E_2 is the modulus of the fibre in the plastic region, σ_y and ϵ_y are the stress and strain at the yield point.

The toughness (W) of a plant fibre can be then approximated by:

$$W = \frac{1}{2}E\epsilon_y^2 + E\epsilon_y(\epsilon_f - \epsilon_y) + \frac{1}{2}E_T(\epsilon_f - \epsilon_y)^2 \tag{3.5}$$

According to Keckes, during a tensile test, the change in MFA (μ) is connected to strain by Equation 3.6 [Keckes et al., 2003]:

$$\mu(\epsilon) = \mu_0 - cot\mu_0\epsilon \tag{3.6}$$

where μ_0 is the initial microfibril angle.

In a theoretical case as μ approaches 0, Equation 3.6 becomes:

$$\epsilon_f \equiv \frac{\mu_0}{cot\mu_0} \tag{3.7}$$

Substituting Equation 3.7 into Equation 3.5, the toughness of a plant fibre can be approximated by a second degree polynomial equation depending on μ_0:

$$W = \epsilon_y^2\left(\frac{E_1}{2} + \frac{E_2}{2} - E_1\right) + \epsilon_y\left(E_1 + E_2\right)\frac{\mu_0}{cot\mu_0} + \frac{E_2}{2}\left(\frac{\mu_0}{cot\mu_0}\right)^2 \tag{3.8}$$

The toughness was expected to vary as a second order polynomial function of $\mu_0/cot\mu_0$. In Figure 3.14, the toughness was plotted as a function of $\mu_0/cot\mu_0$.

The experimental points could be described by a quadratic fit (R^2=0.88) which was consistent with the bilinear model. Yet, in contrast to observations in wood, there was no optimum MFA in terms of toughness within the investigated range [Reiterer et al., 2001].

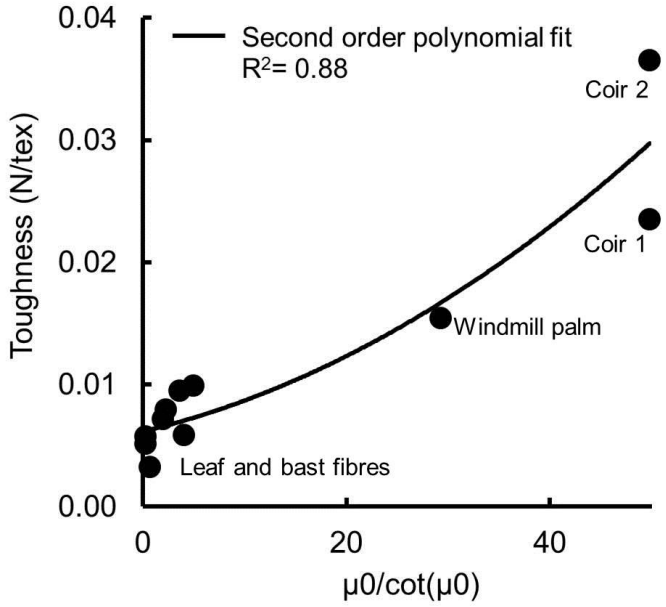

Figure 3.14: Toughness plotted as a function of $\mu_0/cot(\mu_0)$ for the fibres presented in Tables 3.6 and 3.7). The black continuous line represents a second order polynomial fit, $R^2 = 0.88$.

Reiterer et al. proposed that the reason for the higher energy absorption of wood at at higher MFA was due to the predominance of inelastic deformations compared to elastic deformations in tensile testing [Reiterer et al., 2001]. This observation was also applicable to the present fibres. The difference between the elastic and inelastic contribution to toughness was calculated by the integral of the stress-strain curve before and after the yield point (Figure 3.13). As such, European flax deformation was considered elastic, and despite having a tenacity 4 times higher than coir fibres, its toughness was up to 7 times lower. In the case of harakeke fibres, even though the yield point was not as distinct as for coir fibres, harakeke fibre stress-strain curves deviated from linear deformation and had a significant inelastic contribution making them suited for energy absorption

applications while retaining a high strength and stiffness.

The mechanisms behind the inelastic deformations have been discussed by others [Köhler and Spatz, 2002, Baley, 2002, Gierlinger et al., 2006]. It was generally thought that the fibres underwent a series of deformations starting with the realignment of macroscopic defects within the fibres and deformation of the amorphous region of the cellulose microfibrils [Thygesen et al., 2007, Basu, 2012, Placet et al., 2012]. This was followed by the elastic deformation of the hemicellulose/lignin matrix until its shear strength was exceeded which corresponded to the yield point [Burgert and Dunlop, 2011]. Beyond the yield point, the plastic deformation was caused by the realignment of the cellulose microfibrils up to a point where, due to the helical structure of the microfibrils, the realignment was impeded by lateral compression of the cell preventing further reorientation [Köhler and Spatz, 2002]. At this stage, the cells can only then slip past each other up to the point where intercellular failure occurs.

In terms of molecular mechanisms, Gierlinger et al. found that cellulose and lignin deform simultaneously up to 0.5% in strain in a single fibre of spruce wood according to Raman spectroscopy. Beyond a strain of 0.5%, only the C-O-C signal of the cellulose changed, indicating stretching of the cellulose back bone prior to fibre failure [Gierlinger et al., 2006]. Earlier, Hinterstoisser et al., reported that at the molecular level the strain is distributed via the glucose ring, C-O-C ether linkage, and O(3)H $\cdots$ O(5) intramolecular hydrogen bond according to dynamic FT-IR spectroscopy [Hinterstoisser et al., 2003].

3.3.8 Influence of the hemicellulose content on the damping coefficient of plant fibres

The damping coefficient was strongly correlated to the hemicellulose content (Figure 3.12) which was consistent with literature [Entwistle, 2005, Keryvin et al., 2015]. Entwistle suggested that the energy losses are explained by the hemicellulose molecular bonding structure and hydrogen bonding with other chemical components. Recently, the viscous behaviour of the flax fibres was correlated with to the amorphous component content (e.g. pectin, hemicellulose) [Keryvin et al., 2015].

When plotting the damping coefficient as a function of hemicellulose content, an upward trend can be observed even though the scatter was large with a $R^2 = 0.21$ (Figure 3.15). No correlation between the damping coefficient and cellulose or lignin content could be found (Appendix D, Figure D.1). This finding was reinforced by the study of harakeke fibres. In the different sections of the harakeke fibres, the hemicellulose content was similar while the cellulose and lignin contents changed (Table 3.2). However, no significant difference in the damping coefficient was observed. Therefore, it was assumed that the compositional variation of lignin and cellulose within these levels did not influence the damping coefficient.

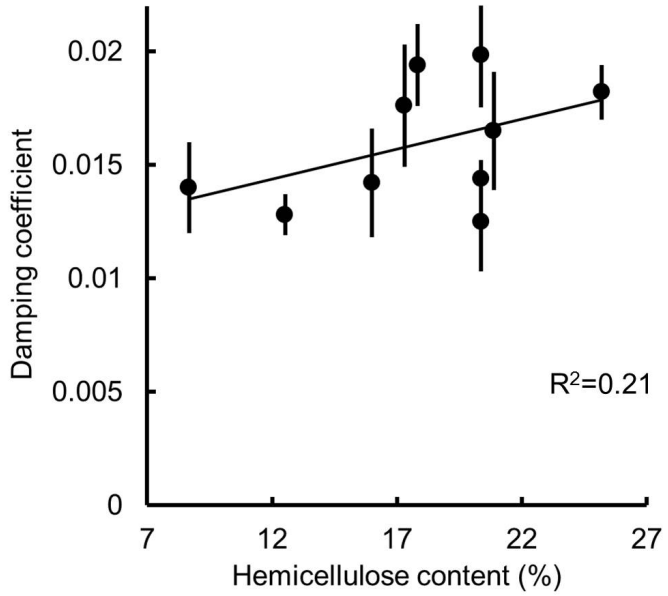

Figure 3.15: Damping coefficient as a function of chemical composition hemicellulose content. The error bars represent the 95% CI.

The vibrational energy loss was reported to increase almost linearly with the hydration of hemicellulose [Entwistle, 2005]. Segerman reported that the damping coefficient typically decreased by 3.5% for each 1% decrease in the moisture content [Segerman, 2001]. The hydration of the hemicellulose was reported to cause swelling in the cell wall, and variation in MFA and lattice of the cellulose crystal structure [Baley, 2002, Placet et al., 2012, Zabler et al., 2010]. The penetration of

water into the cell wall of flax fibre lead to an increase in the cellulose misalignment relative to the axis of the fibre cell, leading to an increase in the spacing between the cellulose microfibrils [Astley and Donald, 2001, Jarvis, 2005, Placet et al., 2012].

The energy dissipation is enhanced by increased molecular motion [Ebrahimzadeh and Bertilsson, 1998, Newman, 2005, Bremaud et al., 2010]. It is thought to occur by (1) motion of water molecules and (2) hydrogen bonding shifts between hydrated hemicellulose and cellulose. The first mechanism relies on the water molecules capacity to move freely due to their small size hence dissipating energy as it was observed in immersion situation (Appendix E). The second mechanism depends on water content and the chemical composition of the hemicellulose [Entwistle, 2005]. The hemicellulose molecules do not have the same mobility due to their size, molecular structure and different conformations. Newman suggested that galactans are more mobile than glucomannan in a hydrated state by comparing the T_{1C} and T_{2C} relaxation parameters using solid state ^{13}C NMR in *Pinus radiata* [Newman, 2005]. However, in the present study, no correlation could be observed between the hemicellulose type and the damping coefficient.

3.4 Conclusions

In Chapter 3, selected plant fibres were characterised for their mechanical properties (strength, stiffness, strain, toughness and damping), physical property (morphology and MFA) and chemical composition (hemicellulose, cellulose and lignin content). Correlations between variables were studied using PCA.

The highest mechanical properties in terms of stiffness and strength were observed for bast fibres, while leaf and mesocarp fibres exhibited the highest toughness. The stress-strain curve exhibited a distinct yield point for fibres with MFA greater than 20°, indicating the onset of irreversible deformation of the hemicellulose and lignin matrix. In the case of fibres with MFA below 20°, no yield point was defined and the transition between elastic and plastic deformation was progressive.

The difference between the mechanical properties in plant fibre could be explained by considering the function the fibres in the plant (e.g. stiffening, protecting, conducting water). Fibres from the stem are arranged in a circular fashion

providing very high bending stiffness that enables the plants to grow higher. Fibres from the leaf are aligned with the base of the leaf, participating in the transport of the photosynthesis products and water through the plant. These fibres present a compromise in flexibility and strength. In mesocarp fibres such as coir or leaf/stipe fibres such as windmill palm, the fibres are tissues protecting the seed or trunk against microbial attacks and impact.

In terms of energy absorption properties, the toughness of the technical fibres increased with MFA and was correlated with fibres containing high level of lignin and low levels of cellulose. It was also shown that toughness and MFA followed second order polynomial function in the MFA range of 5° to 46°. The damping coefficient was only related to the hemicellulose content but not to the type of hemicellulose. No correlation could be found between the damping coefficient and the variation of MFA unlike what was found by others for wood [Bremaud, 2012].

Due to their hydrogen bonding components, plant fibres are sensitive to moisture content. Previous studies have observed the effect caused by moisture on the mechanical and damping properties of cellulosic fibres such as wood and hemp [Ebrahimzadeh and Bertilsson, 1998, Entwistle, 2005, Placet et al., 2012]. The moisture content was influenced by the chemical composition of the plant fibres. Fibres containing high levels of hydrophilic compounds and low levels of lignin would be preferable for vibration damping applications if used in a hydrated state, and the decrease of stiffness was acceptable. If water was identified as an ideal solvent to naturally penetrate the cell wall and increase the damping coefficient of the fibres, clearly its volatility would be impractical in real composite applications and products. Chapter 4 aimed to investigate potential additives without issues of volatility in order to alter the damping behaviour of harakeke fibres. Harakeke fibres presented intermediate chemical properties, MFA and the highest combination of mechanical properties that made them appropriate candidate for composite reinforcement.

Chapter 4

Influence of hydrogen bonding compounds on the damping coefficient of harakeke fibres

4.1 Introduction

It was shown in the previous chapter that the MFA and chemical composition influence the strength, stiffness and toughness of plant fibres, but only the hemicelullose content influenced the damping coefficient.

Studies have shown that the damping property of wood was influenced by water due to by the interaction between water molecules and the hydroxyl groups (-OH) present in the fibres, particularly within the hemicellulose [Ebrahimzadeh and Bertilsson, 1998, Entwistle, 2005]. Yet, the presence of water in plant fibres meant for composite reinforcement is a drawback that hinders the manufacture of composites, particularly when the process involves temperatures higher than 100 °C [Celino et al., 2014, Thuault et al., 2014]. In Chapter 4, hydrogen bonding capable compounds of low molecular mass were investigated. The aim was to test compounds that potentially had a similar plasticising effect to water but without its volatility at processing temperature between 110 to 150 °C .

Dimension stability of cellulosic fibres is particularly important in the field of wood preservation [Hill, 2006]. Past research showed that various hydrogen bond-

ing capable compounds (e.g. propane-1,2,3-triol known as glycerol, polyethylene glycol) are able to impregnate the cell wall of wood fibres and prevent wood from swelling or shrinking with changes in moisture [Hill, 2006, Wallstrom, 1998]. Typically, wood is saturated with such bulking compounds in solution and dried at 100 °C to remove water. The bulking compounds become locked in the cell wall of the wood fibres due to their hydrogen bonding affinity and high boiling point (e.g. 290 °C for glycerol) [Thuvander et al., 2001, Hill, 2006]. A Swedish study showed that glycerol exchanged with water in the cell wall of wood fibres. Glycerol improved the strength, strain and work to failure of wood by decreasing irreversible drying stresses [Thuvander et al., 2001]. Moreover, the larger the bulking compound molecules, the less volatile they are and the more likely they will remain in the fibres. However, a compromise in size of the molecules is required to enable sufficient penetration into the cell walls. Bains found that PEG polymers with a degree of polymerisation $\geq$ 1000 units could only penetrate the cell wall if it was first swollen by a solvent such as ethanol [Bains, 1986].

Song et al. used ethylene glycol to simulate water as a hydrogen bonding medium for DMTA analysis of wood in the temperature range of 20 to 140 °C. They examined the variation of T_g in different types of wood and maturity stages. Extractive biopolymers from heartwood were found to prevent ethylene glycol from being absorbed by the cell wall, resulting in a higher T_g compared with the sapwood in which the ethylene glycol penetrated with greater ease [Song et al., 2014]. Mild chemical treatments can therefore be used to swell the cell wall of the fibres and remove a portion of the extractive compounds, hence, improve plasticiser impregnation [Li et al., 2007, Kabir et al., 2012].

The present work aimed to replace the plasticising effect of water (Chapter 3) with a polyol (e.g. glycerol or its oligomers). At low level of concentrations, the polyols were expected to contribute to energy dissipation via the Velcro® effect that is caused by the repetitive making and breaking hydrogen bonds [Kretschmann, 2003, Keckes et al., 2003]. Mild chemical pre-treatments were used to remove dust and residual extractives, and enhance the diffusion of the plasticiser into the fibre. The fibre was then soaked in a dilute solution of plasticiser and subsequently dried to remove water and lock the polyols into the cell wall. Plasticisers were selected for their low volatility, toxicity and cost. Pre-

treatment and polyol impregnation combinations were studied by their influence on the damping coefficient (tan δ) and stiffness (E') of the fibres. Liquid state NMR was used to investigate the potential variation of PG3 mobility when impregnated in harakeke fibres. Solid state NMR was used to examine changes in the molecular mobility of cellulose and hemicellulose caused by PG3. The experiments were restricted to harakeke fibres as they presented the highest combination of mechanical properties, hence great potential for composite reinforcement (Chapter 3).

4.2 Solid state nuclear magnetic resonance (NMR) relaxation

NMR spectroscopy is based on a physical phenomenon in which the nuclei of certain atoms, when exposed to a magnetic field, absorb and re-emit electromagnetic radiation. This energy occurs at a specific resonance frequency which depends on the magnetic field and magnetic properties of the atoms.

The time required for the nuclei to return to equilibrium after excitation is called the relaxation time. Two principal relaxation processes are:

- T_1 or spin-lattice or longitudinal relaxation : T_1 is a time characteristic of the nuclei related to the dissipation of the magnetic energy imposed by the spectrometer. It provides information on the energy that is dissipated to the molecular framework.

- T_2 or spin-spin or transversal relaxation : T_2 is a time characteristic related to the precession or nutation of the nuclei, shifting from synchronous to asynchronous. It provides information on the energy dissipated to neighbouring nuclei.

Relaxation of magnetisation in NMR experiments is dependant on the molecular motions of the chemical compounds and their environment. Studies on wood have shown that the T_{2H} relaxation was different depending on the chemical compounds observed (e.g. cellulose, hemicellulloses) and their hydration states [Newman, 2005, Hill, 2010]. In this work, the T_{2H} relaxation of proton parameter

is used to determine if the polyols have an effect on cellulose and hemicellulose relaxations.

4.3 Experimental procedures

4.3.1 Materials

The extraction of the harakeke fibres was performed as described in Appendix B. Fibres were only extracted from the middle section of the leaf to ensure that the MFA was a constant, although the influence of MFA on the damping coefficient was not found to be significant (Chapter 3). Propane-1,2,3-triol and poly-propane-1,2,3-triol were used as-received (Solvay chemicals). For convenience purpose, the chemicals were designated under their common names: glycerol for propane-1,2,3-triol and poly(propane-1,2,3-triol)-3 for polyglycerol-3 (PG3). The molecular structure of the glycerol and PG3 are presented in Figures 4.1. The dynamic viscosity of glycerol and polyglycerol were 1 and 41 Pa.s, respectively. The molecular mass of glycerol was 92.1 g mol^{-1}. The average molecular mass of the polyglycerol was 250 g mol^{-1}. The mixture included triglycerol (47 wt. %), di-and tetramer (33 wt. %) and oligomers larger than the tetramer ($\leq$ 20 wt. %). The designation of PG3 was used for the polyglycerol as the distribution of oligomers peaked at the trimer. The boiling point of the glycerol was 290 °C, while the flash point of PG3 was $\geq$ 250 °C.

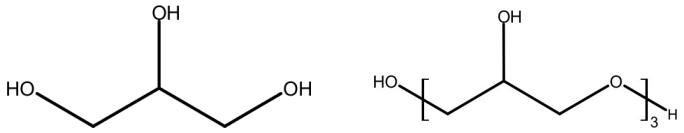

(a) (b)

Figure 4.1: Chemical structure of (a) propane-1,2,3-triol (glycerol) and (b) poly(propane-1,2,3-triol)-3 (PG3).

4.3.2 Methods

All tested fibre bundles were ∼1 m in length, extracted from the upper part of the leaf with similar linear density (AppendixB, Figures B.1 and B.2). The fibre bundles were weighed after conditioning at 23 °C and 50% RH for a week and re-weighed after drying at 105 °C until constant mass in order to calculate the moisture content. The oven dry mass was obtained on 50 mg of fibre bundle after 1 h at 105 °C and measured in air tight containers cooled to room temperature on a 5 decimal balance using a Mettler AT261 Delta range scale (Metler Toledo,Switzerland). The fibre bundles were chemically treated and re-weighed after drying at 105 °C to determine mass loss due to the chemical treatment. They were then soaked in the plasticiser solutions and dried again to measure the mass of absorbed chemical. They were then re-equilibrated at 23 °C and 50% RH for a week to attain a final moisture content. A total of 24 fibre bundles were chemically treated and impregnated separately.

The effects of the pre-treatment and impregnation on tan δ and E' were examined independently and in combination. The design of experiment approach used in this work is presented in Table 4.1. The effects of the pre-treatment and impregnation on tan δ and E' of the fibre bundles were analysed by analysis of variance using the software Minitab version 15.1.0.0 (Minitab Inc.) and fitted with a linear model. The validation of the model is presented using the graphical residual analysis for the damping coefficient and the storage modulus in the Appendix G, Figures G.1 and G.2.

1- Pre-treatment

1. None: Fibres were used straight after extraction and conditioning.

2. Boiling water: Fibres were boiled in water for 10 min and dried at 105 °C for 30 min.

3. NaOH: Fibres were immersed in a solution of 1 wt. % NaOH for 2 h at 45 °C , neutralised in 0.1 wt. % HCl to pH 7, washed with distilled water and dried at 105 °C for 30 min.

Table 4.1: Design of experiments showing 2 factors at 3 and 4 levels.

Factors	Levels
1- Pre-treatment	1- None 2- Boiling water 3- NaOH
2- Impregnation	1- Glycerol low 2- Glycerol high 3- PG3 low 4- PG3 high

2- Impregnation

1. None: No impregnation
2. Glycerol 2%: pre-treated fibres were soaked in an aqueous solution of 2 wt. % of glycerol overnight at 60 °C
3. Glycerol 10%: pre-treated fibres were soaked in an aqueous solution of 10 wt. % of glycerol overnight at 60 °C
4. Polyglycerol 2%: pre-treated fibres were soaked in an aqueous solution of 2 wt. % of polyglycerol overnight at 60 °C
5. Polyglycerol 10%: pre-treated fibres were soaked in an aqueous solution of 10 wt. % of polyglycerol overnight at 60 °C

4.3.3 DMA and optical microscopy

The damping coefficient and storage modulus (tan δ and E') were determined using the test as described in Chapter 3 (Section 3.2.5). Specimens of 100 mm in length

were cut out of the middle of the technical fibres following the pre-treatment and impregnation steps. The specimens were all conditioned at 23 °C and 50% RH for a week prior to testing by DMA.

Optical microscopy was performed as described in Chapter 3 using a stereo microscope Leica MZ12.5 fitted with a video camera (Leica DC 100). The fibre quality was assessed using a loop test to detect the presence of inhomogeneities and defects [Bos, 2004].

4.3.4 Liquid state NMR

Liquid state NMR experiments were collected at 300 K using a Bruker AVANCE III spectrometer (Bruker BioSpin, Rheinstetten, Germany) operating at 400.13 MHz proton frequency and equipped with a 5 mm BBO probe. The data was acquired and processed using the software TOPSPIN 3.2 (Bruker BioSpin, Rheinstetten, Germany). The 1H spectral width was set to 8223.7 Hz and 300 K complex points were recorded during an acquisition time of 3.985 s and a recyle delay of 1 s. Spectra were processed with a line broadening factor of 0.20 Hz. All spectra were calibrated using the residual water in D_2O at 4.79 ppm (H2O, OH). The specimens investigated were harakeke fibres impregnated by aqueous solution of PG3 at 10 and 50 wt. %, then dried in an oven at 105 °C for 2 hours and run in D_2O. The control sample was 50 wt. % PG3 in D_2O.

4.3.5 Solid state NMR

Solid state NMR experiments were performed using a Bruker Avance AVIII 200 operating at a ^{13}C frequency of 50.32 MHz and ^{1}H frequency of 200.13 MHz. Specimens were cut into small pieces using a razor blade and placed in a 4 mm zirconia rotor fitted with a Kel-F® cap. The sample was then spun at 5 KHz in a 4 mm Bruker SB MAS probe. The peaks of interest were the C4 cellulose (interior of the crystal) at 89.3 ppm (Figure 4.2) and the acetyl group of the hemicellulose at 21.8 ppm (Figure 4.3) [Pfeffer and Gerasimowicz, 1989]. The latter one is generally uncommon for hemicellulose but harekeke fibres are known to have acetylated hemicellulose [Newman et al., 2007]. Small amount of lignin

were detected, however the methoxyl lignin peak at 56 ppm was not defined enough to integrate reliably (Figure 4.3).

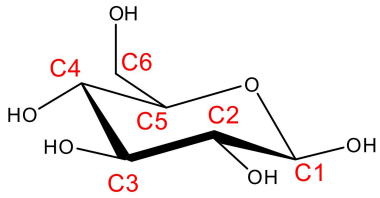

Figure 4.2: Carbon numbering used for carbohydrates (as shown for β-D-glucopyranose). Courtesy of Dr Stefan Hill [Hill, 2010]

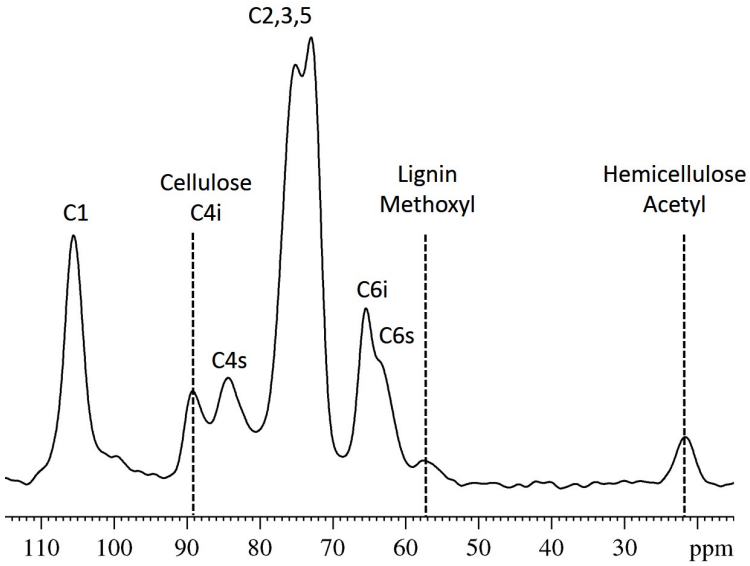

Figure 4.3: Typical solid state NMR spectrum of harakeke fibres.

A standard cross-polarization/magic angle spinning (CP/MAS) NMR pulse sequence was used. Each 3 μs proton preparation pulse was followed by a 1 ms cross-polarization contact time. This was followed by 30 ms of data acquisition during which high powered proton decoupling was applied. A recycle delay of 1.5 s was used between scans for a total of 3072 scans. The time domain free induction decays (FIDs) were summed per data point for a total of 16 points per experimental condition and Fourier transformed with 25 Hz Gaussian line broadening to obtain

the final frequency domain spectra. The spectra were linear baseline corrected in the 0 to 120 ppm region.

T_{2H} was calculated using the normalised plot of the signal fitted with a modified Weibull function [Newman, 1987, Hill, 2010] as presented in Equation 4.1:

$$I = I_0 + A\ exp\left(\frac{-t^{\mu}}{\mu 2^{\mu} T_{2H}^{\mu}}\right)\ sin\left(\frac{\pi(t - t_s)}{t_{\pi}}\right) \tag{4.1}$$

where I is the NMR signal, I_0 is an intensity offset, A is the amplitude, and t, t_s and t_{π} are constants determined by the pulse sequence. μ is a factor that describes the shape of the damped oscillation (μ =1 describing an exponential function and μ=2 a Gaussian function).

The normalised nutation decay plots of the ^{13}C NMR signal using the peak area of the cellulose (89 ppm) and hemicellulose (21.8 ppm) were fitted with Equation 4.1 using Origin 8.0 software (OriginLab Corporation) to obtain the value of T_{2H}.

4.4 Results and discussion

4.4.1 Plasticiser calibration using glycerol

A calibration curve was constructed to determine the relationship between the impregnating solution concentrations and fibre uptake. Four solutions were prepared with concentration of plasticiser of 5, 10, 25 and 50 wt. %. The fibres were then immersed in solution overnight. The plasticiser content was calculated by taking the oven-dry mass of the fibres before impregnation and after impregnation. The impregnation was linear up to 50 wt. % with a 1 to 1 ratio of glycerol absorbed by the fibre to the concentration of the impregnating solution (Figure 4.4). Plasticiser levels above 10 wt. % saturated the fibres and residual plasticiser could be seen at the surface of the fibres (Figure 4.5). If such fibres were used as a composite reinforcement, the plasticiser could decrease the fibre/matrix adhesion and compromise the mechanical properties of the composite [Greenspan, 1963, Borodulin, 2013]. Thus the concentration levels of the impregnating solutions were selected

at levels of 2% and 10% of plasticiser per dry mass of fibre.

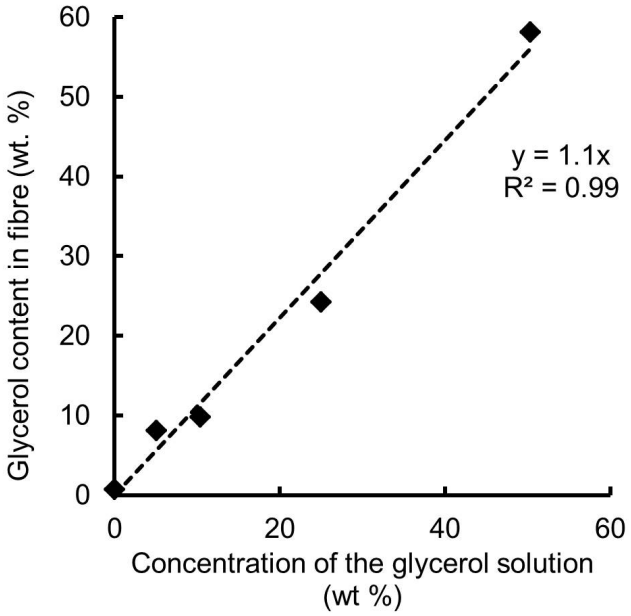

Figure 4.4: Glycerol calibration for fibre impregnation with linear regression fit.

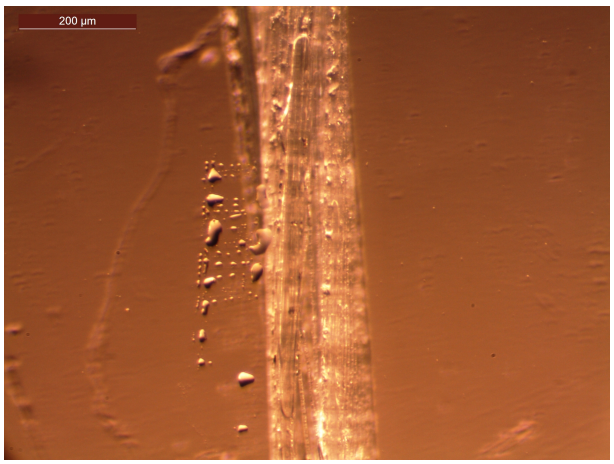

Figure 4.5: Transmitted light micrograph of a harakeke fibre impregnated with 25 wt. % of glycerol solution. The micrograph shows residual glycerol that transferred from the fibre surface to the microscope slide.

4.4.2 Mass and moisture content variation after pre-treatment and impregnation

The mass loss due to the boiling water treatment was 5.2% (±0.9%). It was similar to results reported by Richter on harakeke fibres [Richter et al., 2011] and corresponded to the loss of residual cuticle material [Thamae and Baillie, 2007] (Table 4.2). The mass loss due to the NaOH treatment was 17.8% (±1.6%) and was attributed to the loss of acetyl groups and xylan [Newman et al., 2007].

Table 4.2: Mass variation in wt. % of fibres after pre-treatment and impregnation steps.

	No	Glycerol		PG3	
	impregnation	2%	10%	2%	10%
No pre-treatment	NA	-1.0	9.7	-0.9	10.3
Boiling water	-5.2	2.5	7.9	2.6	13.7
NaOH 1%	-17.8	2.3	9.9	2.9	13.1

In the cases of fibres without pre-treatment and 2% impregnation, fibres have lost around ∼1% despite the potential plasticiser addition to the mass (Table 4.2). The negative variation was attributed to the loss of water soluble compounds in the fibres that counter balanced the absorption of plasticiser. The rest of the data points were consistent with the calibration curve (Figure 4.4), confirming a 1 to 1 ratio of solution concentration to fibre uptake for the glycerol. The ratio was slightly higher for the PG3 than the glycerol especially at 10% concentration where the ratio was 1.3 to 1. The uptake of PG3 by the fibres was higher after pre-treatment. The removal of water soluble compounds from the fibres, facilitated the absorption of the PG3. However, this effect was not observed for glycerol and was attributed to their differences in molecular mass.

The average moisture content of the fibres before treatment was 10.3% (± 0.5%) as was found in Chapter 3 (Table 4.3). The moisture contents after pre-treatment were lower by ∼1 wt. % compared to the non-pretreated fibres which indicated that hydrophilic compounds were removed as reported previously [Li et al., 2007, Kabir

Table 4.3: Moisture content in wt. % after pre-treatment and impregnation steps.

	No impregnation	Glycerol 2%	Glycerol 10%	PG3 2%	PG3 10%
No treatment	10.3	4.3	2.5	5.0	2.5
Water 100°C	8.7	3.8	1.4	2.0	1.6
NaOH 1%	8.9	3.6	1.0	3.1	1.8

et al., 2012]. The moisture content after impregnation were only a fraction of the non-treated fibres which was consistent with literature values of PEG treated wood (Table 4.3) [Akitsu et al., 1993]. The pre-treatments were expected to decrease the amount of hydrophilic compounds and facilitate the impregnation of polyols. Therefore it was presumed that the lower moisture content was a combined effect of removing soluble hydrophilic compounds from the fibre and having plasticiser occupying hydrogen bonding sites that could otherwise attract water molecules.

4.4.3 Liquid state NMR of the impregnated harakeke fibres

The signal of the protons between 4-3.8 ppm corresponded to the protons closer to oxygen atoms (hydroxyl and close to hydroxyls). The peak signals in the spectrum of the fibres impregnated with 10 wt. % solution of PG3 were broader and not as resolved as the control one. In addition, no shift in the peak signals were obvious compared to the control (Figure 4.6 (a) and (c)). The lack of resolution and the broadening could be attributed to the limited amount of PG3 in the fibre bundles and/or the restricted mobility of the PG3 molecules in the fibre cell wall caused by hydrogen bondings with polysaccharides. The higher resolution of the peaks in the spectrum of the fibres impregnated at 50 wt. % solution of PG3 (Figure 4.6 (b)), was believed to be caused by the transfer of PG3 from the harakeke fibre bundles to the D_2O solution.

Hydrogen bonding of PG3 in the cell wall could restrict its mobility (e.g. broadening of the peak signal) to solid-like. In solid state NMR, the relaxation parame-

ters of the polysaccharides contained in the cell wall (e.g. cellulose, hemicellulose) can be determined to assess the plasticisation caused by a hydrogen bonding chemical such as water [Hill, 2010]. The next section reported the variation of the proton relaxation time parameter T_{2H} as an indicator of the penetration of PG3 into the cell wall of the harakeke fibre bundles.

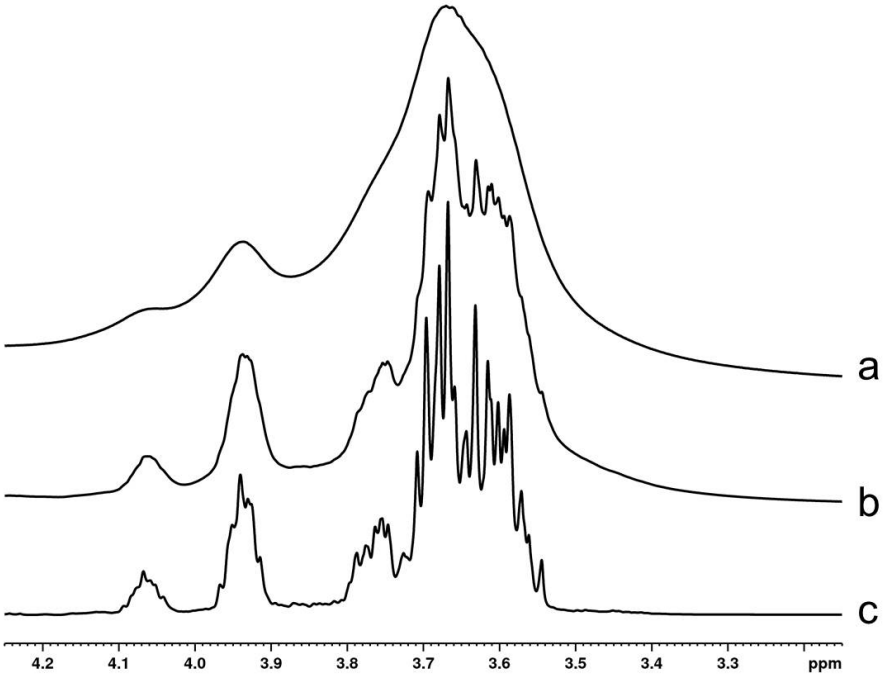

Figure 4.6: Liquid state NMR spectra overlay of (a) Harakeke fibres impregnated with 10 wt.% PG3 solution, (b) Harakeke fibres impregnated with 50 wt.% PG3 solution and (c) Control: 50 wt. % of PG3 in D_2O.

4.4.4 Solid state NMR relaxation of the impregnated harakeke fibres

Fitted damped oscillations are presented on Figures 4.7 and 4.8 for non-pretreated harakeke fibres impregnated with PG3 (10 wt. %) after oven drying at 103 °C for 1 h.

The results of the T_{2H} determined by the fits are presented in Table 4.4. Hill found values of T_{2H} for hydrated wood of 9.4 μs for cellulose and 12.6 μs for

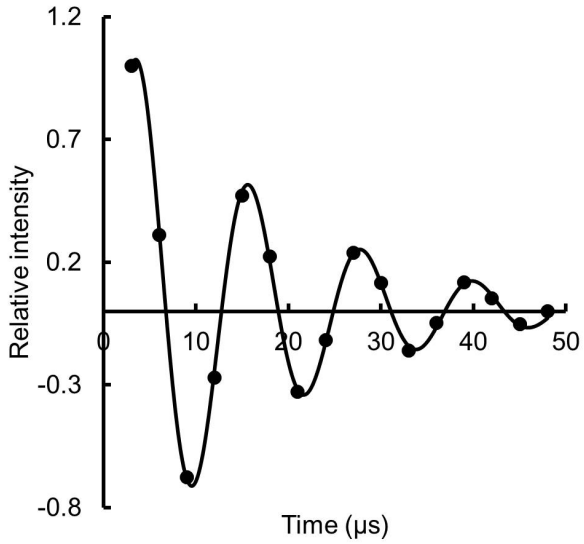

Figure 4.7: Nutation decay plot fitted with Equation 4.1 for the cellulose signal (89 ppm) of non-pretreated harakeke fibres impregnated with PG3 (10 wt. %).

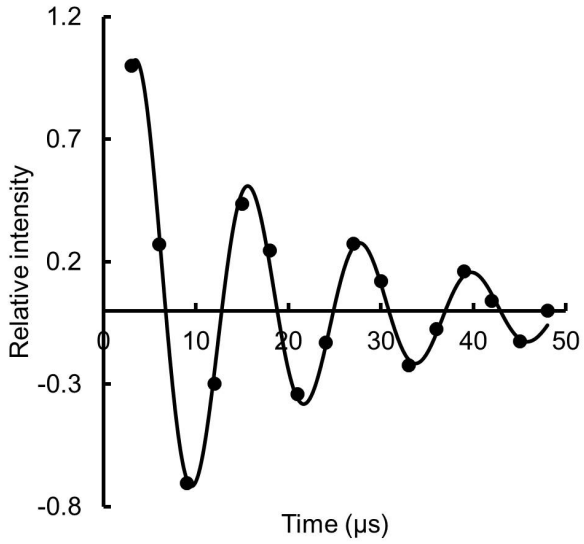

Figure 4.8: Nutation decay plot fitted with Equation 4.1 for the hemicellulose signal (21.8 ppm) of non-pretreated harakeke fibres impregnated with PG3 (10 wt. %).

hemicellulose which was consistent with the values found in this study [Hill, 2010]. The shorter the values of T_{2H}, the more rigid or confined the structure is.

The values of T_{2H} for the cellulose trended up from 8.2 to 8.9 μs in the dry and wet stage, respectively (Table 4.4). The value of the cellulose signal for the PG3 impregnated harakeke was intermediate at 8.4 μs, however, the values for the 3 different states were not statistically significant as the variation overlapped. The cellulose mobility was therefore not significantly affected by water-saturated and PG3 conditions. Conversely, the hemicellulose T_{2H} relaxation was influenced by the environmental conditions in spite of a large RMSD. In water-saturated conditions, the hemicellulose T_{2H} was twice the value of the dry state. With 10% PG3 impregnation, the T_{2H} was intermediate between the dry and wet states, showing that the hemicellulose retained a greater molecular mobility compared with those of the non-treated oven-dried state (Table 4.4). This latter observation indicated that PG3 impregnated successfully the cell wall of the harakeke fibres.

Table 4.4: T_{2H} values for different fibre treatments. The value in brackets represent 1 standard deviation.

	T_{2H} Cellulose (μs)	R^2	T_{2H} Hemicellulose (μs)	R^2
Dry harakeke	8.2 (0.4)	0.99	8.7 (0.8)	0.99
Harakeke PG3 (10 wt. %)	8.4 (0.3)	0.99	9.9 (1.0)	0.99
Wet harakeke	8.9 (0.7)	0.97	15.4 (4.0)	0.94

4.4.5 Influence of the pre-treatment and impregnation on E' and tan δ

The analysis of variance showed that all factors (pre-treament, type of polyol and polyol level) had significant effects on E'. The pre-treatment without impregnation decreased E' from its original value by ~25% for boiling water and ~75% for sodium hydroxide. The stiffness of the fibres was larger for glycerol impregnated fibres than PG3 (Figure 4.9). An increase in stiffness between no impregnation

and 2 wt. % was observed. This increase was counter-intuitive as the addition of platiciser was expected to decrease stiffness. However, a similar phenomenon was described for hemp and flax fibres where the modulus and strength increased with relative humidity up to 70-80% [Baley, 2002, Placet et al., 2012]. This phenomenon was attributed to the capacity of the cellulose microfibrils to realign towards the fibre axis as the hemicellulose/lignin matrix plasticised [Placet et al., 2012]. In this work, the oscillating strain level (0.05%) were not large enough to attribute the stiffening effect to MFA realignment. Alternatively, it was previously proposed that water in wood acts as an interlayer between cellulose and hemicellulose, playing a structural role in the mechanical properties of wood [Hill, 2010]. In this present work, it was therefore believed that up to a certain threshold, the polyols enhanced the stress-transfer between the hemicellulose and cellulose microfibrils resulting in an increase in stiffness. Beyond 2%, the impregnation of polyol caused E' to decrease as levels increased from 2% to 10% indicating over-plastification (Figure 4.9).

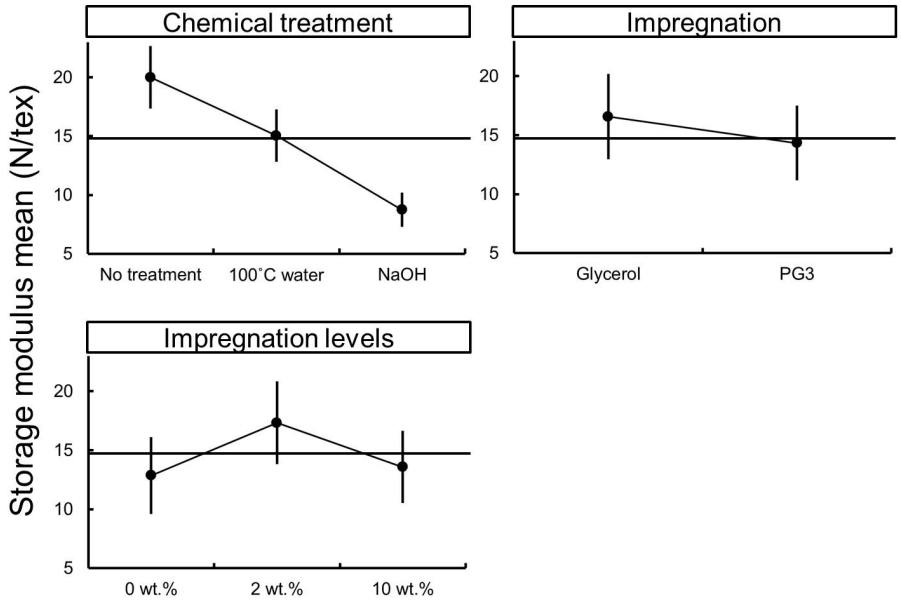

Figure 4.9: Main effects of the pre-treatment, impregnation and impregnation level on the storage modulus. The error bars are the 95% CI.

The variations in tan δ followed inverse trends that those of E'. Both boil-

ing water and sodium hydroxide pre-treatments increased tan δ from 38 to 50% of the non pre-treated value. The difference in polyol type indicated that PG3 impregnated fibres exhibited a higher damping than those impregnated with glycerol. In addition, polyol level at 2% decreased tan δ while it increased it at 10% (Figure 4.10).

When considering the mass loss of the fibres during the pre-treatment, the more severe the pre-treatment and mass loss were (none < boiling water < NaOH), the higher the decrease in E' and increase in tan δ. The best compromise between E' and tan δ was observed for the boiling water treatment where both E' and tan δ were above the overall averages. In terms of impregnation type, glycerol and PG3 were fairly equivalent. Conversely, the effect of the polyol level on E' and tan δ was significant, especially between 2 to 10% impregnation, where its influence shifted from stiffening to plasticising.

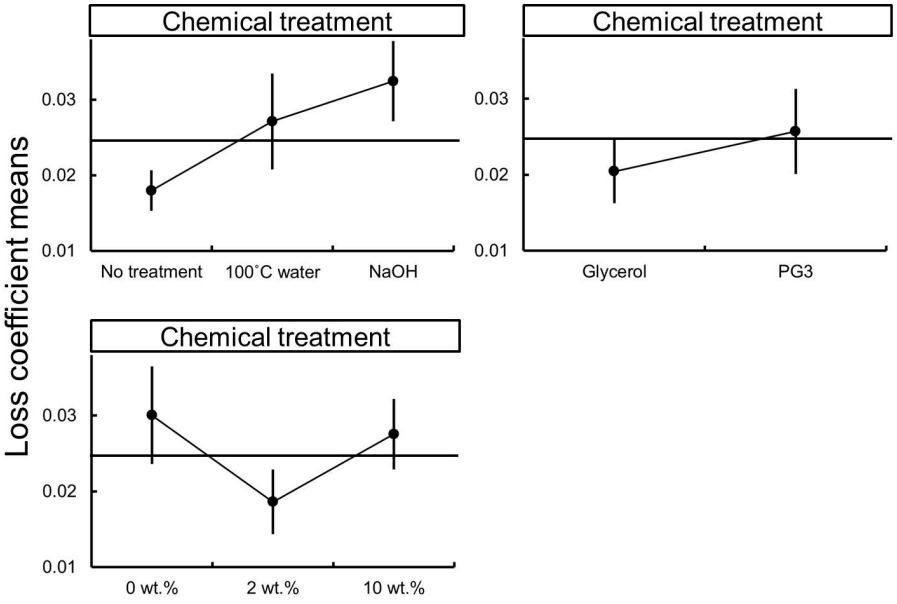

Figure 4.10: Main effects of the pre-treatment, impregnation and impregnation level on the damping coefficient. The error bars are the 95% CI.

The higher variation of properties for the fibres pre-treated with boiling water and consecutively impregnated suggested that the polyol had an easier access into the cell walls of the harakeke fibres than the non pre-treated fibres. In the case of

the sodium hydroxide pre-treated fibres, the mass loss was so large (17.8 wt. %) that the variation in the polyol level did not influence E' nor tan δ unlike the boiling water pre-treatment. The fibres were potentially degraded after the sodium hydroxide pre-treatment.

4.4.6 Impact of the pre-treatment and impregnation on the physical aspect of the fibres

The pre-treatments influenced the physical appearance of the fibres (Figures 4.11). The original fibres were homogeneous and formed a consistent loop showing no sign of defects (Figure 4.11 (a)). The boiling water pre-treatment caused 5.2% mass loss, however, no sign of inhomogeneity or damage were visible on the fibres which indicated that the mass loss was mainly attributed to surface cuticle and no structural compounds were removed (Table 4.2, Figure 4.11 (b)). In contrast, the sodium hydroxide pre-treatment weakened the fibre by removing 17.8% of dry mass and kinks were observed during the loop test which was consistent with the degradation hypothesis mentioned above (Figure 4.11 (c)).

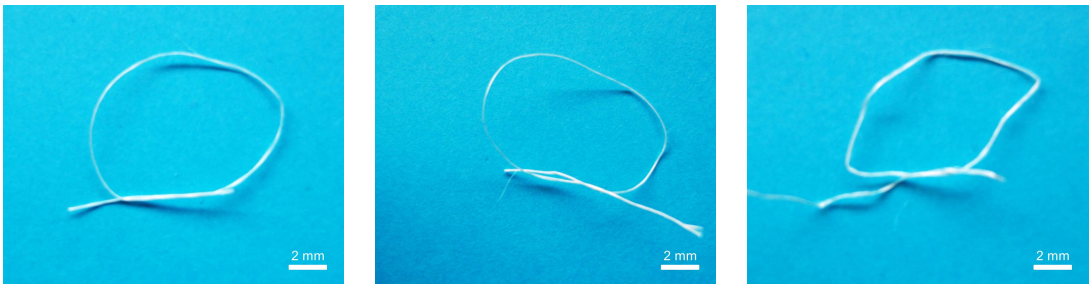

(a) (b) (c)

Figure 4.11: Loop test of the fibres of harakeke fibres after (a) no-pretreatment, (b) water 100 °C , and (c) NaOH treatment.

The surface of the fibre without pre-treatment was irregular which was consistent with the presence of residual compounds following the extraction of the harakeke leaves (Figure 4.12 (a)). After the boiling water pre-treatment, the residual compounds were almost completely removed leaving a smooth fibre surface with

a 5.2% mass loss without compromising the structural integrity of the fibre (Figure 4.12 (b)). The sodium hydroxide pre-treatment had a similar effect as boiling water upon the fibre surface but in addition caused defibrillation of the fibre cells which explained the decrease in storage modulus as the fibres no longer behaved as a cohesive bundle (Figure 4.12 (c)). The increased damping in the fibre pretreated with sodium hydroxide was therefore mainly attributed to the de-cohesion of the technical fibre into fibre cells instead of being induced by a hydrogen bonding mechanism.

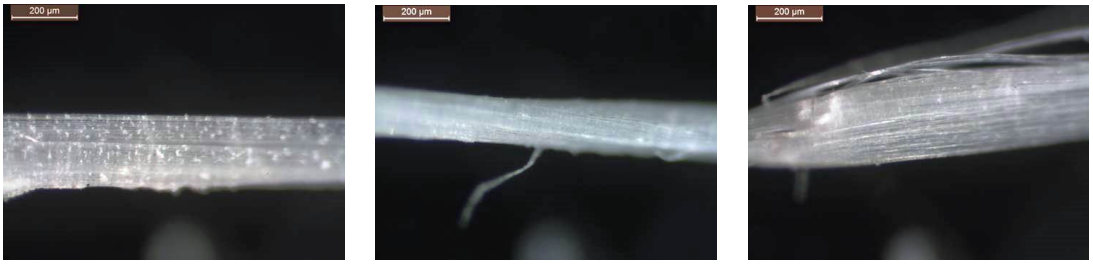

(a) (b) (c)

Figure 4.12: Reflected light micrographs of the surface of harakeke fibres after (a) no pre-treatment, (b) water 100 °C , and (c) NaOH treatment.

4.5 Conclusions

Harakeke technical fibres were impregnated with hydrogen bonding capable polyols, with and without pre-treatments, at different concentration levels. Subsequently, the mechanical properties of the fibres were investigated in terms of stiffness and damping.

The polyols were found to successfully impregnate the fibre cell wall of harakeke fibres and improved their damping coefficient suggesting that hydrogen bonding is an influencing factor that modified the damping property of cellulosic fibres. The impregnation within the cell wall was improved by removing residual cuticle material. However, further extraction using 1 wt. % sodium hydroxide solution lead to fibre defibrillation and defect formation. The increase in damping coefficient for

the sodium hydroxide pretreated fibre was therefore attributed to the de-cohesion of the fibre bundle.

Low levels of plasticisers improved the stiffness of fibres. This observation was tentatively attributed to an improvement in stress-transfer from the hemicellulose/lignin matrix to the cellulose microfibrils.

Solid state NMR indicated that the hemicellulose T_{2H} of fibres impregnated at 10 wt. % PG3, and then oven-dried at 105 °C , was intermediate between oven-dried and water saturated fibres. This intermediate value of T_{2H} suggested that the hemicellulose remained plasticised to a certain level after oven drying.

In the following chapter, polyol impregnated fibres were used as reinforcement for composite structures. The composites were manufactured under vacuum in compression moulding using processing temperatures of 110 to 150 °C . The damping property of these composites was studied to assess if the improved damping coefficient of fibres impregnated with polyols was observed in the damping coefficient of the whole reinforced composite.

Chapter 5

Utilisation of polyol compounds to improve vibration damping of plant fibre composites

5.1 Introduction

In the previous chapters, the damping properties of plant fibres were examined. It was found that the influencing parameters were the hydration level of the fibre, presence of hydrogen bonding compounds and the physical morphology of the fibre.

Chapter 4 focused on the efficiency of low molecular weight, low volatility hydrogen bonding compounds for mimicking the effect of water in the plant cell wall to improve the damping coefficient of the fibres. The findings reinforced the hypothesis that hydrogen bonding was the major cause of damping in plant fibres and two polyol were identified. The aim of Chapter 5 was to impregnate fibres as in Chapter 4 and measure the damping coefficient of composites reinforced with such fibres using acoustic and forced oscillation methods.

5.1.1 Damping at resonance using acoustic method

Measuring the quality factor (Q) of a resonance is a fast non-destructive method to obtain the damping coefficient of a material at the resonant frequency. The quality factor is equivalent to the inverse of the damping coefficient η (also called loss

coefficient) for level of damping $\eta < 0.1$ (Chapter 2, Equation 2.6) [Kinra, 1992]. The test relies on striking a specimen and recording the decay of the oscillations. A Fourier transform is then performed on the recording and the quality factor is determined from the width of the resonance peak.

The longitudinal waves in a beam are described as the tensile-compressive deformation of a volume. The longitudinal waves are not susceptible to the fixture set-up and occur in a higher frequency range than the flexural or bending wave. The flexural waves are the most important waves when studying vibrating structures, since they are the main cause of sound radiation [Cremer et al., 2005, p 95]. When measuring the oscillation of the flexural waves, the location of the support (e.g. rubber bands) is important to avoid external damping contributions (Figure 5.3). The supports are placed at the defined locations (nodes) depending on the mode of vibration being studied (Figure 5.1). In this study, the location of the nodes for the third and fourth flexural mode were chosen at the extreme ends (Figure 5.1).

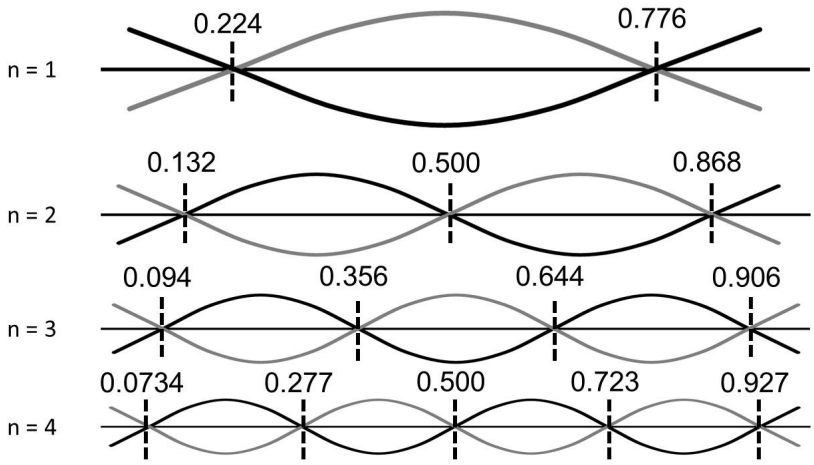

Figure 5.1: First four bending shapes and nodes (Numbers give the location of nodes in fraction of length from left end) adapted from [Stockey, 2002]

5.1.2 Time and temperature superposition (TTS)

Another successful method to measure and model the damping behaviour of material is to use DMTA equipment (Chapter 2).

The main limitation of the DMTA on vibrations experiments arises in the range of oscillations that can be applied. The DMTA allows data collection of forced oscillation between 0.01 Hz which is a practical limit (time constraint) and 100 Hz which is the physical limit of the instrument. Beyond this range, mechanical data collection is difficult. However, there is often a time dependence of the properties of polymers and composites in addition to temperature effects due to viscoelastic behaviour. As the mechanical frequency is increased the position of the transitions shift to a higher temperature since the polymer chains require more energy to respond within a shorter time scale. Thus, time and temperature can have equivalent effects on the rheological properties of linear viscoelastic materials that allows the use of time and temperature superposition (TTS) techniques to model the properties of materials beyond the frequency limits of the experimental set up. A so-called master curve is constructed by shifting the data of interest (e.g. storage or loss moduli) to overlap and form a single curve relative to a reference temperature.

Master curves are constructed using shift factors derived from the Williams, Landel, Ferry (WLF) and Arrhenius equations (Appendix J). These equations are used to calculate the activation energy or creep compliance over an extended period of time. Even though, the WLF approach is only valid when studying rheologically simple materials (single relaxation), they still provide useful comparative data when applied on composite [Pothan et al., 2003, Goertzen and Kessler, 2007]. Sucessfull comparative data of tan δ and E' could be obtained using TTS in vibration damping research [Sutton et al., 1999]. The details of the WLF and Arrhenius equations are presented on Appendix J.

In this work, the master curves were compared with reference composites with the aim of characterising the effect of polyol impregnation of European flax fibre on the viscoelastic response of flax-fibre-reinforced epoxy composites.

5.2 Experimental procedures

5.2.1 Material

European flax fabric was purchased from Composites Evolution Ltd under the trademark Biotex. The yarn is twistless, and weave types include 2/2 twill. The wrapping yarn is made from PET, that it is double-wrapped and represents a nominal 13 wt. % of the fabric when oven dried at 105 °C. The fabric was used as received. The gramage of the fabric was 420 g m^{-2} and the linear density of the yarn was 250 tex. A pre-treatment was done prior to the impregnation to clean the fabric of dust particles and enable an easier penetration of the polyol in the fibres (Chapter 4). It consisted in boiling the flax fabric for 30 minutes, drying it at room temperature and further drying at 105 °C for two hours. The mass loss for 1055 g of fabric was 2.01% by weight.

Plain-weave aramid fabric (Kevlar ® K49 from Dupont) with an areal weight of 170 g m^{-2}, and 2/2 twill carbon fabric (Made from Toray 300 yarn) with a areal weight of 240 g m^{-2} were purchased from Fibretech Solutions Ltd in Rotorua. The aramid and carbon fibre-reinforced composites were used for comparisons with the flax-reinforced laminate. Glycerol and polyglycerol-3 (PG3) were as described in Chapter 4, Section 4.3.1.

The resin system of the composites was based on diglycidyl ether of bisphenol A (DGEBA) purchased as EPON 828 from Shell Chemicals, and methyl-tetrahydrophthalic anhydride purchased as Lindride 52 from Lindau Chemicals. The catalyst was methyl-imidazole purchased from Sigma Aldrich. The ratio of resin:curing agent:accelerator was 100:87.5:1.5, as reported in literature [Nishino et al., 2000].

5.2.2 Plasticiser impregnation calibration

In Chapter 4, single technical harakeke fibres had a 1 to 1 weight ratio of polyol uptake to the concentration of the impregnating solution. Preliminary tests on impregnation of fabrics have shown that the absorption of plasticiser could be a 1 to 3 ratio (not presented here). In the case of European flax fabric, the ratio may have differed and a calibration was remeasured to remain below 5% by

weight uptake in the fabric. 1 L solutions of plasticiser were made at 1%, 2% and 5% in weight of glycerol and PG3. For each impregnation, two plies of 280 x 160 mm^{-2} were cut and dried at 105 °C for 2 h, weighed, and soaked for 24 h in the plasticiser solution. The ratio of fabric to solution mass was 1:50. The plies were then removed from the solutions, dried at room temperature for 2 h, dried overnight at 45 °C and dried for 1 h 105 °C and finally weighed for mass uptake.

5.2.3 Preparation of the composite laminate

The resin was mixed and degassed for 1 h in a desiccator at room temperature. Plies of 280 ×160 mm^2 were impregnated with resin one at a time by hand lay up and pre-cured separately at 105 °C for 10 min. The prepreg laminae were then stacked on an aluminium plate to give a symmetric [0,90] cross-ply spacers and placed in a vacuum bag. The laminate stack was kept under vacuum at room temperature for 1 h and then placed in a 30 tons hydraulic hot press (Siempelkamp, Krefeld, Germany) to be consolidated and cured (Figure 5.2).

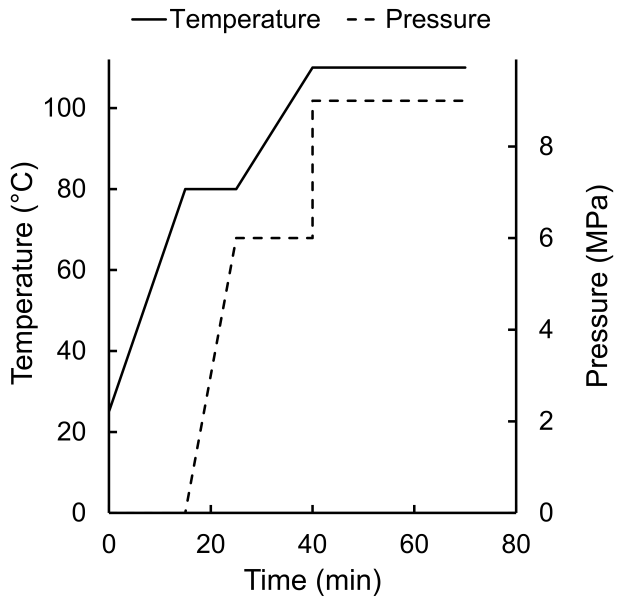

Figure 5.2: Temperature and pressure profiles for forming the composites.

The composite laminates were allowed to cool overnight under vacuum at room temperature, and then post-cured in 2 steps at 105 °C for 24 h and at 150 °C for an additional 6 h. The carbon, aramid and flax fibre-reinforced epoxy laminates had final thicknesses of 1.4, 1.7 and 2.8-2.9 mm, respectively.Each flax-fibre composite was made in duplicate.

Three to four specimens from each panel were cut on a band saw in 250×25 mm in dimensions and conditioned for a week at 23 °C and 50% relative humidity prior to acoustic testing. Three-point bending specimens for DMTA of 56×5 mm were cut and equilibrated in the same conditions. The 40 mm span of the DMTA support was to small to test the specimens of the flax composite to the ASTM D5023-07 (span = 16 x thickness) however, the introduction of random artefacts caused by sanding laminates to smaller thicknesses was not considered appropriate [ASTM D5023-07]. In order to avoid sawing artefacts (e.g. edge roughness or small fissures), all specimens edges were sanded with an 80 then 150 grit sand paper with the exception of the aramid specimens. Due to the toughness of aramid fibres, the composites were cut with a metal band saw and the edges were trimmed with a razor blade.

5.2.4 Physical properties of the composite laminates

Fibre weight fractions in the composite laminates were obtained by dividing the oven-dried mass of the reinforcement after impregnation by the mass of the post-cured laminate panel. Conversion to a volume fraction required a value of density for the impregnated fibre. The density of the fibre was calculated based on the density of the composite, density of the epoxy (1160 kg m^{-3} as determined by pycnometry), and the rule of mixtures, neglecting the presence of voids. The moisture content was calculated from the conditioned weight of the composites stored until constant weight at 23 °C , 50% RH and their oven-dried weight (overnight at 105 °C and brought back to room temperature in a desiccator containing dry silica gel).

5.2.5 Acoustics test

Each specimen was excited by a manual impulse and the resulting vibration decay was recorded with a microphone (THS 130P10 SN6156) plugged to an amplifier from National Instruments (NI USB-4431) as described in the ASTM E1876-09 (Figures 5.3) [ASTM E1876-09]. In the case of flexural resonance testing, the specimens were suspended at nodal points to minimise the influence of the system suspensions, and the exciter and the sensor were placed at anti-nodes [Wei and Kukureka, 2000], [Cremer et al., 2005, 226]. The sampling rate was 50 kHz and sampling durations were 0.1 and 1 s for the measurement of the longitudinal and flexural moduli respectively.

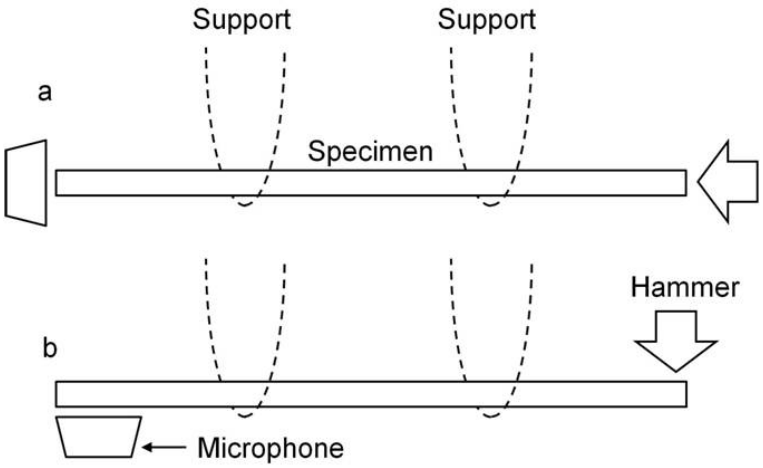

Figure 5.3: Free-free resonance frequency set up to determine the damping coefficient and stiffness in (a) longitudinal mode and (b) flexural mode.

Longitudinal and flexural moduli were calculated from Equations 5.1 and 5.2 respectively [Cremer et al., 2005, p 226] [Schmitz and Smith, 2011, p 310]:

$$E_{c,tensile} = 4\rho L^2 f_n^2 \tag{5.1}$$

$$E_{c,flexural} = \frac{48\pi^2 \rho L^4 f_n^2}{(\beta_n L)^4 h^2} \tag{5.2}$$

where ρ is the density in kg cm^{-3}, L and h are the length and thickness of

the beam in meters respectively, f_n is the resonant frequency at the n^{th} mode and $\beta_n L$ is the constant associated with the n^{th} flexural mode ($\beta_1 L$=4.73, $\beta_2 L$= 7.853, $\beta_3 L$= 10.996, $\beta_4 L$=14.137, etc.)

Damping coefficients were calculated using the half-power bandwidth b of the fundamental resonance at frequency $f_r$using the relationship described in Equation 5.3 (Appendix A, Figure A.3) [Cremer et al., 2005, 232].

$$\eta = C \frac{b}{f_r} \tag{5.3}$$

where:

$$C = \frac{1}{\sqrt{n^2 - 1}} \tag{5.4}$$

where $n^2 = \sqrt{5}$ and $\eta = b/(2f_r)$. When $n^2 = \sqrt{2}$, it is referred to as the 3 dB method and $\eta = b/(f_r)$ [Cremer et al., 2005, 226].

5.2.6 DMTA

Three-point bending specimens with a 40 mm span were tested using a TA RSA-G2 DMTA equipment with 0.5 N of pre-load. Tan δ and complex moduli were recorded. 2 to 3 replicates of each panel were tested for each type of test.

The first test involved a temperature scan from -25 °C to 180 °C at 5 °C min^{-1}, at 1 Hz oscillation and 0.1% strain. The effect of the plasticiser on the T_g of the composite was determined.

The second test involved an isothermal frequency sweep from 0.1 to 10 Hz at 0.1% strain at -40, -30, -20, -10, 0, 10, 20, 30, 40, 50, 60, 70, 80, 90, and 100 °C . The TTS master curves were assembled using the software package Trios 3.0.2 (TA instruments) (Figure 5.4). The shifting and overlay of curves was performed manually and the superposition was calculated using the Arrhenius law. The plots of shift factor versus 1/T are provided in Appendix J to validate the utilisation of the Arrhenius model.

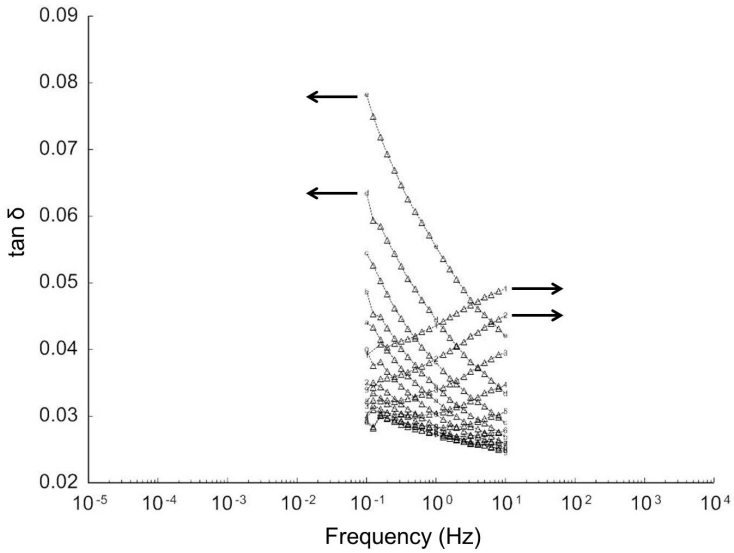

(a)

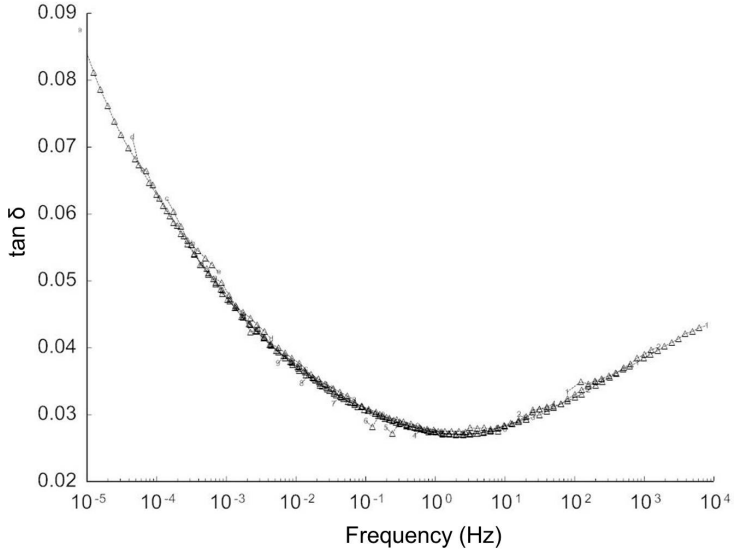

(b)

Figure 5.4: An example of a typical TTS master curve analysis of PG3-impregnated flax composites showing an (a) isothermal frequency sweep, black arrows point toward the translation necessary to obtain the master curve, and (b) master curve of the combined isothermal frequency sweep at a reference temperature of 20 °C.

5.2.7 Microscopy

Optical microscopy was done with a Leica MZ12.5 stereomicroscope. Field-emission scanning electron microscope (FESEM) images were obtained using a Jeol JSM-6700 F instrument. Specimens were taken from the fracture surface of the reinforced composites with the exception of the aramid fibre composite that did not produce clean fracture and was microtomed instead. Specimens were fastened onto a support with a 12 mm diameter disc of carbon tape. The support and the samples were coated with chromium under 10^{-4} to 10^{-3} mbar vacuum and scanned at a 3 kV acceleration voltage.

5.3 Results and discussion

5.3.1 Plasticiser calibration solution

Both glycerol and PG3 impregnated the fabric in proportion to the concentration of the plasticiser solution used (Figure 5.5). The linear regression fit indicated that the uptake of plasticiser was 1.81 times the concentration of the soaking solution. In the case of single fibres, the uptake was almost 1:1 (Chapter 4). This showed a large influence of the preform shape and/or the type of fibres. Also it was shown in Chapter 3 and Appendix E that the uptake of water was hindered by the lignin content. Thus the difference in the polyol uptake was also likely due to differences in the lignin content between harakeke (6.8 wt. %) and European flax fibres (3.2 wt. %) (Chapter 3, Section 3.3.1).

Beyond 5 wt. %, excess polyol was noticed at the surface of the fibres and if embedded as a composite might have interfered with the curing of the resin and prevented adhesion between the fibres and the matrix. As mentioned, the impregnation level in the fabric was intentionally kept below 5 wt. %. Thus, an impregnation plasticiser concentration of 2 wt. % was selected as the pre-treatment of the textiles by referring to the calibration curve (Figure 5.5). Glycerol uptake by the fabric was higher than expected, whereas PG3 was lower. However values were within the range determined by the calibration curve (Figure 5.5).

Table 5.1: Mass uptake of 2 wt. % plasticiser impregnation for composite preforms.

	Calculated	Measured	Variation (%)
Glycerol	3.64	4.12	+ 13.2
PG3	3.62	2.97	- 18.0

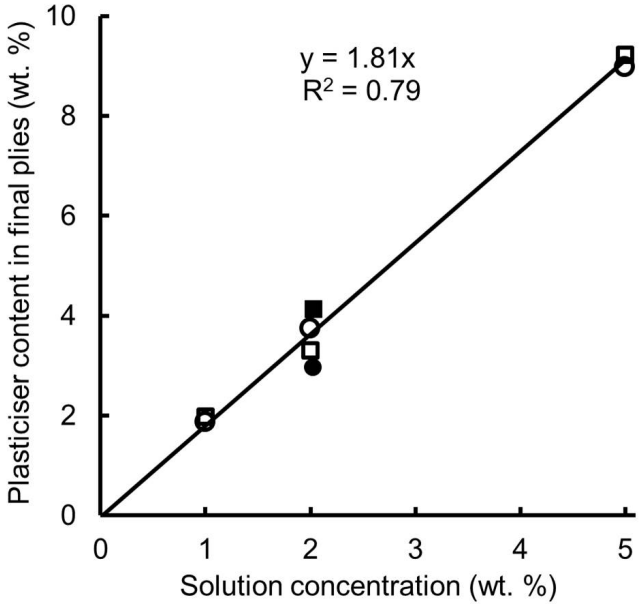

Figure 5.5: Plasticiser uptake from the impregnation treatment. The squares represent glycerol and circles represent PG3. Each point represents a ply of 20 g with the exception of the black filled symbol that represents 8 plies (160 g). The solid line represents the least squares best fit y = 1.81 x, $R^2 = 0.79$

5.3.2 Effect of the impregnation treatment on the physical characteristics of the composites

The presence of a polyol did not affect the fibre volume fraction composites manufactured under similar conditions which indicated that the polyol had a no impact or very little effect on the volume of the reinforcement (Table 5.2). The influence of polyol addition was however noticed by the increase of around 1% in the density of the final composite. The equilibrium moisture content of the flax composite laminates were similar for all composite, showing that the polyol did not influence the moisture absorption of the composite (Table 5.2). The fibre volume fraction for the replicate flax composites "B" were very similar to the composites series "A" and the subsequent stiffness and damping results for the "A" and "B" series were averaged.

Table 5.2: Composites physical characteristics, A and B are designation to distinguish replicate composites.

	Ply sequence	Densities kg m^{-3}	Fibre volume fraction	Moisture content wt. %
Carbon	[0/90/0/90/0]	1364.6 (12)	0.52	-
Aramid	[0/90/0/90] s	1252.3 (15)	0.53	-
Flax (No polyol) A	[0/90]s	1241.6 (4.4)	0.47	1.73 (0.05)
Flax (No polyol) B	[0/90]s	1238.0 (5.6)	0.48	
Flax (Glycerol) A	[0/90]s	1251.4 (10.5)	0.48	1.78 (0.09)
Flax (Glycerol) B	[0/90]s	1253.5 (5.4)	0.47	
Flax (PG3) A	[0/90]s	1250.4 (5.7)	0.48	1.78 (0.06)
Flax (PG3) B	[0/90]s	1255.9 (2.5)	0.48	

5.3.3 Influence of the impregnation on the tensile and flexural properties of the European flax composites

The impregnation of the flax textile by glycerol and PG3 decreased by around 10% both tensile strength and modulus of the final flax fibre-reinforced composite laminates (Table 5.3) and by 20% of the flexural strength and stiffness (Table 5.4). Treatment with glycerol degraded the mechanical properties to a greater extent than PG3 in general. This could be due to the higher content of glycerol relative to the fibres treated with PG3 (e.g. 4.12% and 2.97%) and/or a greater plasticisation effect of the glycerol due to its lower molecular weight and viscosity.

Obataya et al. reported that up to 8 wt. % of water in wood, the stiffness increased by 10% [Obataya et al., 1998]. In the case of the present study, it indicated that the polyols did not have the same effect than water possibly due to the molecular size difference or that particular threshold content observed in other studies was exceeded [van Voorn et al., 2001, Placet et al., 2012]. The values of strain at maximum stress were comparable between the different flax fibre-reinforced composites, with a marginal improvement for the reinforcement impregnated with PG3 which increased the composite plastic deformation by 0.2%.

The polyol impregnation generally increased the toughness of the composites (work to fracture) indicating that the fibre cells or microfibrils are sliding past each other or that the interface epoxy/fibres has changed (Tables 5.3 and 5.4). The interface fibre/epoxy is commented further in the microscopy section 5.3.7.

Table 5.3: Tensile properties of the flax fibre composites. Numbers in brackets are 95% confidence interval.

	Young's modulus (GPa)	Ultimate tensile strength (MPa)	Strain to failure (%)	Toughness (MJ/m^3)
Flax (No polyol)	8.1 (0.5)	54.6 (1.2)	1.55 (0.16)	0.69 (0.23)
Flax (Glycerol)	7.1 (0.5)	47.2 (2.1)	1.49 (0.26)	0.60 (0.32)
Flax (PG3)	7.3 (0.5)	49.5 (0.2)	1.75 (0.21)	0.73 (0.24)

Table 5.4: Flexural properties of the flax fibre composites. Numbers in brackets are 95% confidence interval.

	Young's modulus (GPa)	Ultimate flexural strength (MPa)	Strain to failure (%)	Toughness (MJ/m^3)
Flax (No polyol)	3.3 (0.2)	49.4 (4.8)	1.86 (0.16)	0.52 (0.11)
Flax (Glycerol)	2.0 (0.4)	39.2 (4.2)	1.95 (0.35)	0.60 (0.15)
Flax (PG3)	2.3 (0.2)	40.8 (5.0)	3.01 (0.41)	0.74 (0.12)

5.3.4 Acoustics properties of the composites

Matrix dependence properties

Acoustic tests on the unreinforced epoxy, in longitudinal and flexural modes, gave distinctly different values for the damping coefficient: $\eta_m = 0.033$ for longitudinal vibrations at 3369 Hz and $\eta_m = 0.013$ for flexural vibrations at 58 Hz (Figure 5.6). The dependence on frequency was consistent with published data for unreinforced epoxy, reporting an increase in damping coefficient by a factor of two over the frequency range 50-500 Hz [Gibson and Plunkett, 1976]. The frequency dependence of η_m was investigated in greater detail through additional acoustic testing, in flexural mode, at resonance frequencies above the fundamental frequency (Figure 5.6). Values of the elastic modulus were $E_m = 3.2$ and 2.8 GPa for longitudinal and flexural testing respectively.

Influence of the impregnation on the tensile and flexural moduli of the flax composites

The moduli values of the flax composites extracted from the vibrational testing in the longitudinal mode were in close agreement with that from the tensile testing (Table 5.3 and 5.5). The flexural modulus was almost constant for the first four modes of vibration. Thus, a mean value of the flexural modulus was calculated for each type of composite (Table 5.5). Here again, there was a 3 to 5% decrease in the modulus of elasticity when polyols were added, and the magnitude of the decrease was consistent with the replacement of cellulose by polyol in the fibre weight

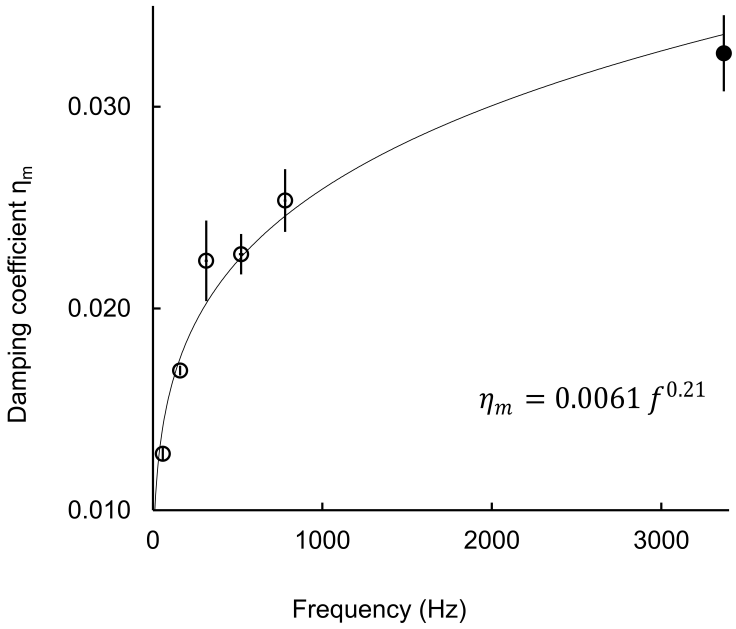

Figure 5.6: Longitudinal and flexural acoustic damping coefficient on unreinforced resin as a function of frequency, plotted as filled and unfilled circles respectively, the curve represents the least-squares best fit, $R^2 = 0.987$. The error bars represent the 95% CI.

fraction. The moduli determined in flexural mode were 16 to 20% lower than those determined in longitudinal mode. This known characteristic in acoustics testing is a result of the approximation in the modulus calculations using Equation 5.2 which does not take into account the effects of lamina structure in the thickness direction [Ramtekkar et al., 2002] as well as potential dependence of mechanical properties with frequency [Divos and Tanaka, 2000, Ouis, 2002].

Table 5.5: MOE and damping coefficient determined in longitudinal and flexural mode from acoustic testing. Numbers in brackets are 95% confidence interval.

	E flexural (GPa)	E tensile (GPa)	Damping coefficient η
Carbon	41.7 (1.0)	52.8 (0.5)	0.0059
Aramid	28.9 (0.4)	34.8 (0.3)	0.0150
Flax (No-polyol)	6.5 (0.1)	7.8 (<0.1)	0.0174
Flax (Glycerol)	6.2 (0.1)	7.4 (<0.1)	0.0192
Flax (PG3)	6.3 (0.1)	7.5 (<0.1)	0.0217

Influence of the impregnation on the damping coefficient of the flax composites

Values of the damping coefficient were found to be functions of frequency for all composites (Figure 5.7). The damping coefficient increased with increasing frequency for the flax composites. In contrast, the damping coefficient decreased with increasing frequency for the carbon and aramid fibre composites. Moreover, the damping coefficient for the flax fibre composites was greater than those of the aramid and carbon fibre composites. That observation was consistent with a recent report that flax-twill epoxy composites have a relatively high loss coefficient compared with carbon-twill epoxy composites [Duc et al., 2014]. The experimental values were plotted against the logarithm of frequency (Figure 5.7) and linear least-squares fitting was used to obtain values of the damping coefficient at 100 Hz (Table 5.5). The determination of the damping coefficient at 100 Hz was chosen arbitrary, and only used to compare the merit of the different composites in

terms of damping. The treatment of flax fibre with polyols resulted in composites that exhibited a higher damping coefficient than untreated flax fibre composites over the entire range of frequencies. The damping coefficient at 100 Hz of the flax fibre composites was increased by 10 and 25% with the glycerol and PG3 treatment respectively. The relatively large effect of PG3 compared to glycerol on the damping coefficient is further discussed in Section 5.3.8.

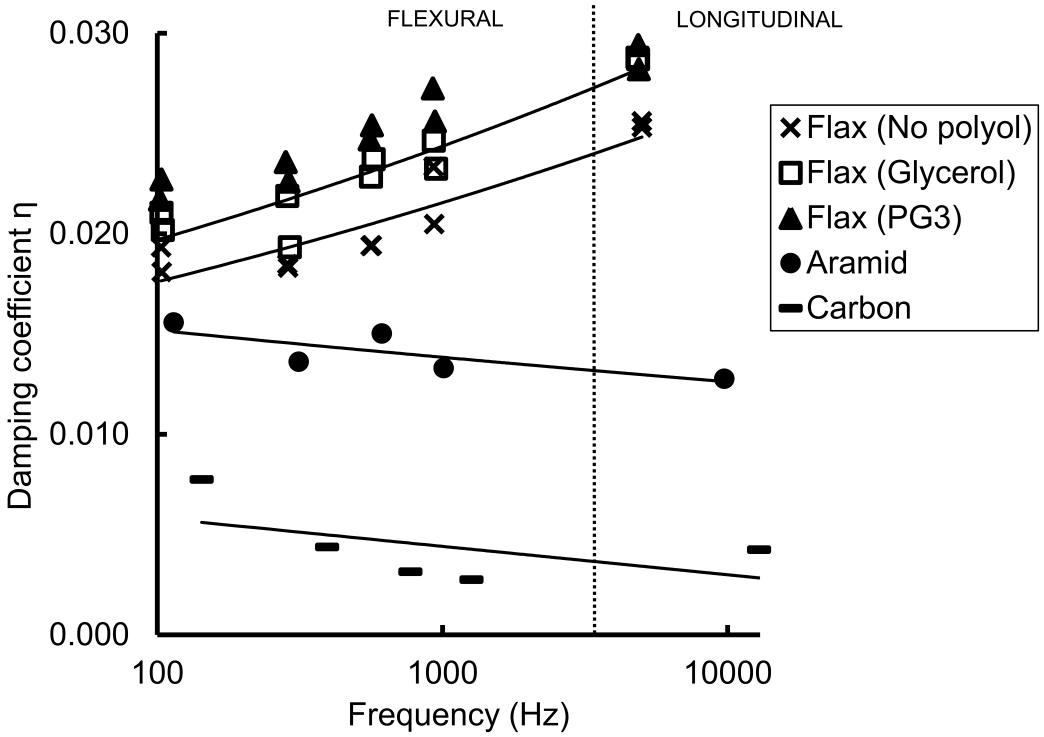

Figure 5.7: Semi-logarithmic plot of the damping coefficient as a function of the resonant frequency. The black lines represent linear least-square fits.

5.3.5 Influence of the polyol treatment on the dynamic thermo-mechanical properties

The composites were found to be fully cured and no thermal transitions were observed for the impregnated flax composites suggesting that the polyol did not interfere with the cure of the epoxy resin (Figure 5.8) [Thuvander et al., 2001].

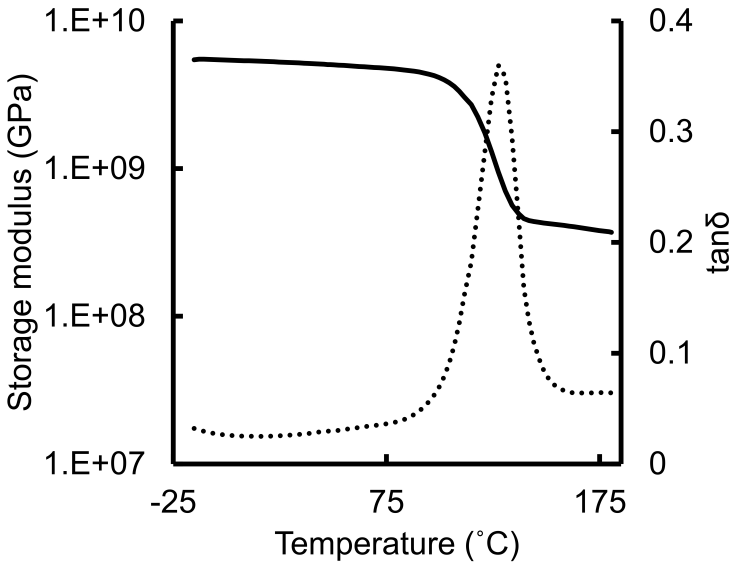

Figure 5.8: Typical temperature scan in DMTA, showing the storage modulus and tan δ (flax-PG3 composite specimen). The black line represents the storage modulus and the dotted line represents tan δ.

The temperature at maximum tan δ was similar for all the flax composites. The aramid fibre composite exhibited a T_g that was ∼12 °C lower in comparison to the other composites (Table 5.6). Similarly to the acoustic tests reported in the previous section, PG3 increased vibration damping more than glycerol, despite a lower loading of polyol on the fibres (Table 5.6). The improvements were 13% for the glycerol treatment and 21% for the PG3 treatment when comparing tan δ at room temperature.

The plots of tan δ against temperature indicated a single thermal transition for all composites, attributed to the glass transition temperature (T_g) of the resin (Figure 5.9). A gradual increase of the tan δ in the range of 25 to 75 °C was attributed to the T_g of the PET (T_g = 65-80 °C) present in the flax textile. The polyol-impregnated flax fibre composites exhibited a T_g that was slightly higher than the untreated flax composite, an observation tentatively attributed to local cross-linking of the polyols and the anhydride epoxy resin sytem.

Previous work on the vibration damping of other bio-based composites has re-

Table 5.6: Results of dynamic temperature ramp scans (5 °C min^{-1}) in oscillation (1 Hz, 0.1% strain) in 3-point bending mode. The number in brackets is the 95% confidence interval calculated on 3 specimens for the aramid and carbon composites and 5 specimens for the flax composites sampled from two different composites of the same formulation.

	Storage modulus at 20 °C (GPa)	Loss modulus at 20 °C (GPa)	tan δ at 20 °C	Max tan δ position (°C)
Resin	2.7	0.05	0.018	154
	(0.2)	(0.01)	(0.002)	(2)
Carbon	43.6	0.22	0.005	130
	(3.3)	(0.03)	(0.001)	(1)
Aramid	13.1	0.43	0.033	117
	(0.6)	(0.05)	(0.005)	(1)
Flax (No polyol)	5.6	0.16	0.029	129
	(0.3)	(0.03)	(0.004)	(3)
Flax (Glycerol)	4.8	0.19	0.035	136
	(0.1)	(0.04)	(0.004)	(4)
Flax (PG3)	5.1	0.22	0.044	134
	(0.1)	(0.03)	(0.005)	(1)

vealed the presence of local maxima in tan δ as a function of temperature. For example, coir fibre reinforced composites exhibited a number of separate peaks in tan δ that were attributed to the matrix, fibres, and fibre-matrix interface [Geethamma et al., 2005]. The flax fibre-reinforced composites did not exhibit maxima over the temperature range investigated, although the presence of a shoulder was observed within the main tan δ peak for the carbon fibre-reinforced composite (Figure 5.9). Successive temperature scans were then performed on the carbon fibre-reinforced composite to ensure the shoulder was not an artefact of incomplete curing of the epoxy. However, the presence of this shoulder persisted. Similar observations of a secondary transition have been made for carbon fibre composites [Atkinson and Jones, 1996]. The presence of a secondary transition in carbon fibre composites was attributed to the formation of an interphase at the fibre-matrix interface that may have resulted from a chemical reaction between the sizing on the fibre and anhydride in the resin. It has also been suggested that anhydride hardeners react with functional groups on the fibre surface and reduce the cross-link density close to the fibre surface, leading to a localised interphase with a lower glass transition temperature than the rest of the matrix [Atkinson and Jones, 1996].

5.3.6 Modelling tan δ of the composites as a function of frequency using time and temperature superposition (TTS) principle

Similarly to the acoustic experiments, the carbon and aramid fibre composites exhibited either constant or lower tan δ with increasing frequency compared with the flax composites (Figure 5.10). The comparison between the impregnated and non-impregnated flax composites was not as straight forward as for the acoustic tests. Error due to the TTS overlay lead to variation as large as the actual difference in tan δ of the different flax composites, and therefore, potential variations between the impregnated and non-impregnated flax composites on the TTS overlay were not reliable. While TTS is robust for rheologically simple systems, it application here was limited to supporting the acoustic results.

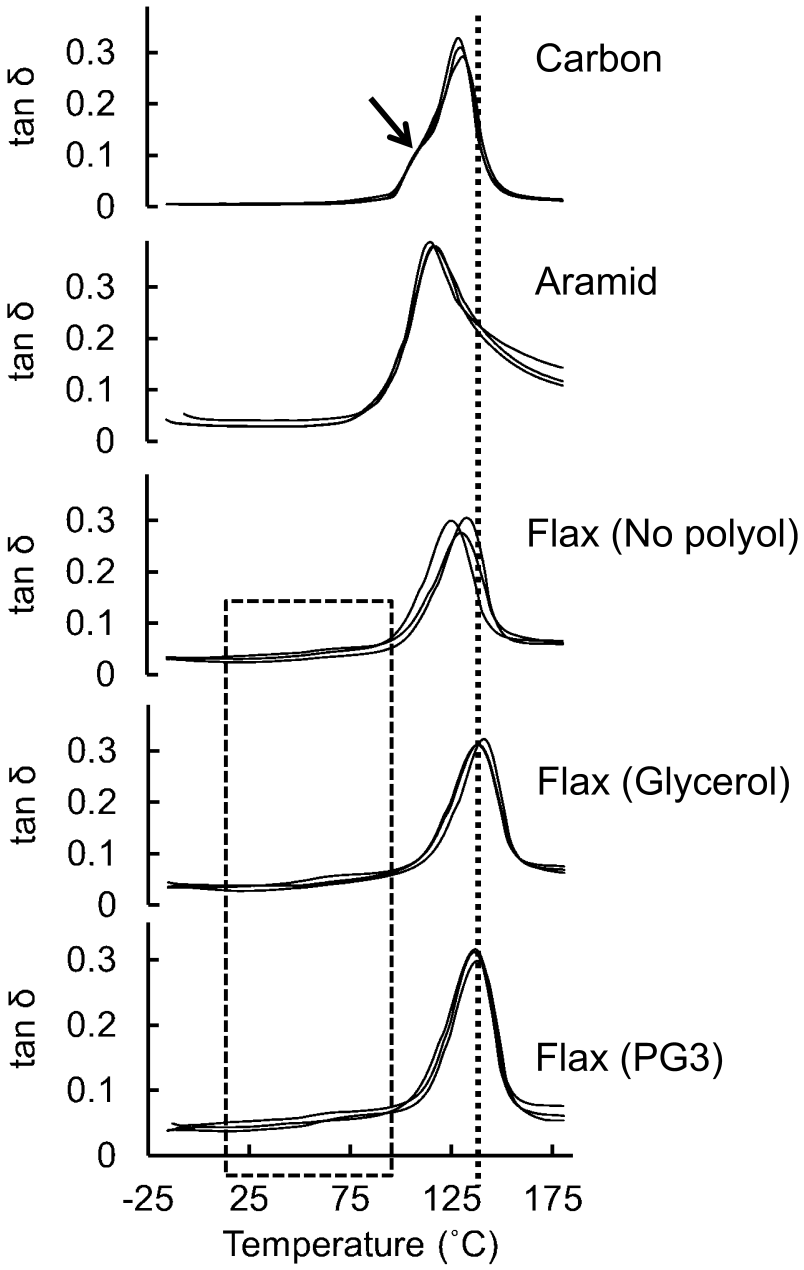

Figure 5.9: tan δ as a function of temperature for the different types of reinforcement. The arrow indicates a shoulder observed for the carbon fibre composite. The dotted rectangle highlights the low temperature region of the flax fibre composites.

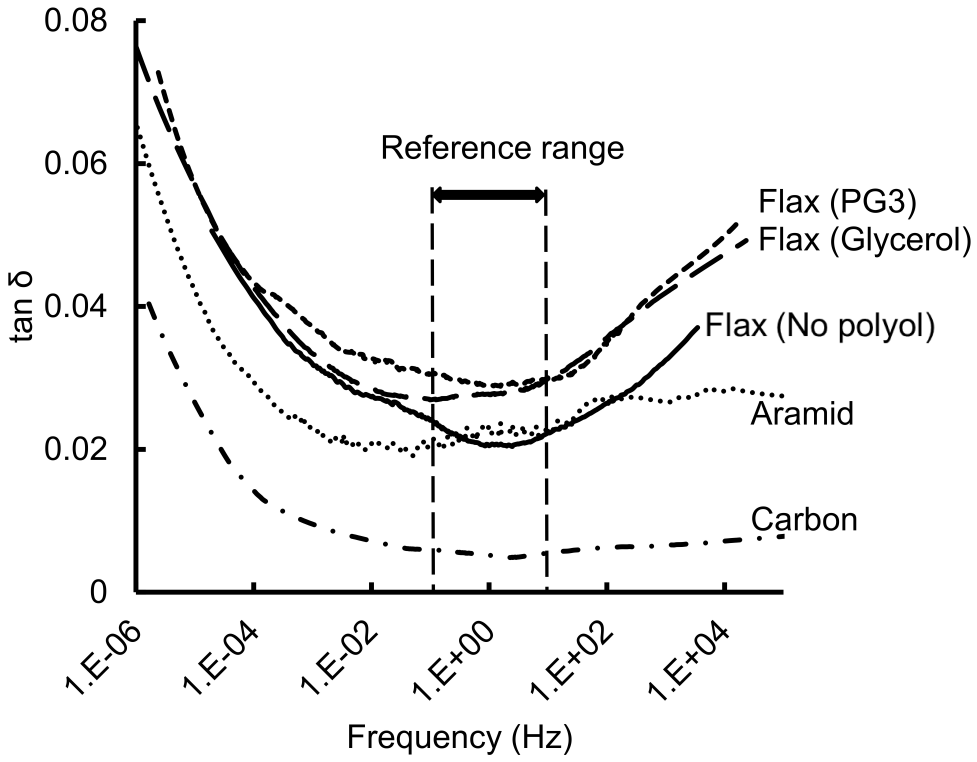

Figure 5.10: TTS overlay of the different reinforced composites at a reference temperature of 20 °C .

5.3.7 Composite fracture behaviour

In the case of the aramid-fibre reinforced composite, the cut surface showed poor bonding at the interfaces between the fibre and matrix (Figure 5.11 (a)). The fibre surfaces were smooth and seldom showed broken matrix particles clinging to the aramid fibres. This poor bonding was consistent with the DMTA results, which showed the tan δ peak at a temperature approximately 12 °C less than for the other composites (Figure 5.9). Weak interfaces between fibre and matrix were thought to act as stress concentrators and energy sinks that contributed to an increased damping [Geethamma et al., 2005]. In the case of the carbon composite, strong adhesion between the fibre and matrix was observed (Figure 5.11 (b)). Broken particles of matrix were left clinging to the surfaces of the fibres after fracture, indicating failure within the matrix rather than at the fibre-matrix interface. This observation was consistent with the shoulder in the tan δ plot against temperature, which was attributed to chemical reactions between sizing on the fibre and the anhydride in the resin (Figure 5.9) (Section 5.3.5) [Atkinson and Jones, 1996].

As mentioned, the flax yarn was also composed of PET fibres (Figure 5.12 (a) and (b)). When looking at the frature of the composite (Figure 5.13), the fracture of the flax composites was likely caused by a weak interface between the PET and the epoxy matrix. Indeed, the flax fibre surfaces were defibrillated compared to their original state in the yarn while the PET fibre were unchanged showing little adhesion with the epoxy matrix (Figure 5.12 (c) and (d)).

The fracture surfaces for the flax fibre-reinforced composite did not show any visible difference between the non-impregnated specimens and those impregnated with glycerol or PG3 (Figures 5.14 (a) and (b)). This indicates that at these levels of impregnation, the polyols remained in the cell of the fibre cell and did not hinder the adhesion between the flax fibre bundles and the epoxy/anhydride matrix. The increased toughness observed in the tensile/flexural data was therefore attributed to sliding between the fibre cells and/or the sliding of the microfibrils into the cell wall (Section 5.3.3). A mixture of failure mechanisms was indicative of the strength of the fibre-matrix interface, with both fibre and interfacial failure being clearly observed (Figures 5.15).

Figure 5.15 (a) presents a non-debonded fibre despite the obvious adjacent

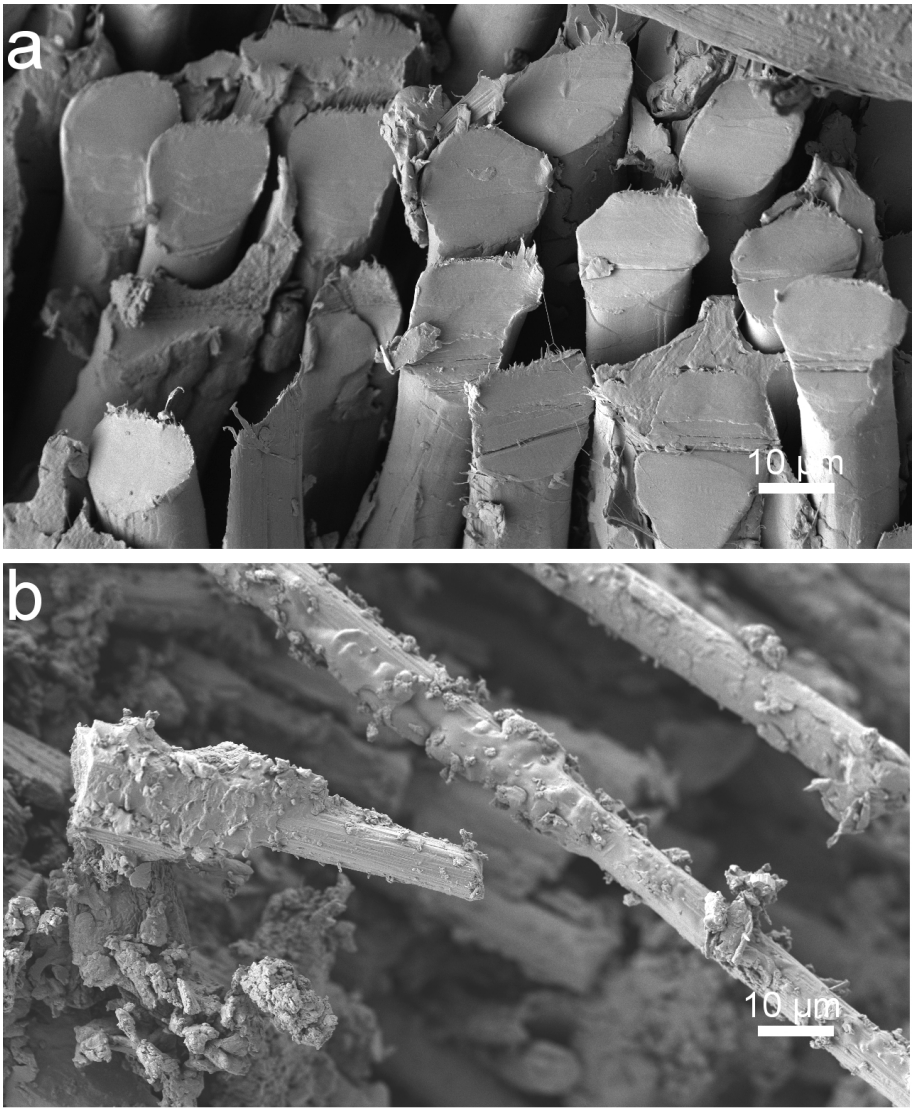

Figure 5.11: Scanning electron micrographs of the (a) cut surface of the aramid fibre-reinforced composite, and (b) fracture surface of the carbon fibre-reinforced composite.

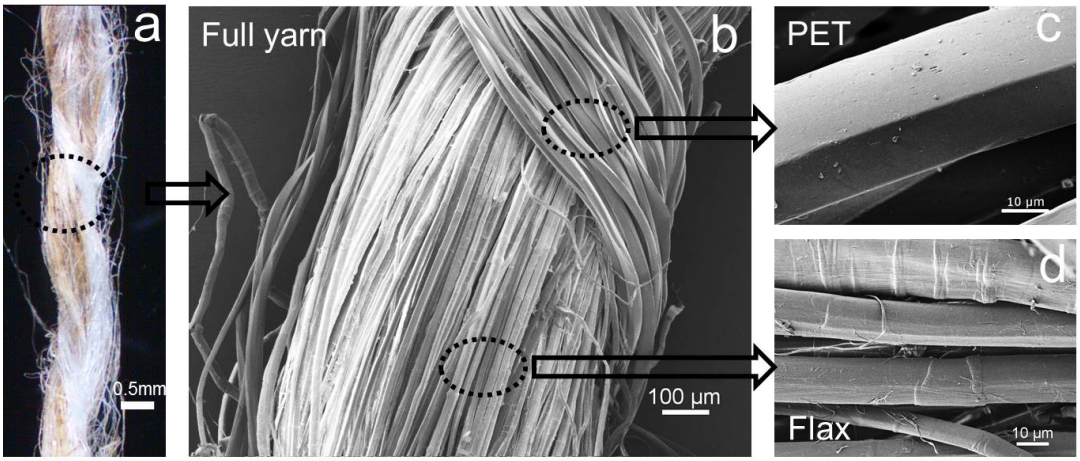

Figure 5.12: Flax yarn sampled from the twill fabric (a) reflected light micrograph of the flax yarn with PET wrap in white, (b) scanning electron micrograph of the yarn with the PET wrap, (c) scanning electron micrograph of surface features of a PET fibre, and (d) scanning electron micrograph of surface features of flax fibres.

failure. The failure seemed to have been initiating from a kink band as an imprint in the matrix suggested and as it was reported by others [Hughes, 2012]. The presence of residual fragments of primary cell walls embedded in the adjacent epoxy matrix was evidence of extensive fibre-matrix bonding. The macrofibrillar structure of embedded cell wall fragments in the epoxy was indicative of secondary cell wall matter (Figure 5.15 (b)). In contrast, failure occurred mainly within the matrix of the carbon fibre-reinforced composite (Figure 5.11 (b)).

In Section 5.3.5, it was proposed that the anhydride hardener acted as compatibiliser between the flax fibre and epoxy matrix. FESEM confirmed that hypothesis as strong adhesion between flax fibre and epoxy could be observed after fracture. Flax fibres surfaces were torn apart showing ribbons of microfibrils (Figure 5.13). The strong adhesion between fibres and epoxy also implied that damping in the flax fibre-reinforced composite did not originate from poor fibre matrix bonding. The increased flexural strain to failure observed earlier in Section 5.3.3: 1.86 % for the non-impregnated fibres and 3.01 % for the PG3 impregnated fibres indicated that PG3 plasticised either between cells interface or within the cell wall but not at the fibre matrix interface (Table 5.4).

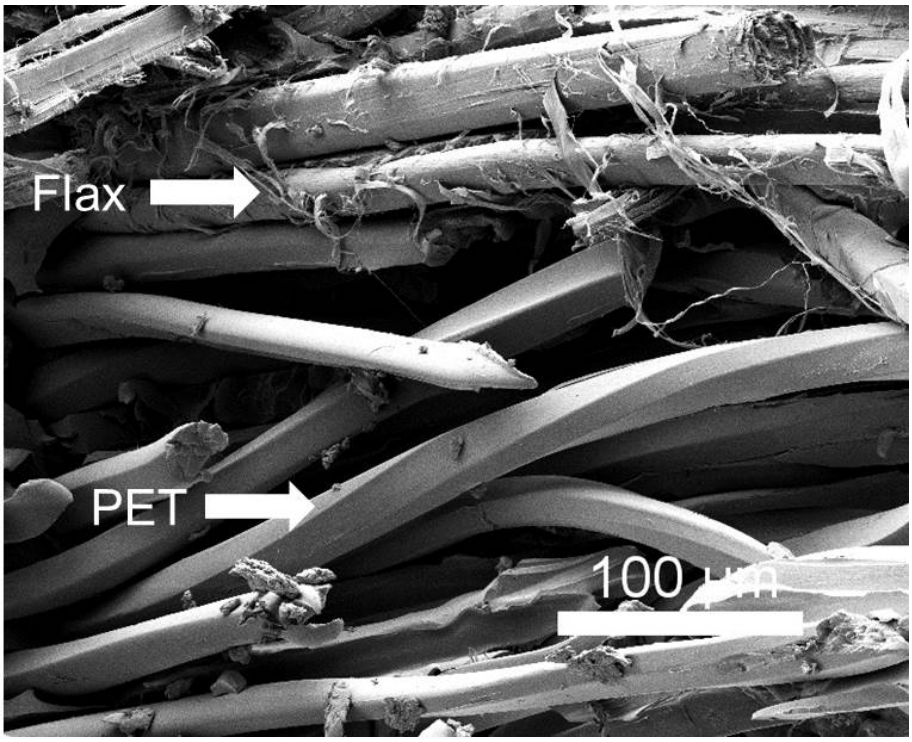

Figure 5.13: Fracture surface of a flax reinforced composite showing different surface features between the flax and PET fibres.

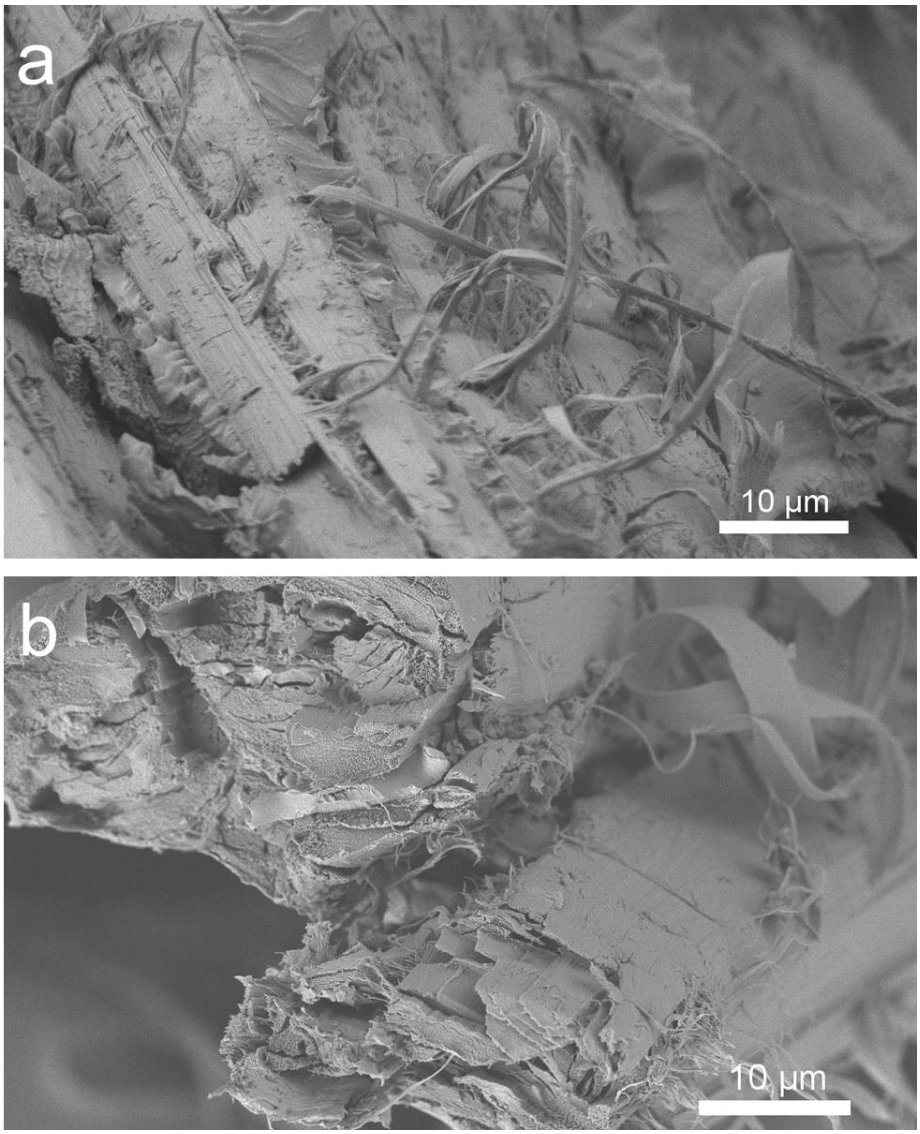

Figure 5.14: FESEM of flax reinforced composite fractures (a) No impregnation, and (b) PG3.

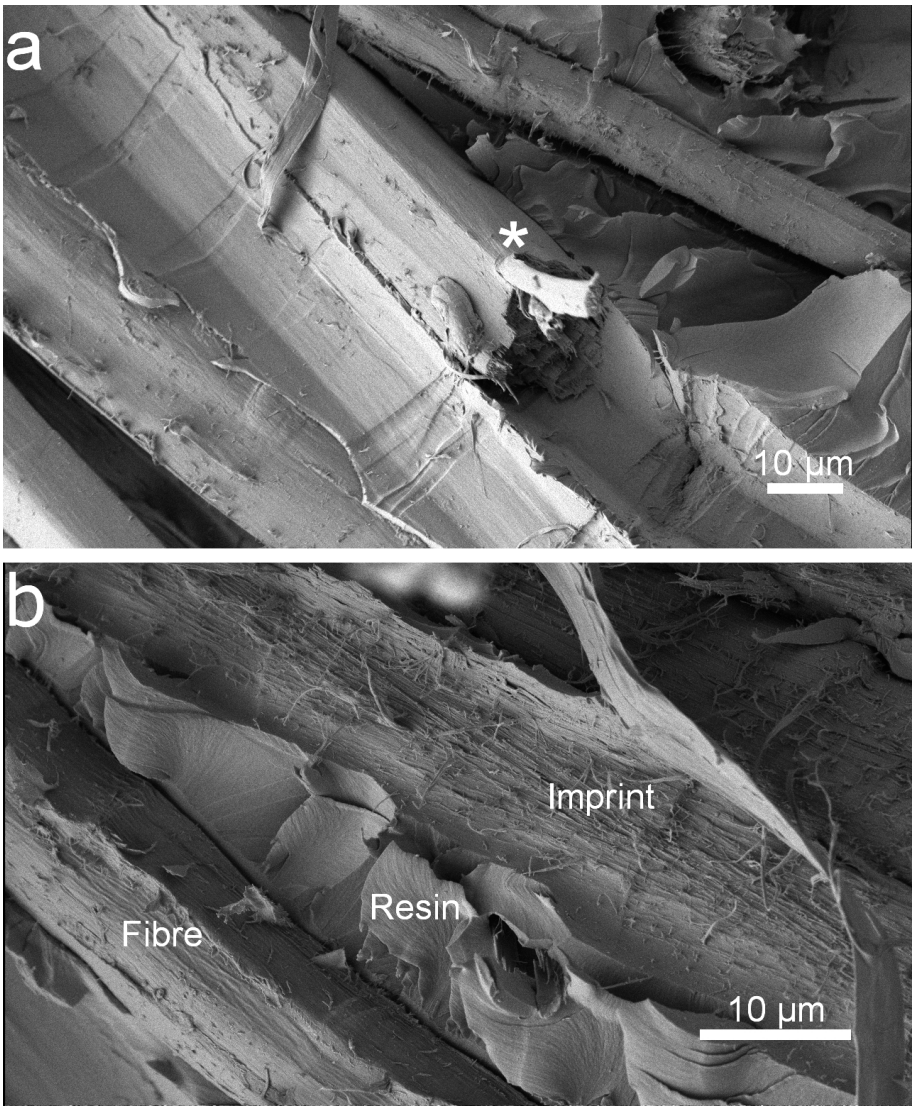

Figure 5.15: Scanning electron micrographs of fractured surfaces of the flax fibre-reinforced composite (PG3 impregnated) showing (a) a broken but non-debonded fibre (marked with a star), leaving an imprint where the remainder of the fibre was removed; and (b) epoxy matrix with residual fibrous cell wall materials where a fibre was torn out during fracture.

A FESEM image of a broken end of a flax fibre cell (Figure 5.16 (a)) shows concentric layers of macrofibrils and ribbons of fibrils pulled apart. This layered structure can be seen more clearly at higher magnification (Figure 5.16 (b)). The absence of an empty lumen indicated collapse of the fibre during processing, and was consistent with a mechanism for vibration damping that involves friction between layers of macrofibrils in cell walls, rather than energy loss involving cavities such as empty lumens. An earlier study attributed vibration damping, at least in part, to intra-cell wall friction, without being specific about the location of the moving parts within the cell wall [Duc et al., 2014].

5.3.8 Proposed damping mechanism of the polyol in flax fibre

In the stick-slip model for energy absorption in wood, weak interactions such as hydrogen bonds connect two adjacent cellulose microfibrils, in much the same way as the hooks and loops of Velcro® connect adjacent surfaces [Kretschmann, 2003, Keckes et al., 2003]. Water molecules may provide additional hydrogen bonds between the adjacent surfaces. However, moisture was a minor component relative to the glycerol or PG3 content of the polyol impregnated flax fibre in the present work. Each glycerol molecule has 3 hydroxyl groups, while the trimer of glycerol has 5 hydroxyl groups. Therefore, the polyols are able to form bridges of hydrogen bonds between the surfaces of cellulose microfibrils (Figure 5.17). It is proposed that the larger number of hydroxyl groups on the trimer increases the probability that a polyol molecule will hydrogen bond adjacent cellulose surfaces (Figure 5.17). Thus, the larger hydrogen bonding capacity of PG3 could be a possible reason for the increase in vibration damping compared with glycerol.

5.4 Conclusions

Oligomeric compounds impregnated into cellulosic fibres were shown to influence vibration damping of plant fibres alone and embedded in a polymer matrix (Chapters 4 and 5). These findings combined supported the hypothesis that vibration damping in plant fibre composites was enhanced by hydrogen bonding compounds

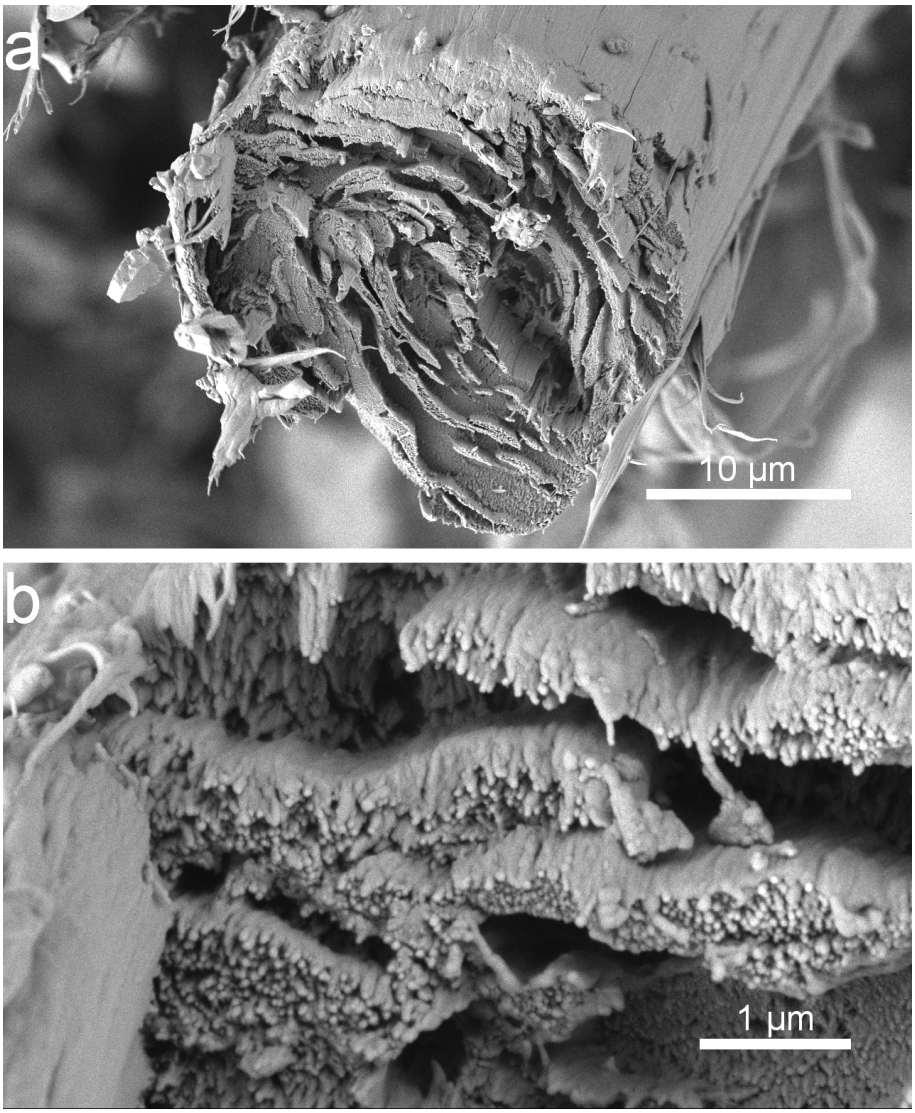

Figure 5.16: Scanning electron micrographs of fractured surfaces of the flax fibre-reinforced composite (No impregnated) showing (a) a broken end of a fibre cell, illustrating concentric layers of cell wall matter; and (b) individual cellulose microfibrils within layers.

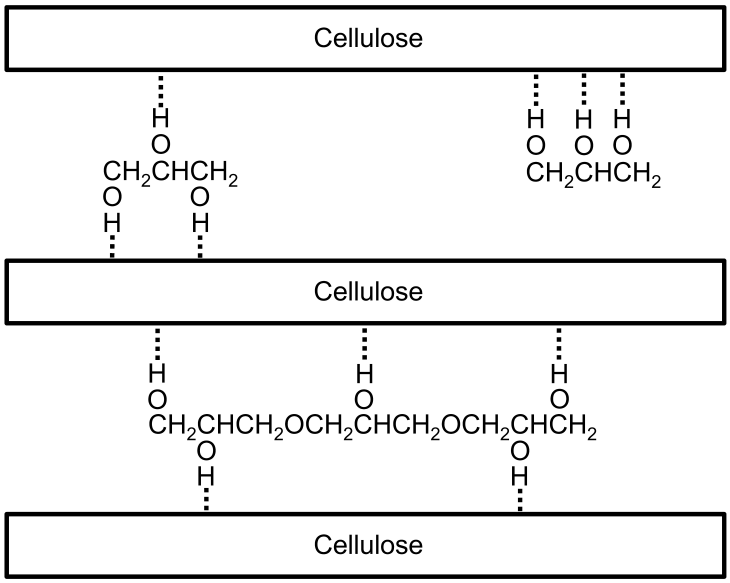

Figure 5.17: A schematic representation of glycerol (above) and a glycerol trimer (below) bridging gaps between cellulose microfibrils. Dotted lines represent hydrogen bonds.

that can break and reform in the cell wall.

There was no evidence of plasticiser released into the matrix at levels below 5% making polyol impregnation suitable for composite manufacture. PG3 performed better than glycerol in terms of the product stiffness and damping coefficient which was likely due to its larger molecular mass and larger number of hydroxyl groups.

The anhydride hardener reacted with plant fibre surfaces as a compatibiliser that explained the higher thermal stability of the impregnated flax composites and ruled out damping caused by poor fibre-matrix interface.

When considering stiffness and damping, the order of highest to lowest performance at room temperature was aramid, carbon, flax impregnated with oligomers and then untreated flax composite. However, this ranking changed with increasing frequency. Unlike aramid or carbon fibre composites, damping in flax composites increased with frequency.

In terms of commercial product development, if high damping is required with modest stiffness, flax fibre is an ideal candidate especially considering the low cost of flax fibres compared to carbon or aramid fibres. Carbon fibre is however undoubtedly superior where stiffness is the only requirement. Aramid combines both stiffness and damping properties, yet aramid fibre composites would be expensive and require particular tooling for post-processing (e.g. metal saw for cutting) which make the use of these fibres very targeted.

Both performance in terms of stiffness and damping is required in sporting equipment (e.g. racquets, bike frames, snowboards). Thus, the compromise of properties offered by single fibre type composites is limiting in these applications. A possible way to tailored the required properties is to combine different types of fibres to make hybrid composites. Hence, Chapter 6 focused on the properties of hybrid composites and their compromise between stiffness and damping.

Chapter 6

Stiffness and damping in plant fibre hybrid composites

6.1 Introduction

Chapter 5 showed that polyol treated flax fibres improved the damping coefficient of a laminate reinforced with such fibres. It was also observed that the improvement in damping lead to a decrease in stiffness and strength. Despite the potential of plant fibres composite in vibration damping applications [Gomina, 2012, Duc et al., 2014], the loss in ultimate tensile strength and stiffness is a problem restricting the utilisation of plant fibres to non-structural applications [Wambua et al., 2003, Summerscales et al., 2010].

The low strength of plant fibre composites can be mitigated by hybridisation of natural and man-made fibres especially carbon fibres[Van Raemdonck, 2008, Dhakal et al., 2007, Jawaid and Khalil, 2011, Nunna et al., 2012, Fiore et al., 2012, Dhakal et al., 2013, Angrizani et al., 2014]. Carbon fibres improve the required specific strength of the overall composite, while plant-fibres enhance vibration damping [Van Raemdonck, 2008, Fiore et al., 2012, Dhakal et al., 2013]. The partial replacement of carbon fibre by flax fibre in a bicycle frame is reported to decrease vibration up to 20% [Gomina, 2012], however very little data is available to compare the stiffness-damping trade-off of such hybrid composites.

The aim of Chapter 6 was to study the trade-off in carbon-flax hybrid com-

posites in terms of elastic modulus and damping coefficient. Hybrid composite laminate were manufactured using different ratios of carbon to flax fibre. A hybrid rule of mixtures equation was used to modelled the trade-off in properties.

6.2 Experimental procedures

6.2.1 Materials

The resin system and composite manufacture were similar to those described in Chapter 5. A brief summary is presented below but for further details, refer to Section 5.2.3, Chapter 5. The resin system was based on diglycidyl ether of bisphenol A (DGEBA) and methyl-tetrahydrophthalic anhydride. The catalyst was methyl-imidazole and the ratio of resin:anhydride:catalyst was 100:87.5:1.5 per hundred of resin. The flax 2/2 twill and carbon 2/2 twill had an area density of 420 g m^{-2} and 240 g m^{-2}, respectively. One composite was reinforced with flax hopsack fabric purchased from the same supplier and had an area density of 500 g m^{-2}. Hopsack weave is a variation of a plain weave where two or several yarns in both the warp and weft direction are woven side by side. The resin was mixed at room temperature and degassed for 1 h. The plies were impregnated and pre-cured separately at 105 °C for 10 minutes. The preform was then stacked, in a cross-ply configuration and pressed under vacuum from room temperature to 110 °C using a 30 tons hydraulic hot press (Siempelkamp, Krefeld, Germany). The post cure was done at 110 °C for 24 h and at 150 °C for an additional 5 h. The combination of laminate configurations are given in Table 6.1. The carbon volume content was calculated by dividing the thickness of the composite by the total number of ply. The mean thickness of one carbon-epoxy and flax-epoxy ply were 0.256 and 0.743 mm respectively. Specimens were cut from the panels for mechanical property characterisation and conditioned for at least two weeks at 23 °C and 50% relative humidity prior to testing.

Table 6.1: Laminate configuration and carbon-epoxy volume content in the hybrid composite.

Laminate configuration [a]	Carbon volume content
$[0_F/90_F/0_F]$	0
$[0_F/90_F/0_F]$ [b]	0
$[0_F/90_C/0_F/90_F/0_F/90_C/0_F]$	0.10
$[0_F/90_C/0_F]_s$	0.15
$[0_F/90_C/0_F/90_C/0_F]$	0.19
$[0_F/90_C]_s$	0.26
$[0_C/90_F]_s$	0.26
$[0_C/90_C/0_F/90_C/0_C]$	0.58
$[0_C/90_C/0_C/90_C/0_C]$	1

[a] F=Flax, C=Carbon

[b] Hopsack flax weave. All others fabric were 2/2 twill weave

6.2.2 Quasi-static mechanical properties of the hybrid composites

Quasi-static mechanical tests were performed to measure the tensile and flexural strength of the hybrids and compare the value of the elastic modulus with those measured by acoustics. 5 to 8 specimens from each panel were cut in 220 × 25 mm dimensions for tensile testing and 5 to 10 specimens were cut in 100 × 12.6 mm for 3-point bending testing. All static properties were determined on an Instron universal machine with load cell of 10 kN with the exception of the carbon hybrid in tensile mode. Due to the higher strength of the carbon hybrids, these specimens were tested on an Instron with a 40 kN load cell. The 3-point bending tests were carried out at a displacement rate of 1.1 mm min^{-1} following the standard ASTM D790-10 [ASTM D790-10]. The tensile tests were carried out using a 25 mm gauge length extensometer and a displacement rate of 2 mm min^{-1} following the standard ASTM D3039/D3039M-14 [ASTM D3039/D3039M-14]. In the case of the carbon-hybrid, the tensile strain was measured using the displacement of the transverse and the initial gage length.

6.2.3 Acoustic property measurements

The acoustic test was carried out in the same way than Chapter 5. A brief summary is given below but for further details, refer to Section 5.2.5, Chapter 5. Each specimen was excited by an impulse, and the resulting vibration decay was recorded with a microphone plugged to an amplifier. Damping coefficients were calculated from the half-power bandwidth b of the fundamental resonance frequency. MOE were calculated in longitudinal and flexural mode using from Equations 6.1 and 6.2, respectively [Cremer et al., 2005, p 226] [Schmitz and Smith, 2011, p 310]:

$$E_l = 4\rho L^2 f^2 \tag{6.1}$$

$$E_f = \frac{48\pi^2 \rho L^4 f_n^2}{(\beta_n L)^4 h^2} \tag{6.2}$$

where ρ was the density in kilograms per unit volume, L and h were the length

and the thickness of the beam in meter respectively, f_n was the resonant frequency at n mode, $\beta_n L$ was the constant associated with the n^{th} flexural mode ($\beta_1 L$=4.73, $\beta_2 L$= 7.853, $\beta_3 L$= 10.996, $\beta_4 L$=14.137 etc.)

6.3 Determination of the ROHM between stiffness and damping coefficient using acoustics properties

A composite material exhibits mechanical properties that are intermediate to those of the reinforcement and matrix component taken separately. These properties can be approximated by using a rule of mixtures (ROM). Similarly, composites that are reinforced with two different types of reinforcement generally will show intermediate properties to the composites based on a single type of reinforcement. The elastic properties of such composites can be predicted successfully using a rule of hybrid mixtures (ROHM) (Equation 6.3) [Venkateshwaran et al., 2012, Zhang et al., 2013]. The ROHM considers the matrix combined with each reinforcement and assumes that no interaction arises between the different reinforcing components [Czigany, 2005].

$$\begin{aligned} P_h &= P_a V_a + P_b V_b \\ V_a &+ V_b = 1 \end{aligned} \tag{6.3}$$

where P_h is the property of the hybrid, P_a and P_b are the individual properties of the composites reinforced with fibre of either type a or b and V_a and V_b are the volume fractions of composite a or b relative to the hybrid. A positive or negative hybrid effect in hybrid composites is defined as a positive or negative deviation of the experimental values from that predicted by the rule of hybrid mixtures [Marom et al., 1978].

6.3.1 Longitudinal mode

The elastic modulus of the laminated hybrid composites was calculated using the ROHM (Equation 6.4) through characterisation of longitudinal vibrations.

$$E_l = \sum_i V_i E_i \tag{6.4}$$

where E_l was the MOE determined in longitudinal mode and V_{fi} is the volume ratio of component i relative to the total volume content with $\sum_i V_i = 1$. The subscript i refers to i^{th} type of fibre.

In the present study, two types of fibre (carbon and flax) were used in the hybrid and Equation 6.4 could be written as:

$$E_l = (E_C - E_F)V_C + E_F \tag{6.5}$$

E_F and E_C were the longitudinal stiffness of the single fibre type composites (F= Flax, C= Carbon) and V_C was the carbon volume content.

Similarly to Chapter 5, Section 5.1.1, the parameter used to describe vibration damping was the damping coefficient (η), which was defined as the amount of energy dissipated over one radian of a vibration cycle relative to the total stored energy [Ungar and Kerwin, 1962].

Previous studies have approximated damping in polymer composites to the viscoelasticity of the matrix [Pothan et al., 2003]. Further work on damping in composites materials have investigated the contributions of the fibres in reinforced composites and shown that the fibres contribution is not negligible [Vantomme, 1995, Zhang and Chen, 2006, Berthelot and Sefrani, 2007]. The damping contribution of the alone fibres embedded in a polymer is difficult to estimate since it depends on the architecture of the reinforcement, fibre-matrix interface and voids fraction. The ROHM has the advantage of considering the hybrid as a proportion of the single fibre composites which encompasses the interface, reinforcement structure and void content. Ungar and Kerwin described the damping in terms of energy concepts such that, damping in lightly damped structures, is a function

of the energy stored in the constitutive elements of the structure [Ungar and Kerwin, 1962]. When applying this concept to different components using the rule of hybrid mixtures, the damping of the composite can be written as

$$\eta_l = \frac{\sum_i \eta_i U_i}{U_l} \tag{6.6}$$

where η is the damping coefficient and U is the elastic energies stored. The subscripts l and i relate to the hybrid composite and composite part reinforced with fibre i respectively.

If the strain is assumed to be evenly distributed between the different composite fractions and all fractions behave in their linearly elastic range, then Equation 6.6 can be written as a function of the elastic moduli:

$$\eta_l = \frac{\sum_i \eta_i E_i V_i}{E_l} \tag{6.7}$$

When applied to carbon and flax fibres hybrids in this work, Equation 6.7 became:

$$\eta_l = \frac{E_C\eta_C - E_F\eta_F}{E_l} V_C + \eta_F \frac{E_F}{E_l} \tag{6.8}$$

The dependence between stiffness and damping could be expressed by combining Equations 6.5 and 6.8 to eliminate V_C variable. The relation between E_l and η_l was then expressed as:

$$\eta_l = \frac{E_F(E_F\eta_F - E_C\eta_C + \eta_F(E_C - E_F))}{E_C - E_F} \frac{1}{E_l} + \frac{E_C\eta_C - E_F\eta_F}{E_C - E_F} \tag{6.9}$$

6.3.2 Flexural mode

The in-plane flexural modulus (E_f) depends on the stacking sequence of the different laminae and the rule of mixtures must take into account the laminate configu-

ration. The flexural modulus of a hybrid laminate can be determined by classical lamination theory (CLT) using the properties of each laminae. The CLT assumes that the laminae are perfectly bonded together, beam thickness is much smaller than its lengths along edges, displacements are small compared to the beam thickness and through-thickness strains are negligible [Tsai and Hahn, 1980].

E_f of a hybrid beam is then calculated using Equation 6.10 [Tsai and Hahn, 1980]:

$$E_f = \frac{12}{h^3\ d_{11}} \tag{6.10}$$

where E_f is the flexural modulus of the hybrid composite, h is the total thickness of the laminate and d_{11} is the flexural compliance of the laminate in kN m^{-1}. d_{11} takes into account the position of the laminae relative to the midplane of the laminate [Tsai and Hahn, 1980].

In this study, the stiffness was similar in both direction of the weave, the laminates were symmetrical and no plies were orientated off-axis. Equation 6.10 could then be simplified and written as:

$$E_f = \frac{8}{h^3} \sum^{h/2} E_i(z_i^3 - z_{i-1}^3)) \tag{6.11}$$

where z represented the upper and lower coordinates of the layers of either the carbon or the flax.

Furthermore, when applied to carbon-flax composite laminate, in the case where the hybrids had a core/skin configuration (Figure 6.1) and the carbon was located on the outer layers, Equation 6.11 could be written as:

$$E_f = (E_F - E_C)\,(1 - V_C)^3 + E_C \tag{6.12}$$

with $V_C \equiv$ 1 - z/h.

When the carbon was located in the core layers of the laminate, Equation 6.11 became:

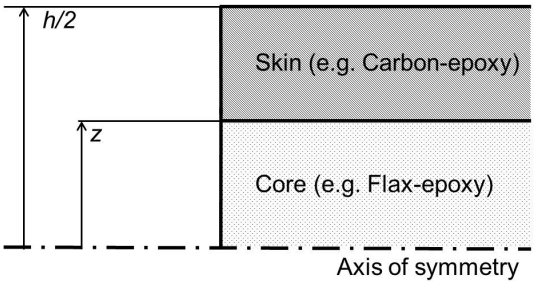

Figure 6.1: Skin-core configuration of a hybrid laminate.

$$E_f = (E_C - E_F)\, V_C^3 + E_F \tag{6.13}$$

with $V_C \equiv z/h$.

Similarly to the MOE, the damping coefficient of a hybrid laminate could be determined using a modified rule of mixtures [Hoa and Ouellette, 1984]. Hoa and Ouellette reported the corresponding rule of mixtures presented by Equation 6.14 as a function of the damping coefficients and flexural stiffness of the different laminae, and the flexural stiffness of the hybrid ([Hoa and Ouellette, 1984]).

$$\eta_f = \frac{8}{h^3 E_f} \sum^{h/2} E_i \eta_i (z_i^3 - z_{i-1}^3) \tag{6.14}$$

where η_f was the damping coefficient of the hybrid in flexural mode, η_i was the damping coefficients of the single fibre type (i) composite in flexural mode.

When the carbon was located on the outer layers, Equation 6.14 could be written as:

$$\eta_f = \frac{(E_F \eta_F - E_C \eta_C)(1 - V_C)^3 + E_C \eta_C}{(E_F - E_C)(1 - V_C)^3 + E_C} \tag{6.15}$$

When the carbon was located in the core layers, Equation 6.14 could be expressed as:

$$\eta_f = \frac{(E_C\eta_C - E_F\eta_F)V_C^3 + E_F\eta_F}{(E_C - E_F)V_C^3 + E_F} \tag{6.16}$$

The expressions of the trade-off could be determined by combining Equations 6.12 and 6.15 for the carbon located on the outer layers and Equation 6.13 and 6.16 for the carbon located in the core layers.

The trade off between could be described with Equation 6.17 for the carbon on the outer layers and Equation 6.18 for the carbon in the core layers:

$$\eta_f = \frac{E_C(E_C\eta_C - E_F\eta_F + \eta_C(E_F - E_C))}{E_F - E_C}\frac{1}{E_f} + \frac{E_F\eta_F - E_C\eta_C}{E_F - E_C} \tag{6.17}$$

$$\eta_f = \frac{E_F(E_F\eta_F - E_C\eta_C + \eta_F(E_C - E_F))}{E_C - E_F}\frac{1}{E_f} + \frac{E_C\eta_C - E_F\eta_F}{E_C - E_F} \tag{6.18}$$

Equations 6.17 and 6.18 showed that the trade-off between stiffness and damping was independent of the ply configuration layout whether the carbon or the flax was on the outer plies. Similarly, when comparing these expressions to Equation 6.9 in longitudinal mode, the equations were also found equivalent.

6.4 Results and discussion

6.4.1 Comparison of the MOE determined by quasi-static and acoustic testing

Value of MOE obtained by static and acoustic tests were similar (Table 6.2). The tensile modulus was slightly larger when measured by acoustic testing, as expected for measurements at a shorter characteristic time, i.e. 1/f = 0.2 ms for longitudinal vibrations, compared with 1/f = 12 ms for flexural vibrations (Table 6.2). In general, the apparent value of the elastic modulus is higher when measured by a dynamic technique, relative to a static technique due to the contribution of

viscoelastic processes having characteristic times similar to that of the test duration [Divos and Tanaka, 2000]. The composite reinforced with flax hopsack weave exhibited similar values of moduli and damping coefficient compared to the 2/2 twill weave-reinforced composite, indicating, in this study, no influence of the weave type in the flax composite.

Further comparison for determining the variation of the elastic modulus using DMTA, acoustic and quasi-static test are presented in Appendix I, that confirmed an equivalence of ± 8% in the different methods for measuring the elastic modulus.

Table 6.2: Comparison of static and acoustic moduli on epoxy reinforced with flax fabric. Numbers in brackets are 95% confidence interval.

Flax	Longitudinal test		Flexural test	
twill	Static	Acoustic	Static	Acoustic
n [a]	8	5	5	5
f_1 [b] (Hz)	NA	5399 (11)	NA	84.8 (0.8)
$E(GPa)$	7.9 (0.9)	8.6 (0.1)	6.4 (0.3)	6.3 (0.1)

[a] n=Number of tested specimens
[b] f_1= First resonant frequency

6.4.2 Stiffness-damping trade-off in longitudinal mode using hybrid rule of mixtures on flax-carbon composites

The variation of E_l increased linearly as a function of carbon-epoxy content and was successfully fitted with Equation 6.5, showing a root-mean-square deviation (RMSD) of 2.6 GPa (Figure 6.2). The ROHM indicated that for each percent of added carbon-epoxy fraction to the hybrid, the stiffness increased by 0.4 GPa (Figure 6.2). These results were consistent with those of Zhang et al. who performed similar experiments on the glass-flax hybrid laminates [Zhang et al., 2013]. They reported that the rule of hybrid mixtures was appropriate to determined the

influence of the glass-epoxy content in the laminate. The corresponding ROHM indicated 0.2 GPa increase per percent of added glass-epoxy fraction [Zhang et al., 2013].

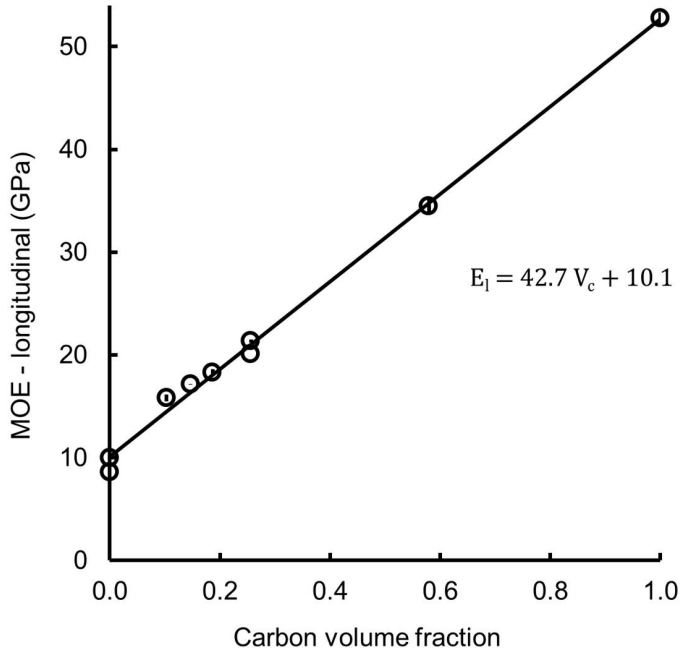

Figure 6.2: MOE in longitudinal mode as a function of carbon volume fraction. The black line represents the hybrid rule of mixtures. The error bars represent the 95% CI.

The variation of η_l determined in longitudinal mode was decreasing non-linearly as a function of carbon-epoxy content. The experimental data points were successfully fitted with Equation 6.8 displaying a RMSD of 0.0007 (Figure 6.3). Between 0 to 20% of carbon content, the damping coefficient decreased by half the original value of flax only composite. Conversely, above 60% of carbon content, no significant increase in damping coefficient was noticeable (Figure 6.3).

When plotting the stiffness as a function of the damping coefficient, the relationship of the hybrid carbon-flax composite could be described by using Equation 6.9 (Figure 6.4). The results indicated that, for low to medium stiffness hybrids (10 to 20 GPa), the loss of damping coefficient was significant. A 20 to 25% increase in stiffness resulted in more than 50% drop in damping coefficient.

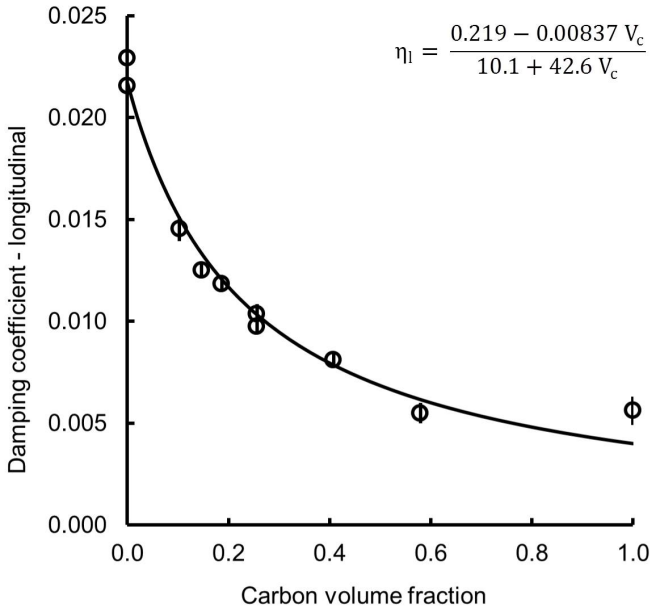

Figure 6.3: Damping coefficient in longitudinal mode as a function of carbon volume fraction. The black curve represents the hybrid rule of mixtures. The error bars represent the 95% CI.

Conversely for the hybrids with higher stiffness (≥25 GPa), a 10% diminution in the damping coefficient resulted in a 50% increase in stiffness (Figure 6.4).

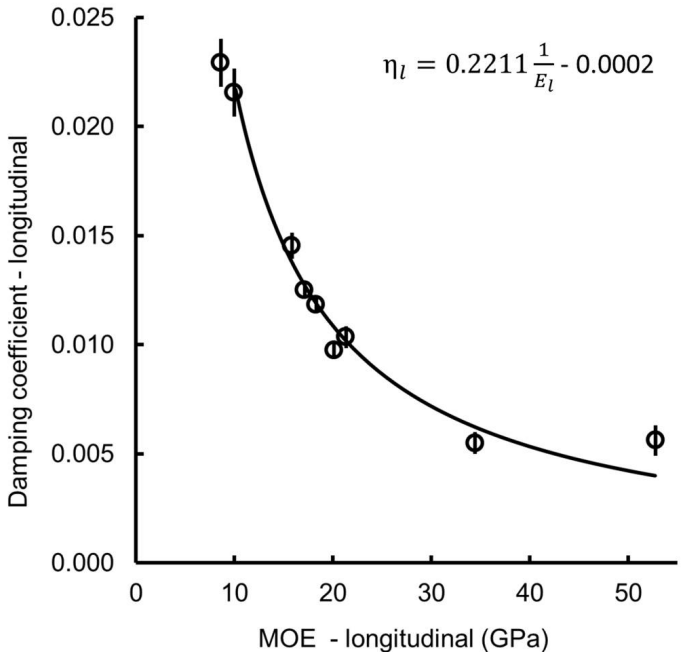

Figure 6.4: Damping coefficient as a function of MOE determined in longitudinal mode. The error bars represent the 95% CI.

6.4.3 Stiffness-damping trade-off in flexural mode using hybrid rule of mixtures on flax-carbon composites

The variation of E_f increased differently as a function of carbon-epoxy content depending on the layout of the hybrid laminate (Figure 6.5). The experimental data points and 2 ROHM presented on Figure 6.5 corresponded to laminate configurations where either the carbon or flax fibres reinforced laminae were located as the outer plies of the hybrid laminate.

In both cases, the experimental data points were consistent with the rule of hybrid mixtures (Equations 6.12 and 6.13). Some composites had an alternative carbon-flax laminate configuration that, for clarity purpose, are not shown graphically but are presented in Table 6.3. The addition of 10 vol. % of carbon ply

on the outer surface of a laminate leads to an increase of around 300% in flexural stiffness. Conversely, at higher fraction of carbon on the outer surface, the variation of stiffness was minor between a hybrid laminate containing 60 vol.% of carbon ply and a laminate of carbon only (Figure 6.5). Similarly, Subagia et al. reported an increase of only 15% in stiffness between a carbon-basalt hybrid laminate, containing 69 wt. % of carbon on the outer surface, and a 100 wt. % carbon laminate [Subagia and Kim, 2013]. When the flax plies were located on the outer surface of the laminate the trend was reversed and larger quantities of carbon were required to improve the stiffness.

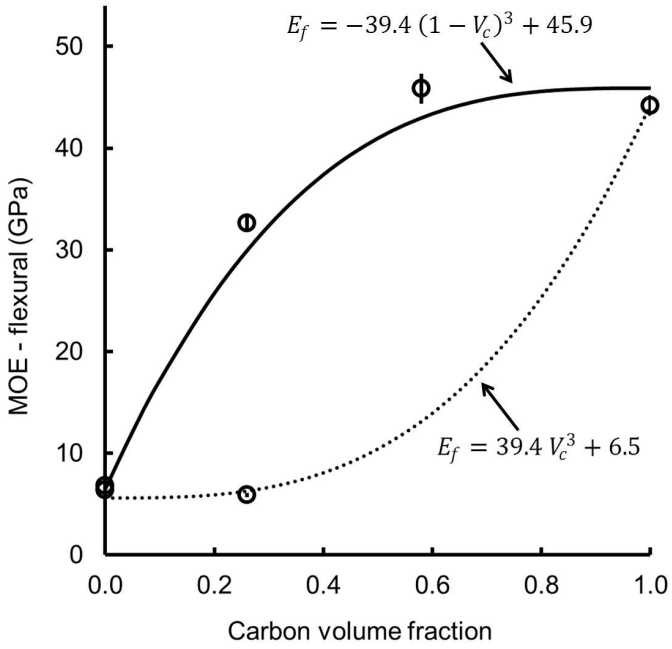

Figure 6.5: MOE in flexural mode as a function of the carbon volume content. The black line represents the carbon on the outside, the dotted line represents the flax on the outside. The error bars represent the 95% CI.

Similarly to the flexural stiffness, the variation of damping coefficient also depended on the ply configuration. The two ROHM models were successfully used to express the non-linear variation of damping coefficient with carbon volume content (Equations 6.15 and 6.16).

Layout configurations where flax and carbon alternated successively were tested

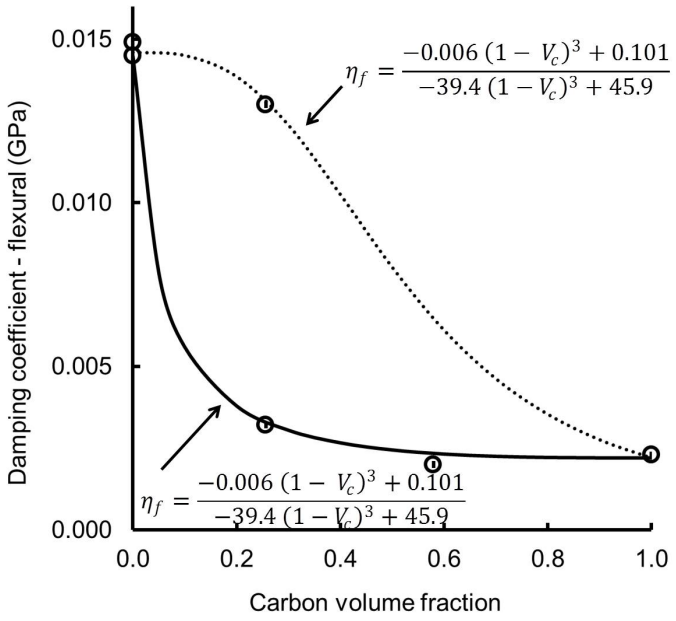

Figure 6.6: Damping coefficient in flexural mode as a function of the carbon volume content. The black line represents the carbon on the outside, the dotted line represents the flax on the outside. The error bars represent the 95% CI.

and were found to have flexural stiffness and damping coefficient located in the area delimited by the two ROHM (Table 6.3). Dorigato et al. reported the flexural stiffness of carbon-basalt hybrid laminates with alternated plies that were consistent with the present work [Dorigato and Pegoretti, 2012].

Table 6.3: Additional data on alternated carbon-flax laminae configuration.

	Elastic Modulus (GPa)			Loss coefficient		
Ply sequence	Model (GPa)	Exp (GPa)	Variation (%)	Model	Exp	Variation (%)
$FC(F)_3CF$	12.8	14.9	16.4	0.0077	0.0087	13.0
$FC(F)_2CF$	11.6	12.2	5.2	0.0085	0.0091	7.1
FCFCF	10.0	9.9	1.0	0.0098	0.0101	3.1

The trade-off between stiffness and damping in flexural mode was not as straight forward as in longitudinal mode in terms of carbon volume content. Indeed, similar carbon fraction could lead to very different mechanical properties depending on the ply configuration (Figures 6.5 and 6.6) [Tsai and Hahn, 1980]. However, when considering the damping coefficient as a function of stiffness, the experimental points were in good agreement with the ROHM determined using Equations 6.11 and 6.14 and also comparable with the longitudinal mode results as expected from the theory section (Figure 6.7). The higher the damping in flexural mode, the lower the flexural stiffness of the laminate. Similarly, Akash et al. observed a 15% increase in the damping coefficient of jute-sisal hybrid laminate compared to jute only laminate that was attributed to a decrease in stiffness [Akash et al., 2013].

6.4.4 Comparison of MOE and damping coefficient between man-made and flax-fibre laminates

The correlation between specific stiffness and damping coefficient was studied by Ono et al. and Bremaud et al. for different species of wood [Ono and Norimoto,

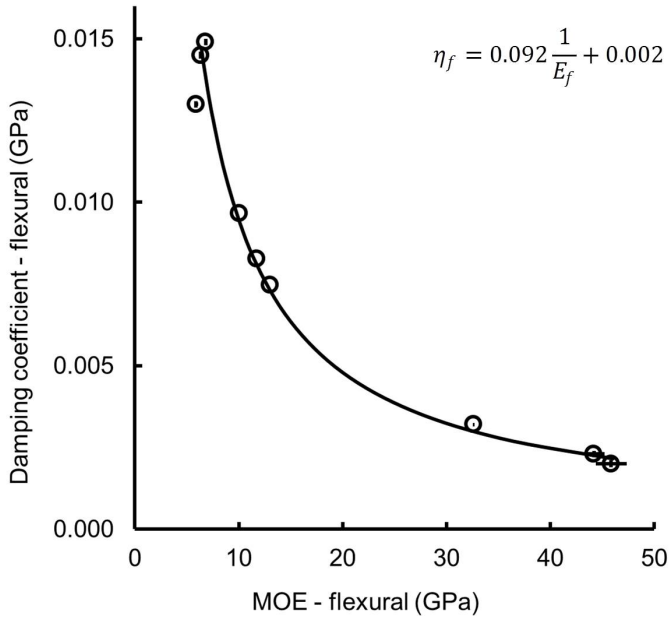

Figure 6.7: Damping coefficient as a function of MOE determined in flexural mode. The error bars represent the 95% CI.

1983, Bremaud et al., 2010]. They fitted arbitrarily decreasing power law functions to describe the shape of curves [Ono and Norimoto, 1983, Bremaud et al., 2010]. In this present work the damping stiffness relationship was expressed successfully with a ROHM using the properties of the single fibre type reinforced composites. The trade-off between properties showed an equivalence in longitudinal and flexural mode.

Thus, when adding flax fibres to increase the damping coefficient of a composite laminate, the goal is to also to minimise the decrease in MOE that could be described as maximising the product $E\eta$. The higher the product, the better the trade-off in the hybrid laminate. When searching for a hybrid combining stiffness and damping properties, it is also possible to rank the single fibre-type reinforced composites using their Eη products .

A study of epoxy resin reinforced with cellulosic fibres quantified the damping property of the composite using the logarithm decrement in flexural mode [Buksnowitz et al., 2010]. The logarithm decrement corresponded to value of damping coefficient of 0.019, 0.018, 0.022 and 0.0022 for flax, hemp, regenerated cellulose,

and glass fibre-reinforced epoxy composites, respectively (Equation 2.6). Concurrently, Buksnowitz et al. reported the corresponding MOE values of 12, 23, 16 and 24 GPa (for flax, hemp, regenerated cellulose, and glass fibre-reinforced epoxy composites, respectively). The product Eη of these composites indicated that in terms of compromise between stiffness and damping, hemp (0.41) performed the best, then regenerated cellulose (0.35), then flax (0.23) and finally glass (0.05) [Buksnowitz et al., 2010]. The product Eη of some of the epoxy composites tested in this work were calculated for resin, aramid, glass, European flax and carbon (Table 6.4). The highest Eη was found for aramid, carbon, flax, glass and resin alone.

In some applications, as for example, maximising the flexural stiffness and vibration damping of a snowboard, the utilisation of hybrid composites is necessary. By comparing Eη of selected laminae and using the ROHM, the hybrid laminates stiffness and damping can be modelled, hence tailored to meet standards in specialised applications.

Table 6.4: Summary of $E\eta$ using the first resonant frequency for the neat resin and composites reinforced with the flax, carbon and aramid fibres.

Ply type	Fibre Volume fraction	Longitudinal		Flexural	
		E η (GPa)	Variation (GPa)	E η (GPa)	Variation (GPa)
Resin	NA	0.108	0.028	0.069	0.003
Aramid	0.52	0.444	0.012	0.470	0.030
Glass	0.50	0.079	0.009	0.098	0.004
Flax	0.40	0.193	0.008	0.108	0.003
Carbon	0.55	0.223	0.055	0.348	0.01

6.4.5 Influence of the carbon content in the tensile and flexural strength of the hybrid composites

Values of the tensile and flexural strength were compared for all composites and plotted versus the carbon volume content (Table 6.5, Figures 6.8 and 6.9). In both the tensile and flexural strength, the relationships looked to be of similar type to the MOE variation with carbon ply content, suggesting that tensile and flexural strength could probably be modelled using a ROHM.

The tensile strength varied linearly with the relative carbon ply content (Figure 6.8) which could be fitted with a ROHM showing a RMSD of 15 MPa (Equation 6.19).

$$\sigma_l = (\sigma_C - \sigma_F)V_C + \sigma_F \tag{6.19}$$

σ_F and σ_C were the flexural strength of the single fibre type composites (F= Flax, C= Carbon) and V_C was the carbon volume content.

The compliance of the tensile strength for hybrid laminates to the ROHM was consistent with literature. Similar trends were found for unidirectional flax/glass fibre composite where the tensile strength of hybrid composites increased linearly with glass content [Zhang et al., 2013].

The flexural strength of hybrid composites was tentatively fitted using a ROHM in past studies [Stevanovic and Stecenko, 1992, Dorigato and Pegoretti, 2012, Subagia and Kim, 2013]. However, the discrepancy between the model and experimental results indicated that the ROHM was not appropriate for fitting the flexural strength of a hybrid laminate. Stevanovic and Stecenko reported that the flexural strength of glass-carbon hybrid laminate varied between 43.6 to 120.5% of the ROHM predicted flexural strength [Stevanovic and Stecenko, 1992]. Similarly, Dorigato et al. found that the flexural strength of some carbon-basalt hybrids deviated from more than 50% from the modelled ROHM [Dorigato and Pegoretti, 2012].

When using the experimental data of the single fibre-type reinforced laminate in the ROHM. The value of flexural strength for the carbon located on the outer

layers varied up to 15% from the theoretical value, indicating a poor fit and a negative hybrid effect (Figure 6.9). The flexural strength data point for the carbon located in the core plies matched the theoretical value, however due to the lack of additional data points, no conclusions other were drawn.

$$\sigma_f = (\sigma_F - \sigma_C)\,(1 - V_C)^3 + \sigma_C \tag{6.20}$$

with $V_C \equiv 1$ - z/h, for the carbon located on the outer layers.

And:

$$\sigma_f = (\sigma_C - \sigma_F)\,V_C^3 + \sigma_F \tag{6.21}$$

with $V_C \equiv$ z/h, for the carbon located in the core layers.

Table 6.5: Laminate configuration and carbon/epoxy volume content in the hybrid composite

Laminate configuration [a]	Tensile strength (MPa)	Flexural strength (MPa)
$[0_F/90_F/0_F]$	62.8 (4.4)	113.0 (1.9)
$[0_F/90_C/0_F/90_F/0_F/90_C/0_F]$	130.7 (13.6)	234.7 (11.4)
$[0_F/90_C/0_F]_s$	162.8 (11.6)	248.4 (7.9)
$[0_F/90_C/0_F/90_C/0_F]$	168.8 (21.7)	249.4 (6.8)
$[0_F/90_C]_s$	214.3 (18.1)	130.9 (3.9)
$[0_C/90_F]_s$	163.5 (11.8)	380.3 (16.5)
$[0_C/90_C/0_F/90_C/0_C]$	329.9 (22.1)	583.6 (36.9)
$[0_C/90_C/0_C/90_C/0_C]$	516.4 (59.4)	741.4 (42.9)

[a] F=Flax, C=Carbon

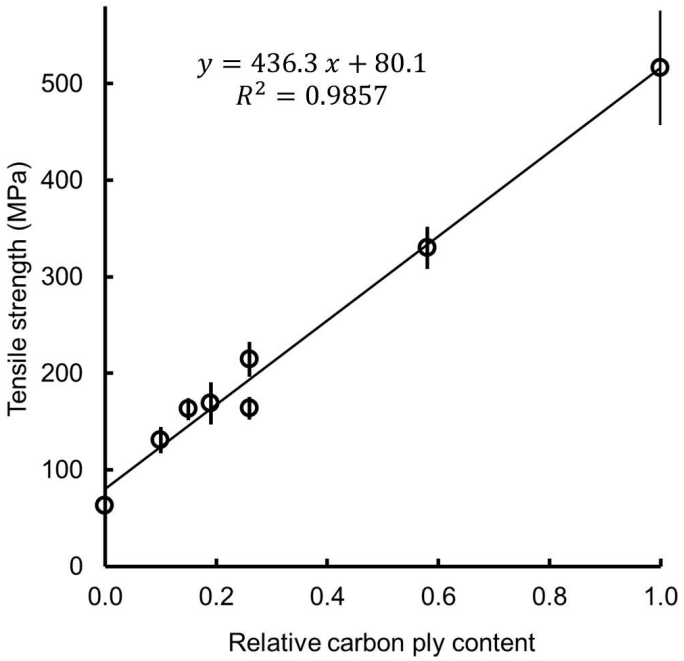

Figure 6.8: Variation of the tensile strength as a function of the carbon ply content. The black line represents the ROHM model.The error bars represent the 95% CI.

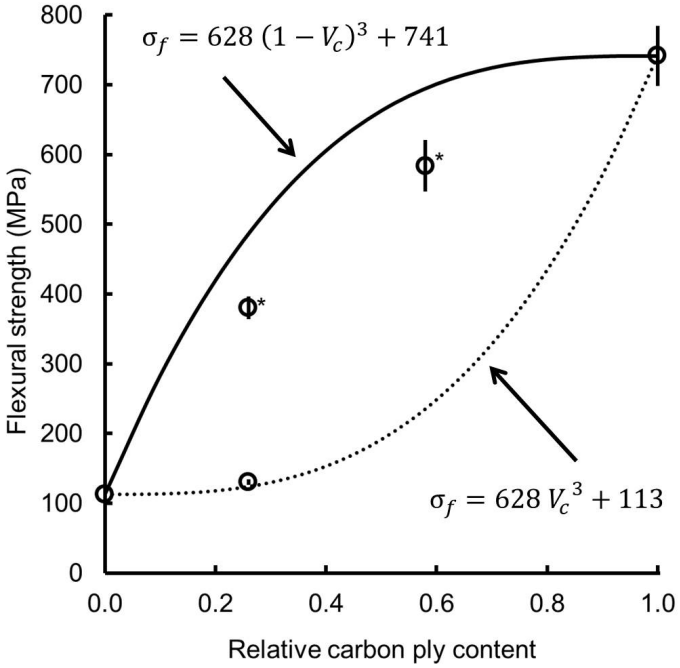

Figure 6.9: Variation of the flexural strength as a function of the carbon ply content. The black line represents the ROHM for the carbon on the outside, the dotted line represents the ROHM for the flax on the outside. The 2 asterisks indicate the laminates containing carbon on their outer layer. The error bars represent the 95% CI.

6.5 Conclusions

Plant fibres in composite reinforcement have become popular due their potential vibration damping properties [Gomina, 2012]. However, their low stiffness and ultimate strength limit their commercial application on their own and encourage the utilisation of hybrid composite such as man-made fibres (e.g. carbon or glass) to mitigate the loss in stiffness and strength [Vanwalleghem, 2010]. Stiffness and damping are antagonist properties and increasing one is generally to the detriment of the other one [Lakes, 2002]. But depending on the material property, architecture, the trade off between stiffness and damping can vary significantly [Lakes, 2002, Bremaud et al., 2010].

In Chapter 6, carbon flax hybrids were manufactured and the stiffness, strength and damping coefficient were studied. In longitudinal mode, the MOE increased linearly as the carbon content increased, and the damping coefficient decreased non-linearly. In flexural mode, the influence of the carbon volume content depended on the layout configuration. In both longitudinal and flexural mode, the experimental data points were successfully fitted with a ROHM. When plotting the damping coefficient as a function of MOE, the damping coefficient displayed a decreasing trend with increasing MOE that was equivalent in longitudinal and flexural mode and could be described by the combinations of ROHM.

The compliance of the experimental data points to the models indicated that the trade-off in stiffness and damping coefficient of hybrid laminates could be predicted and tailored from their single fibre-type properties. The maximisation of the trade-off could be expressed as a maximisation of the $E\eta$ product which depended on the fibre/matrix system of the single-fibre type laminae. Buksnowitz et al. found that $E\eta$ of composite reinforced with hemp fibres was higher than European flax, indicating that hemp maybe more suited than European flax in applications where both stiffness and damping are required [Buksnowitz et al., 2010].

Similar models could be applied for modelling the tensile strength of hybrid laminates, however the ROHM was inaccurate in flexural mode and overestimated the flexural strength at high level of carbon volume content.

Chapter 7

Conclusions

The scope of the thesis was to quantify the damping property of plant fibres used in composite materials and understand the mechanisms that are associated with damping. The hypothesis was that hydrogen bonding of the different chemical compounds (e.g. hemicellulose, cellulose) within the cell wall of the fibres facilitates vibration damping in plant fibres composite. The hypothesis was validated based on the experimental observations on plant-fibres alone and plant-fibre embedded in a composite matrix.

7.1 Summary of the findings

The investigation began with the characterisation of selected plant fibres in terms of origin, morphology, chemical composition, physical and mechanical properties (Chapter 3). Due to the inter-relations between factors, principal component analysis was undertaken to group together factors of similar effect. Damping was found to be positively correlated with high hemicellulose content fibres. No relationship could be found in this study between damping and the amount of water absorbed by the fibres in a conditioned state at 50% RH.

The angle of the cellulose microfibrils was shown not to have an influence on the damping coefficient of plant fibres but was strongly correlated to their toughness under quasi-static load. The relationship between toughness and MFA was successfully modelled using a second order polynomial fit.

Damping has been related to the moisture absorbed by the hemicellulose that involves hydrogen bonding interactions. In Chapter 4, the utilisation of hydrogen bonding capable polyols to replace water and enhance damping was investigated with and without a prior pre-treatment. The polyols increased the high damping coefficient of technical harakeke fibre. Fibres impregnated with polyglycerol had a higher damping coefficient than glycerol. While impregnation with polyol increased the damping coefficient, the stiffness of the fibres was decreased. The molecular interaction between the polyglycerol and hemicellulose was investigated by NMR. The motion of the hemicellulose (monitored using the acetyl group) was found to be intermediate between oven-dried and water saturated fibres. The latter observation indicated that similarly to water, polyglycerol acted as a plasticiser changing the motion of the hemicellulose that could be then be correlated to an increase in damping.

Chapter 5 confirmed the damping improvement of polyol impregnated flax fibres whilst being in an epoxy resin. At levels below 5 wt. %, polyglycerol was more effective than glycerol in improving vibration damping of composites. The experimental results were consistent with polyglycerol forming hydrogen-bonded bridges between concentric layers of cell-wall matter and causing friction between the two layers through stick-slip molecular motion. The polyols were then proposed to act as micro-dampers within the cell wall that can break and reform due to the hydroxyl groups present in the fibre. The acoustic and DMTA results also demonstrated that damping of flax-fibre reinforced composites increased with increasing frequency in contrast to carbon and aramid fibre-reinforced composites. The reasons put forward were that: (i) vibrational energy is dissipated by the heterogeneity of the hierarchical plant fibre structure (e.g. cellulose fibril, single cell, technical fibres) that do not transfer stresses as well as man-made fibres which are single continuous medium, (ii) molecular viscoelastic mechanisms of the different molecular size polyols that vibrate at different frequencies and potentially increase damping with increasing frequency.

Stiffness and damping were shown to be antagonist properties. The final experimental Chapter was focused on describing the trade-off between stiffness and damping by investigating the properties of carbon-flax hybrids. The two properties were found to follow accurately the ROHM both in longitudinal and flexural

mode as a function of carbon-epoxy volume content. However, the relationship between stiffness and damping was shown to be independent of the configuration layout of the composites.

7.2 Future work

The thesis has shown that hydrogen bonding capable compounds influenced the damping of plant fibre-reinforced composites.

The comparison between glycerol and polyglycerol as additives, encouraged investigation of polyglycerols with higher molecular weight, or perhaps other linear polymers bearing hydroxyl groups at intervals along their length.

Additional MFA characterisation (e.g. Nikau, raffia) at the Australian Synchrotron WAXS beam line, would be of interest to strengthen the toughness and microfibril angle relationship.

Unlike wood, the lack of relationship between microfibril angle and damping coefficient in the selected plant fibres suggested that damping in wood could have been caused by a change of chemical composition and not a variation of MFA. Further investigations on different species of wood could be undertaken, reaffirming that hemicellulose content is strongly related to damping.

Additional liquid state NMR study of impregnated fibre bundles in non-polar solvent at different concentration could potentially give information on the polyol saturation levels.

Further DMTA tests could bring further understanding of the hemicellulose chemical interactions at temperatures subzero and their implication in damping. Preliminary investigations on harakeke fibres showed that stiffness changed gradually with temperatures from -10 to 40 °C without any sharp transitions at 0 °C or around 20 °C. It would be of interest to compare the damping coefficient of the selected fibres under the T_g of the hemicellulose and under the freezing point of water.

Appendix A

Damping measurements

A.1 Damping measurement under free oscillation

The equation of movement that characterises vibration can be described as a mass-spring-damper system with 1 degree of freedom as shown on Figure A.1 adapted from [Clough and Penzien, 1980, pp. 41-42].

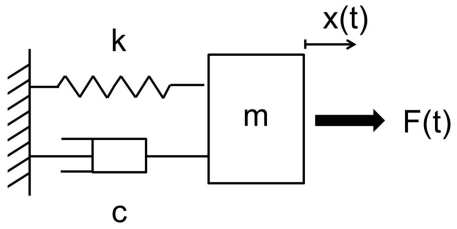

Figure A.1: SDOF with viscous damping.

where x(t) is the displacement, c is the damping constant of the viscous response, m is the mass and k is the stiffness constant of the elastic response. The equilibrium of the forces is given by Newton's second law :

$$F_m = F_c + F_s + F(t) \tag{A.1}$$

where, F_m is the contribution of the inertia force due to the mass (Equation A.2 (a)), F_c is the force caused by the damper and depends on the viscous constant of the damper ((Equation A.2 (b)), F_s is the force caused by the spring which depends on the stiffness of the spring ((Equation A.2 (c)). $F(t)$ is an outside force.

$$F_m = m\ \ddot{x} \tag{A.2a}$$
$$F_c = c\ \dot{x} \tag{A.2b}$$
$$F_s = kx(t) \tag{A.2c}$$

Using Equations A.2, Equation A.1 can be re-written as Equation A.3

$$m\ \ddot{x} = c\ \dot{x} + kx + F(t) \tag{A.3}$$

In the case of free oscillations where $F(t) = 0$, the solutions of the differential equation are of the form:

$$x(t) = A\ exp(-\xi\omega_0 t)\ sin(\omega_d t + \phi) \tag{A.4}$$

Where A and ϕ are integral constants depending on the initial conditions, ξ is the damping ratio, and ω_d is the pseudo frequency. Figure A.2 presents the graphical representation of the solution for an under-damped system.

The vibration damping parameters can be determnined using several methods. In the time domain, when considering two successive peaks from Figure A.2, the ratio of the two amplitudes is equal to

$$\frac{x_n}{x_{n+1}} = exp(2\pi\xi\frac{\omega}{\omega_D}) \tag{A.5}$$

Taking the natural logarithm of Equation A.5, the logarithmic decrement Δ is

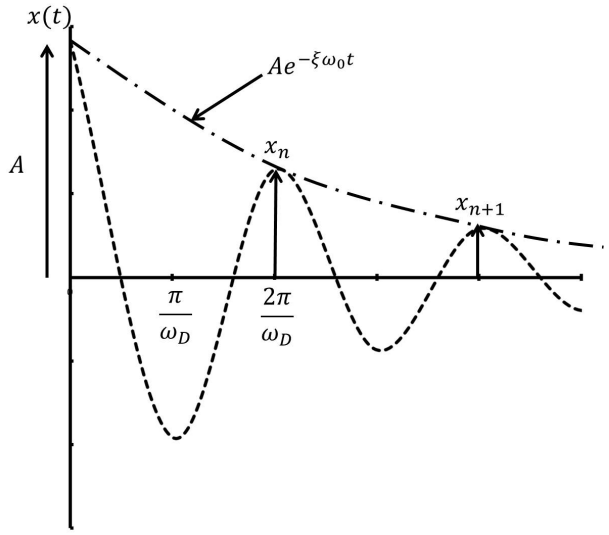

Figure A.2: Under-damped free oscillations.

equal to:

$$\Delta = ln\frac{x_n}{x_{n+1}} = 2\pi\xi\frac{\omega}{\omega_D} \tag{A.6}$$

where

$$\frac{\omega}{\omega_D} = \frac{1}{\sqrt{1-\xi^2}} \tag{A.7}$$

At small level of damping, Equation A.7 can be approximated to:

$$\delta \sim 2\pi\xi \tag{A.8}$$

In the frequency domain, the level of damping can be measured using the shape of the resonant peak and the half-power bandwidth b (Figure A.3).

The damping coefficient is calculated using Equation A.3:

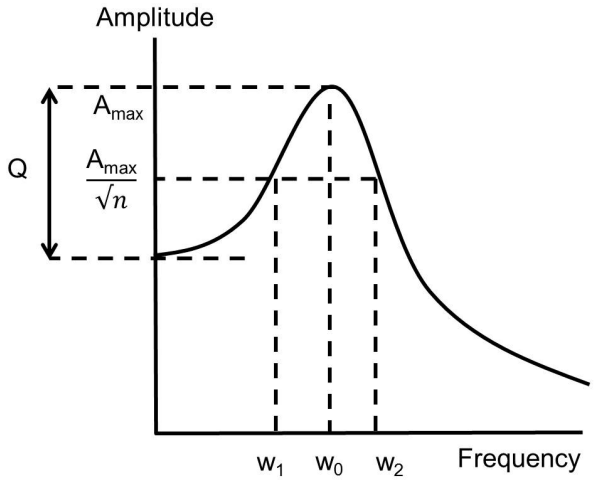

Figure A.3: Half-power bandwidth method of the resonant peak.

$$\eta = C \, \frac{(w_2 - w_1)}{w_0} \tag{A.9}$$

where

$$C = \frac{1}{\sqrt{n^2 - 1}} \tag{A.10}$$

When $n^2 = \sqrt{2}$, $\eta = b/w_0$

Appendix B

Fibre extractions

B.1 Harakeke fibre extraction

Harakeke or *Phormium Tenax* fibres were harvested in July 2011 and 2012 in Rotorua. The fibres consist of parallel strands of sclerenchym cells that lie parallel to the keel of the leaf but overlap each other in a spiral clockwise manner giving the leaf flexibility and toughness [Wehi, 2007, Richter et al., 2011]. Sclerenchyma tissue is associated with the mechanical properties of the plant. The cells in that tissue developed a lignified secondary cell wall which gives strength and rigidity to the fibres to withstand compressive stress [Jarvis, 2005]

The fibre cells differ if the they are extracted from the upped part of the leaf ("glossy") or the bottom part ("matt") as shown in Figure B.1. Maori used to collect only the upper part as it was considered as yielding the best quality fibres.

In order to have fibres free of defects, the fibres were hand-extracted. The fibres were extracted from 3 different locations (top, middle, bottom) and analysed for variation in chemical composition (Figure B.2). The fibres were extracted with a knife (Figure B.3), soaked in water to remove remaining cuticle and dried at room temperature (Figure B.4).

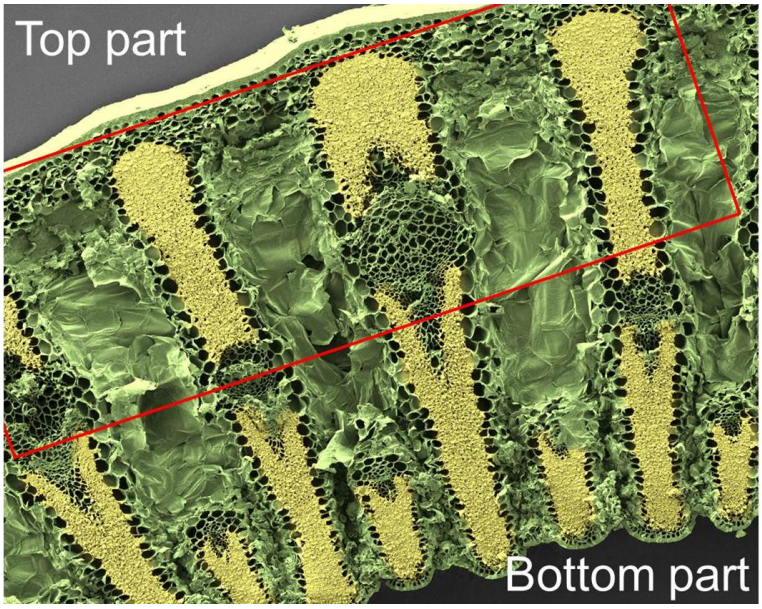

Figure B.1: FESEM of a harakeke leaf cross section, courtesy of Nancy Hati. The yellow sections represent the sclerenchym cells. The square rectangle shows the position where the fibres were of primary interest.

B.2 Other fibre sources

The flax, jute and coir fibres were used as received. The windmill palm fibres were sampled from the dry sheath (Figure B.5 (a)), the nikau fibres were extracted from the stalk (Figure B.5 (b)) and the raffia fibres were extracted from dried leaves that required soaking before extraction (Figure B.5 (c)).

Figure B.2: Harakeke leaves before hand-extraction: (a) harvested leaves around 2 m in length (b) first sectioning to remove the woody part (c) detailed sections ready for extraction.

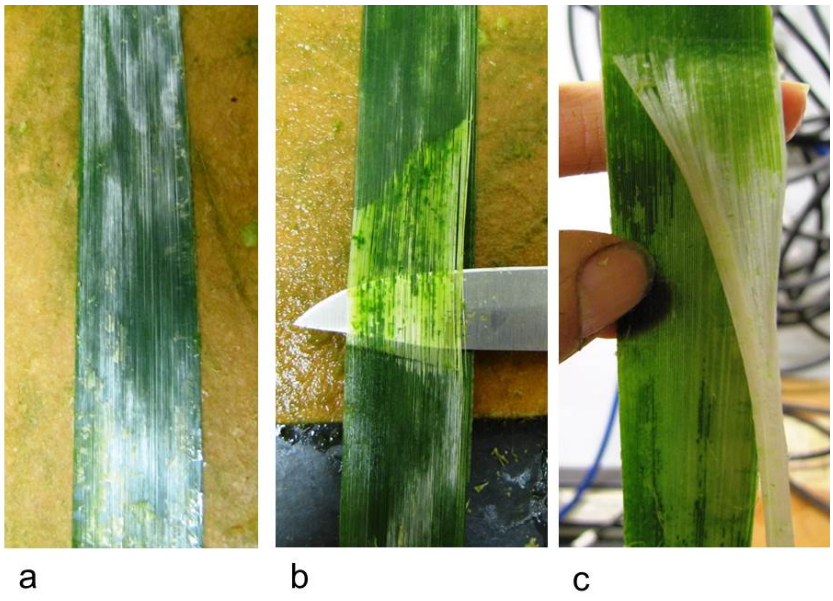

Figure B.3: Fibre extraction process: (a) the waxy surface layer is stripped with a knife blade (b) the fibre cells are lifted with the knife blade (c) The fibre bundles are detached from the rest of the leaf.

Figure B.4: Extracted fibres dried and ready for chemical characterisation. Each jar represents a zone in the leaf.

(a) Windmill palm tree trunk

(b) Nikau palm tree

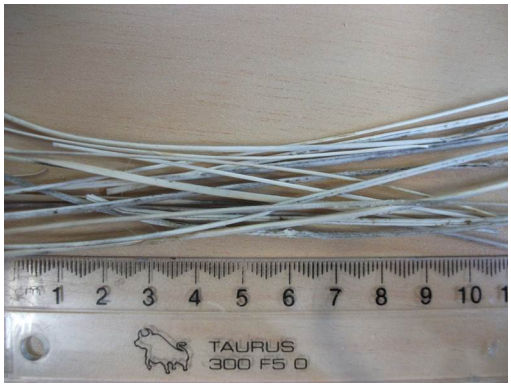

(c) Raffia

Figure B.5: Photographs of the fibre sources: (a) Windmill palm sheath fibres (b) nikau tree, the white arrow points to the section where the fibres where extracted (c) Raffia dried leaf.

Appendix C

DMTA method development

The accurate measurement of the damping coefficient of plant fibres required the determination of the linear visco-elastic range of the fibres and the assessment of the reproducibility over time (cycles).

C.1 Determination of the linear viscoelastic range of the plant fibres

The preliminary work was performed on harakeke fibres. Tension tests were performed using a 10 mm gage length using a pre-load to maintain the fibre and avoid clamping artefacts. The pre-load was calculated as a function of the linear mass (LM) using Equation C.1.

$$F_{preload} = k\ LM \tag{C.1}$$

where k is an arbitrary constant force per tex equal to 0.005 $Ntex^{-1}$.

Typically, a technical harakeke fibre exhibits a strain to failure to 10% strain with a linear region up to 0.5% strain. Thus the first experiment was to determine of the linear viscoelastic range using a strain amplitude sweep from 0.01 to 10% with a log sweep for rapid screening and a linear sweep for an accurate strain range at a frequency of 1 Hz. The linear viscoelastic range was defined as the range where the storage modulus remained constant as a function of strain amplitude

that corresponded to the range of 0.01 to 0.5% strain (Figure C.1).

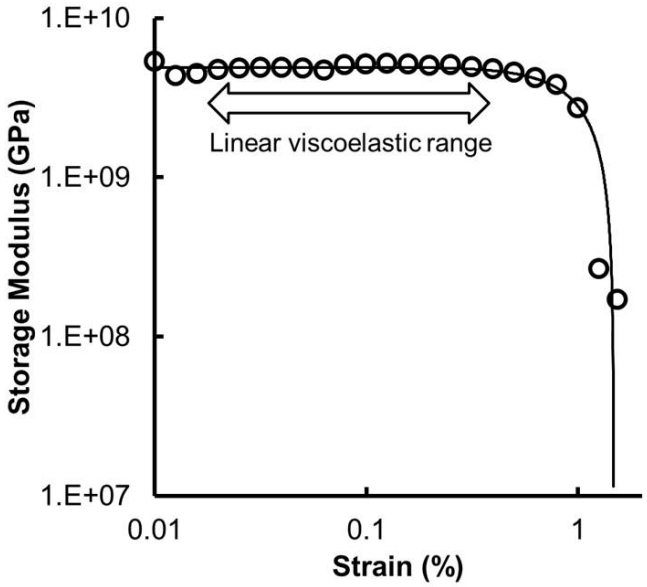

Figure C.1: Strain sweep

The second test was to determine if the damping coefficient of plant fibres was dependent of frequency from 0.1 Hz to 100 Hz. Strain amplitudes ranging from 0.04 to 0.5% were tested in frequency sweep (Figure C.2). At 0.1% strain amplitude and beyond, the strain is not maintained constant across the whole frequency sweep (Figure C.2). Thus, strain amplitude for determining the damping coefficient of fibres was limited to 0.05%.

C.2 Influence of the frequency sweep cycle on the damping coefficient

It was initially observed that the clamping geometries or misalignment of the fibre could cause an overestimation of the damping coefficient and a large scatter of results. Successive frequency sweep were performed until steady state response of the damping coefficient in order to compare the different fibre types (Figure C.3). 20 successive frequency sweeps were used for each fibre. The storage modulus and

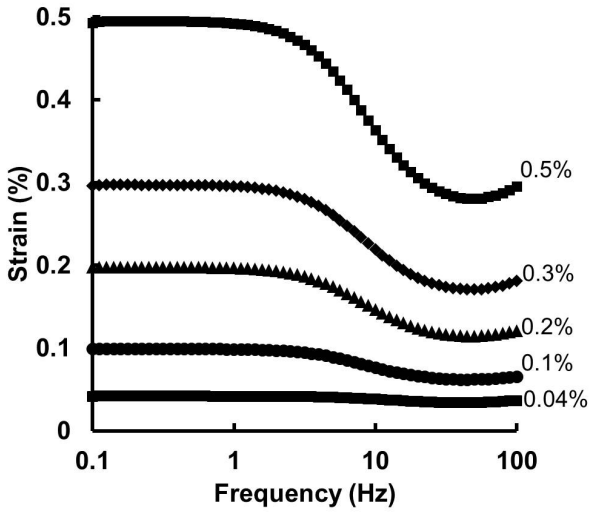

Figure C.2: Variation of strain amplitude during frequency sweep tests.

damping coefficient were then calculated by averaging between the 10^{th} to 20^{th} cycles.

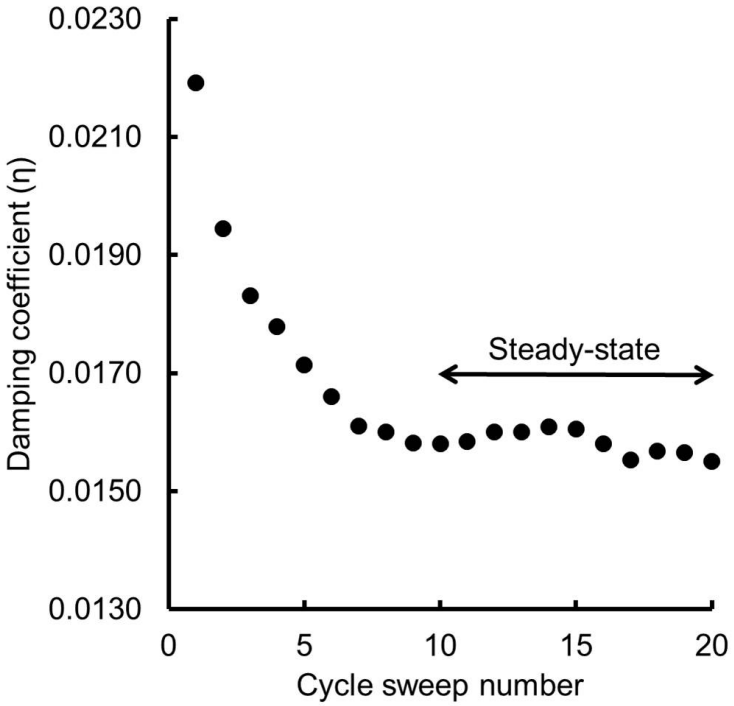

Figure C.3: Influence of the cycle number on the evolution of the damping coefficient.

Appendix D

Principle component analysis

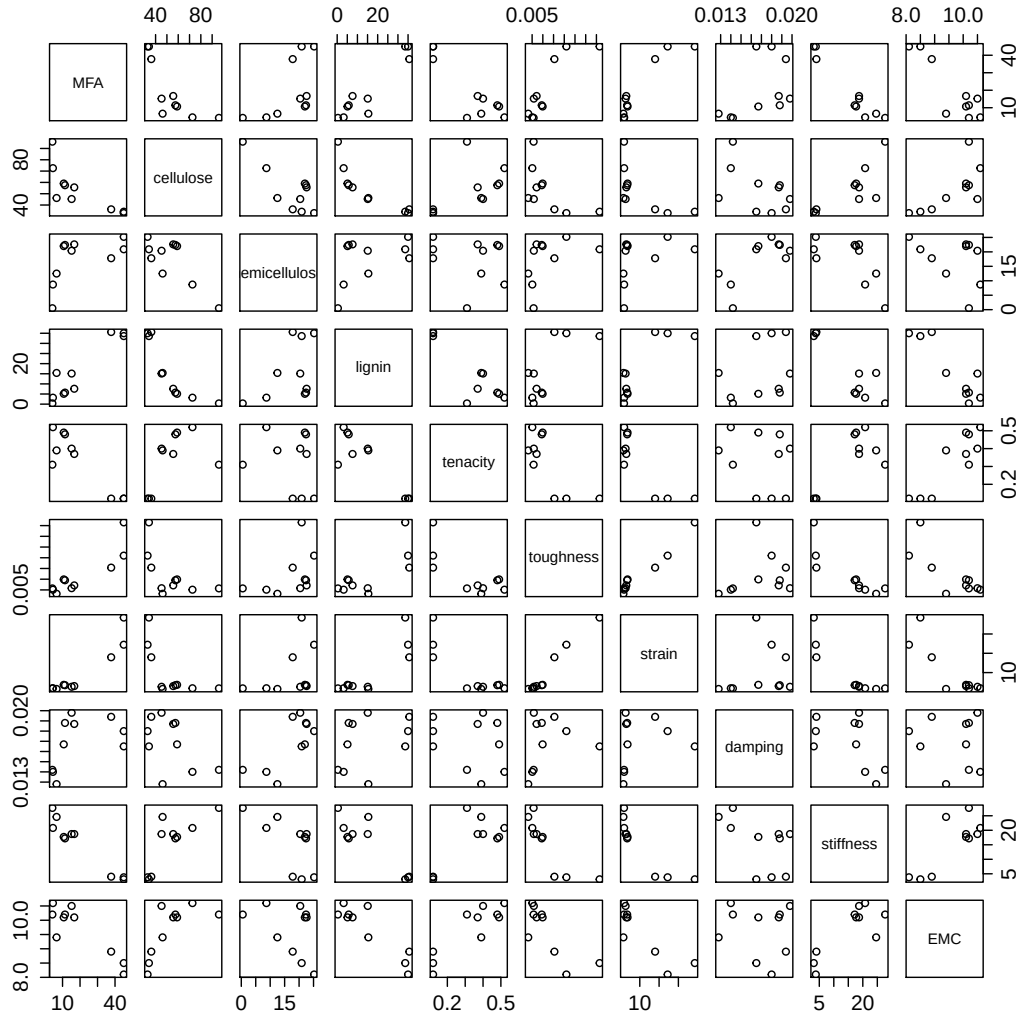

Figure D.1: Scatter plots of the 10 variables.

Table D.1: Coefficient of correlation matrix.

	MFA	cellulose	hemicellulose	lignin	tenacity	toughness	strain	damping	stiffness	EMC
MFA	1.00	-0.77	0.56	0.94	-0.89	0.87	0.93	0.46	-0.96	-0.89
cellulose	-0.77	1.00	-0.77	-0.85	0.55	-0.58	-0.64	-0.49	0.79	0.70
hemicellulose	0.56	-0.77	1.00	0.46	-0.19	0.42	0.39	0.73	-0.63	-0.37
lignin	0.94	-0.85	0.46	1.00	-0.88	0.75	0.85	0.35	-0.90	-0.90
tenacity	-0.89	0.55	-0.19	-0.88	1.00	-0.74	-0.84	-0.25	0.77	0.88
toughness	0.87	-0.58	0.42	0.75	-0.74	1.00	0.98	0.22	-0.84	-0.77
strain	0.93	-0.64	0.39	0.85	-0.84	0.98	1.00	0.21	-0.88	-0.86
damping	0.46	-0.49	0.73	0.35	-0.25	0.22	0.21	1.00	-0.53	-0.11
stiffness	-0.96	0.79	-0.63	-0.90	0.77	-0.84	-0.88	-0.53	1.00	0.80
EMC	-0.89	0.70	-0.37	-0.90	0.88	-0.77	-0.86	-0.11	0.80	1.00

Table D.2: Variance of principal components.

	Comp.1	Comp.2	Comp.3	Comp.4	Comp.5	Comp.6	Comp.7	Comp.8	Comp.9	Comp.10
Standard deviation	2.70	1.26	0.70	0.67	0.37	0.27	0.11	0.06	$\ll$0.001	$\ll$0.001
Proportion of variance	0.73	0.16	0.05	0.05	0.01	0.01	$\ll$0.001	$\ll$0.001	$\ll$0.001	$\ll$0.001
Cumulative proportion	0.73	0.88	0.93	0.98	0.99	$\approx$ 1.0	$\approx$ 1.0	$\approx$ 1.0	1.0	1.0

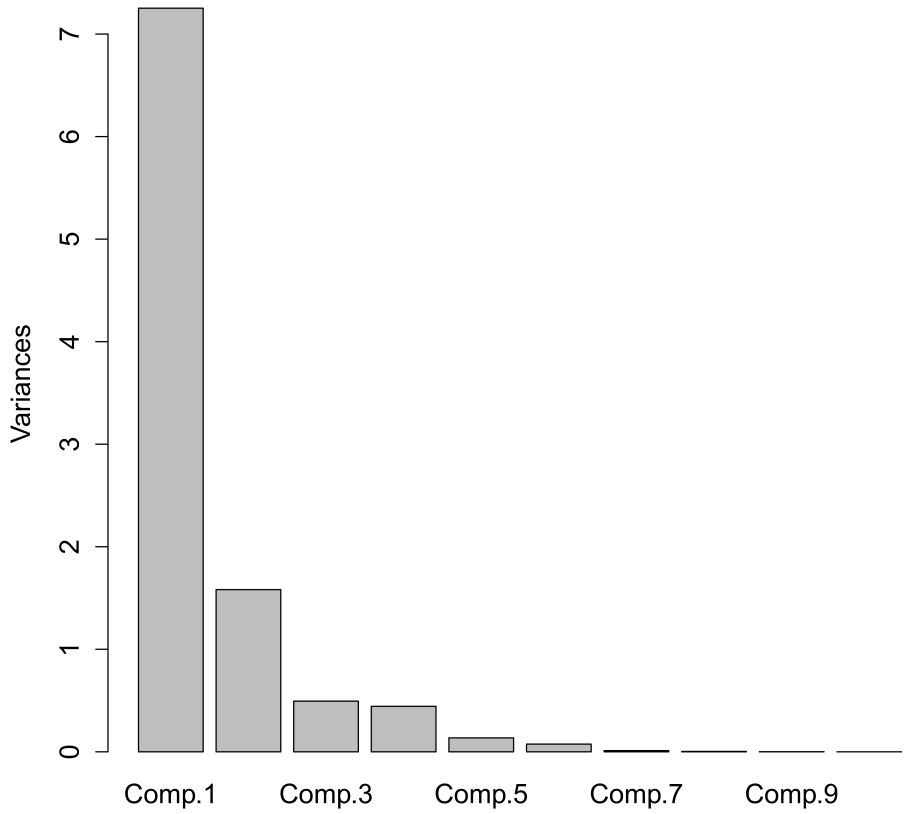

Figure D.2: Variance of each principal components.

Appendix E

Damping of plant fibres in immersion

E.1 Introduction

The aim of this study was to quantify the damping coefficient of non-wood cellulosic fibres immersed in water and correlate the results to those collected in Chapter 3. The fibres were immersion-tested in distilled water at 23°C, using the same methodology as that of Chapter 3.

E.2 Experimental procedures

E.2.1 Materials

The fibres were sampled from the same batch of materials that were used in Chapter 3. Polypropylene fibre from garden twine was used as a control to ensure the difference in damping was not due to fluid inertia. The fibres were left overnight at 23 °C in the immersion cell prior to testing to ensure complete water saturation. The EMC at 50% RH was measured using 5 g specimens with AD-4713 IR balance from A&D Ltd.

E.2.2 Thermogravimetric analysis

The water retention of the fibres after immersion was measured by TGA. A Q500 TA instrument was used to evaluate the amount of water contained in the specimen at saturation. Specimens were heated in platinum pans from 20 to 200 °C in air using a 10 °C/min ramp. 20-30 mg of material was cut in small segments to fit into the TGA pan and soaked overnight in distilled water. Prior to testing, the specimens were dabbed slightly with paper to remove excess water and tested immediately. The water retention value obtained was an average of 5 to 6 replicates.

E.2.3 Damping coefficient and storage modulus determination in water immersion

The damping coefficient and storage modulus were determined using the same test as described in Chapter 3, Section 3.2.5 with addition of an immersion cell. The DMTA immersion cell contained 30 ml of distilled water measured with a graduated syringe and was non-hermetically closed during the test to minimise evaporation. Segments of the technical fibres of 100 mm in length were tested in frequency sweep tensile mode on a RSA-G2 DMTA. The initial gage length was 10 mm. Consecutive frequency sweeps from 0.1 to 100 Hz were performed at 0.05% strain amplitude. Values of tan δ and force at 1 Hz were averaged from the 10^{th} et the 20^{th} frequency sweep to obtain the damping coefficient and storage modulus.

The storage modulus was calculated in Newton per tex as in Chapter 3. Tex is a linear mass unit and was function of the water content. Water absorption in cellulosic fibre influenced the dimensions and mechanical properties of the fibres up to the saturation point beyond which the cell walls cease swelling and the strength reaches a minimum [Berry and Roderick, 2005]. The content of water in the conditioned form was easily calculated by measuring the weight after oven drying. The content of water at saturation was more difficult to determine due evaporation. For consistency, the storage modulus was divided by the oven-dried linear tex of the fibres using the linear mass of conditioned fibres (23 °C, 50% RH) and the average moisture content (Table E.2).

E.2.4 Principal component analysis

The PCA was performed on average value of 6 variables using a correlation matrix. The variables were: cellulose, lignin, hemicellulose content, stiffness (immersed), damping (immersed) and water content at saturation. The same chemical composition results were used from Chapter 3. The PCA was interpreted using R studio version 0.98.945 (RStudio, Inc.) and the results compared with those of Chapter 3.

E.3 Results and discussion

E.3.1 Validation of the experimental set up using polypropylene

Polypropylene (PP) fibres were used as control in order to quantify any variation of tan δ caused by fluid inertia. Polypropylene is hydrophobic and its water absorption is around 0.01 wt. % (Suppliers data) which was considered negligible compared to cellulosic fibres. The increase in tan δ and E' were 2.9% and 9.5% respectively when the PP fibre was immersed in water (Table E.1). However, these values were within the 95% confidence interval of the experimental error and therefore, it was considered that the fluid did not significantly influence tan δ and E'.

Table E.1: Polypropylene damping coefficient and storage modulus results. The number in brackets is the 95% CI.

	50% RH	Immersed water	Variation (%)
Damping coefficient	0.0914	0.0940	2.9
	(0.003)	(0.002)	
Storage modulus	4.2	4.6	9.5
(GPa)	(0.5)	(0.4)	

E.3.2 Water retention in the fibres after immersion

The water content presented large differences between fibre types varying from 31.6 to 74.6 wt. % (Table E.2). The highest water content were found for the bast fibres (e.g. European flax, ramie), then leaf fibres (e.g. sisal) and last were the mesocarp fibres (e.g. coir).

Lower water absorption in coir fibres compared to the other types of fibre has been attributed to air chambers preventing the penetration of water [Symington et al., 2009] and high level of lignin [Müssig, 2010, p 210].

Table E.2: Moisture content in wt. % for conditioned fibres at 23 °C and 50% RH and immersed in water. The value in brackets is the 95% CI.

	Water content	
wt.%	after immersion	95% CI
European flax	74.9	8.1
Ramie	72.0	7.8
Jute	68.1	2.4
Raffia	40.1	5.2
Harakeke	61.0	9.7
Sisal	53.1	9.6
Nikau	50.7	4.7
Windmill palm	37.7	4.6
Coir 1	31.6	5.2
Coir 2	36.9	2.1

E.3.3 Damping coefficient and stiffness of the fibres in water immersion

The damping coefficient and storage modulus of fibres tested in immersion are presented in Table E.3.

Table E.3: Damping coefficient and storage modulus of the plant fibres tested in water immersion.

	Damping coefficient	Storage Modulus (N/tex)
European flax	0.0594 (0.0120)	27.5 (5.4)
Ramie	0.0297 (0.0033)	36.0 (6.0)
Jute	0.0318 (0.0080)	17.9 (5.5)
Raffia	0.0535 (0.0100)	24.2 (4.1)
Harakeke	0.0612 (0.0064)	20.5 (1.9)
Sisal	0.0537 (0.0086)	14.9 (3.3)
Nikau	0.0508 (0.0086)	10.6 (1.3)
Windmill	0.0253 (0.0015)	4.7 (0.5)
Coir 1	0.0279 (0.0021)	2.3 (0.5)
Coir 2	0.0289 (0.0025)	3.2 (0.2)

E.3.4 Correlation between variables using PCA for the immersed state

Similarly to Figure 3.12 (Chapter 3, Section 3.3.6), a strong positive correlation was found between water content, cellulose and stiffness, and a negative correlation was also observed with increasing lignin content (Figure E.1). The negative correlation with lignin supported the observations by Mark et al. and others stating that lignin protects the hydrophilic components of the cell wall [Mark, 1967, Symington et al., 2009].

Water was described as a lubricant between the cellulose microfibrils and the matrix in the cell wall of wood fibres [Hill, 2010]. In this present work, the water content was positively related to the cellulose content in the conditioned 23 °C and immersed state, that reinforced the possibility of water accumulation around the surface of the cellulose microfibrils. In contrast to the conditioned state, no correlation was observed between damping and hemicellulose. These results indicated that at 10 wt. % water or below, damping originated from viscoelastic mecha-

nisms that were not strongly correlated with the moisture content. Conversely, the damping coefficient increased when the water content was higher than 20-30% such that the motion of the water molecules contributed to damping (Figure E.2).

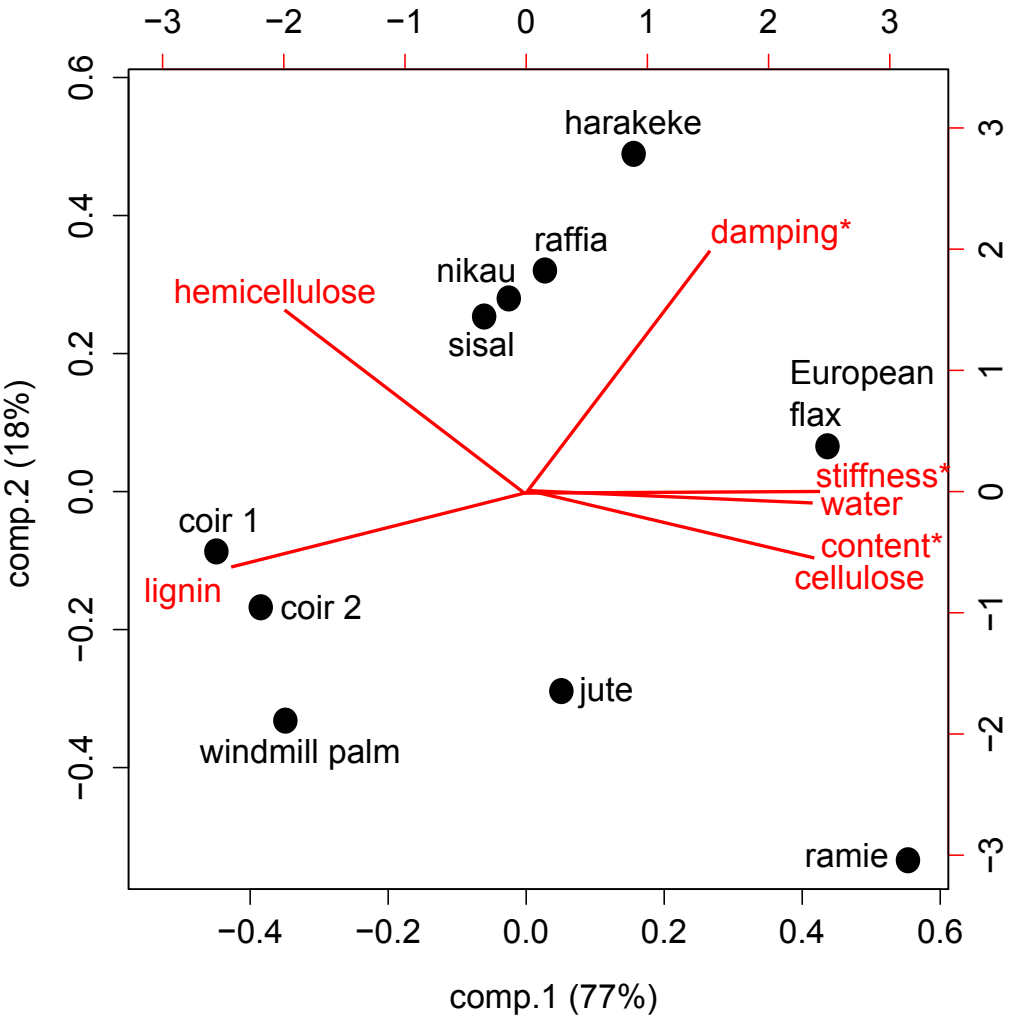

Figure E.1: Bi-plot of the variables (loading and scores) using principal component 1 and 2. The asterisk indicates variables measured in water immersion condition.

During a stress-strain test, high MFA fibres are matrix dominated in the elastic part of the test, hence it is expected that they should be more sensitive to moisture. However, due to the correlation between high MFA and high lignin content (and

subsequently low cellulose content), the increase in damping is low for high MFA fibre.

Most studies of the effect of moisture absorption in wood on vibration damping indicated that moisture increases the damping coefficient due to the presence of hemicellulose [Ebrahimzadeh and Bertilsson, 1998, Entwistle, 2005, Bremaud et al., 2010]. The hemicellulose content nor the type of hemicellulose influenced the variation in damping coefficient (Results not presented here).

E.3.5 Comparison between the conditioned and immersed state

From the PCA of the individual state, the moisture content was not changing the damping coefficient, however, the combination of the data from the conditioned and immersed state, indicated a linear upward trend when plotting the damping coefficient as a function of the water content in the fibres (Figure E.2).

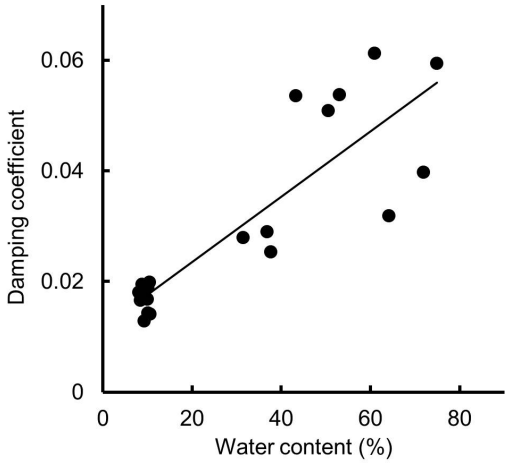

Figure E.2: Damping coefficient as a function of the water content (wt. %). $R^2 = 0.71$

The difference of tan δ and E' (Table E.3) between the conditioned state and immersed state were not the same across all fibre types and could not be explained by differences in water absorption alone. The increase in tan δ was particularly large for raffia, harakeke and flax fibres and lower ($\leq$75%) for coir and windmill

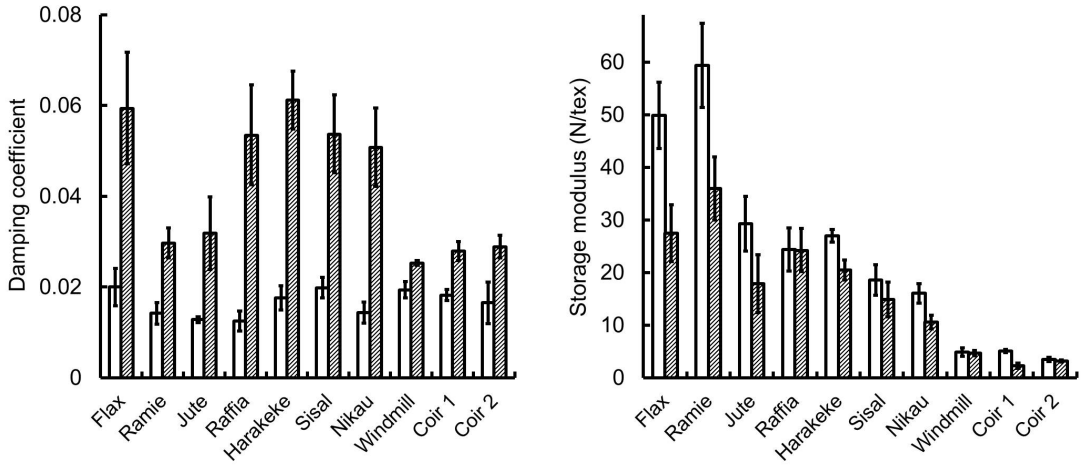

(a) (b)

Figure E.3: Properties of different fibre types immersed in water and conditioned at 23 °C, 50% RH. White bars are the conditioned values, diagonal grey bars are the immersed values. The error bars represent the 95% CI (a) damping coefficient (b) storage modulus

fibres, the increase was associated with the cellulose content that attracted more water.

All values of damping coefficient were higher than those measured in conditioned state (23 °C, 50% RH) in opposition to the storage modulus variation (Figure E.3 (a) and (b)). The water plasticised and softened the fibres, as it penetrated the cell wall, similarly to precedent studies on wood fibres [Ebrahimzadeh and Bertilsson, 1998, Entwistle, 2005].

E.4 Conclusions

In this study, the variation of damping between the water-saturated state and conditioned state was associated with the hydrophilicity of the cellulose microfibrils.

The influence of water content on the storage modulus and damping coefficient of different types of plant fibres was studied. It was observed that water acted as a plasticizer in the fibres and lead to an overall increase in damping and decrease in stiffness. This work also demonstrated in the scope of the investigated fibres,

that a hydration $\leq 10\%$, damping was not dependent on the water content, the chemical composition or MFA of the fibres.

However, trends were observed between the water content and damping when the fibres were immersed in water, with the cellulose and the lignin content being the influencing factors. No clear relationship was observed between the hemicellulose content and damping or stiffness properties.

Damping occurs via the combination of a plasticised matrix caused by moisture and motion of the water molecules. At low level of moisture ($\leq 10\%$), the damping coefficient was associated with hemicellulose content but no obvious trend was seen with water content. At higher moisture content, the hemicellulose was already fully plasticised and the influence of water did not affect further the hemicellulose while it did affect the other hydrophilic compounds (e.g. cellulose). In the immersed state, the fibres were saturated with water and the magnitude at which the absorbed water was penetrating the fibres was an antagonist combination of the cellulose attracting water and lignin preventing water absorption. In the immersed situation, damping was mainly due to dissipation caused by the motion of water molecules.

Appendix F

Influence of kink bands on the damping coefficient of flax fibres and their composites

F.1 Introduction

Debates on whether or not kink bands have an influence of the mechanical behaviour of plant fibres are non-conclusive. When the fibres are embedded in composites, Hughes et al. showed for unidirectional flax fibres that stresses accumulate around the kink bands of fibres [Hughes et al., 2002]. Baley showed for flax fibres that kink bands were the initiation point of failure during tensile tests [Baley, 2004].

Thygensen et al. published a study on the effect of tensile elongation of hemp fibre on kink bands. Similarly to Baley, they reported that the dislocations do not affect the MOR or MOE, but they also showed that dislocations have a viscoelastic behaviour [Baley, 2004, Thygesen et al., 2007]. After realignment of the kink bands under tensile deformation, when the stress is released, Thygensen et al. observed the reappearance of the kink bands partially after 2 weeks and fully after 1 month. The viscoelastic behaviour of kink bands indicates a promising research in terms of explaining the damping behaviour of plant fibres.

The hypothesis of this study was that kink bands act as dampers due to their

viscoelastic properties and were a main contributor to energy absorption in plant fibre composites.

F.2 Material and methods

European flax fibres were obtained from Ag Research (Christchurch, New Zealand) under the form of a twistless yarn. The fibres and the yarn were used as such as control. Straightened flax fibres were obtained by soaking the flax yarn in water, then stretching it in a frame under tensile stress (around 2% elongation) and letting it dry at room temperature.

The morphology of the fibres was characterised by field emission scanning electron microscopy (Jeol JSM-6700 F) and polarised light microscopy (Leica TCS SP5). Dynamic mechanical analysis was carried out on a Rheometrics V to study the damping coefficient of the fibres and the unidirectional reinforced composites. The WAXS experiments were carried out at the Australian synchrotron, using a wavelength = 0.0826561 nm (15 keV) and a CCD detector. X-ray diffraction was used to determine the change in cellulosic microfibril angle (MFA) using the (200) reflection as described elsewhere [Donaldson, 2008].

A low-viscosity epoxy system was prepared by mixing two commercial components: Nuplex resin R300, based on the diglycidyl ethers of bisphenol A and Novolac, and Nuplex hardener H310, containing triethylamine tetramine and isophorone diamine. Resin and hardener were mixed in proportions 5:1 by weight. The composites were made by resin infusion, cured overnight. They were then post cured at 105 °C for 1 h and conditioned at 50% RH and 23 °C for a week prior to testing.

F.3 Results and discussion

The microscopy on fibres indicated that the stretching of the yarn in water unwounded kink bands (Figure F.1 (a) and (b)) and realigned the cellulose microfibrils by 0.7° toward the axis (Table F.1).

The composites reinforced with unstretched and stretched fibres were tested in 3-point bending mode. The damping coefficient of such composite showed a 10%

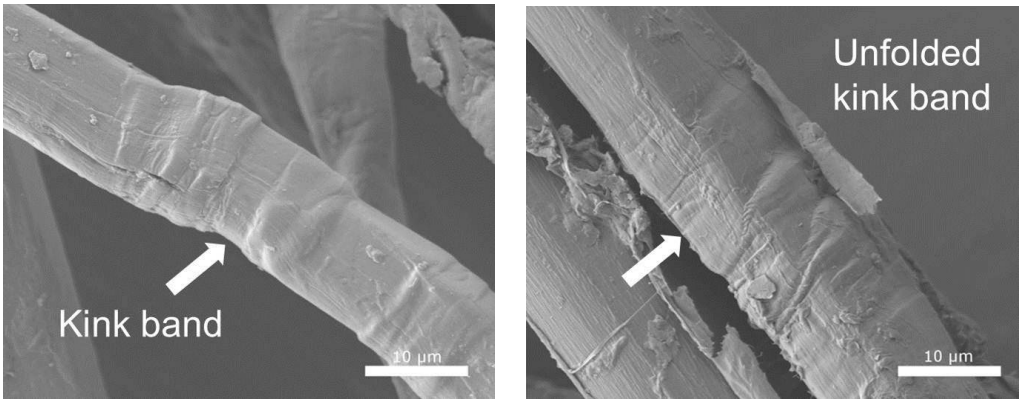

(a) (b)

Figure F.1: Typical kink band on European flax fibres, magnification ×2000 (a) unstretched and (b) stretched.

Table F.1: MFA of the European flax fibre yarn, the standard deviation is given below on 20 scans over 3 yarns.

	Un-stretched	Stretched
MFA (°)	6.4	5.7
SD (°) n=20	0.3	0.3

decrease in damping coefficient. However, the decrease but could be attributed to the decrease of kink bands numbers or the realignment of the cellulose microfibrils or a combined effect of both. The kink bands require local tensile strain up of 10% and beyond to unfold (Figures F.1) [Thygesen et al., 2007]. In the case of vibration where strain tends to be below 0.1%, it is unlikely that the kink bands influence the damping coefficient by viscoelasticity mechanisms. The hypothesis where the damping coefficient decreased after stretching is therefore attributed to the realignment of the cellulose microfibrils by 0.7°.

Table F.2: Damping coefficient of UD composite reinforced with yarn, the value is an average of 3 specimens.

	Un-stretched	Stretched
Damping coefficient	0.0040	0.0036
CI 95	0.0001	0.0001

F.4 Conclusions

When flax fibres are tested free of resin, the fibre stretches non-uniformly. It is believed that first the kink bands become straightened, and then the remainder of the fibre stretches. When flax fibres are embedded in epoxy resin, the fibres stretch uniformly, showing strains within kink bands similar to strains across the remainder of the fibre. The viscoelastic mechanisms involved in stretching the kink band are slow and the electronic micrographs indicated that the unfolding of the kink bands would require larger strain than those withstand during vibration experiments. These findings indicate that the viscoelastic behaviour of kink bands is not directly involved in the vibration damping mechanisms of plant fibres composites. The investigation should then focus on mechanisms that have relaxation constant closer to vibration frequency.

Appendix G

DOE residual plots

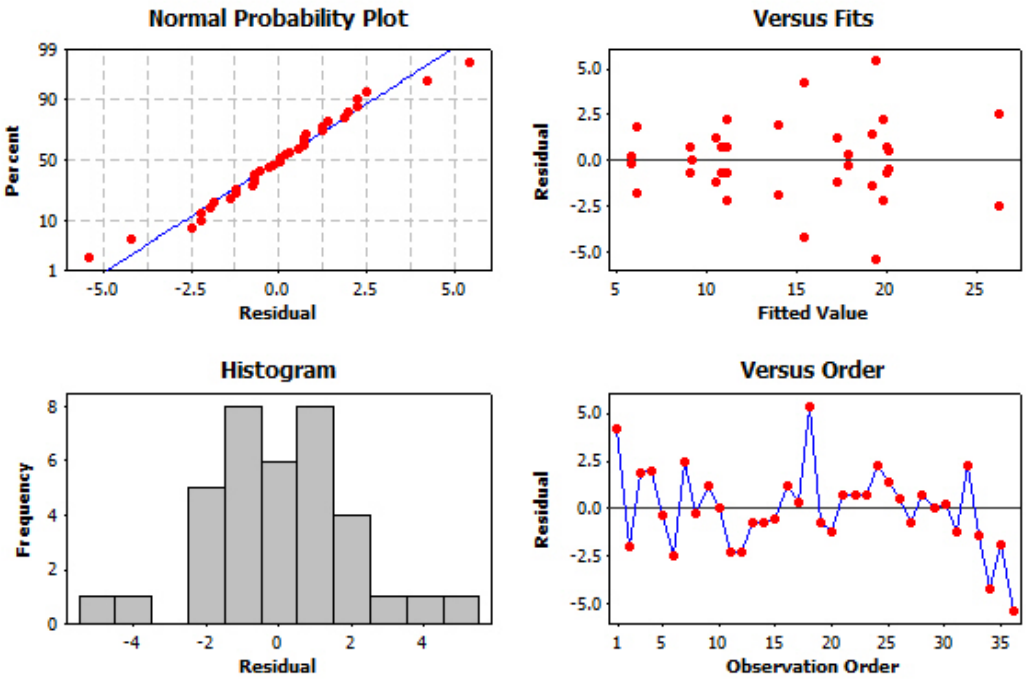

Figure G.1: Residual plots of the elastic modulus.

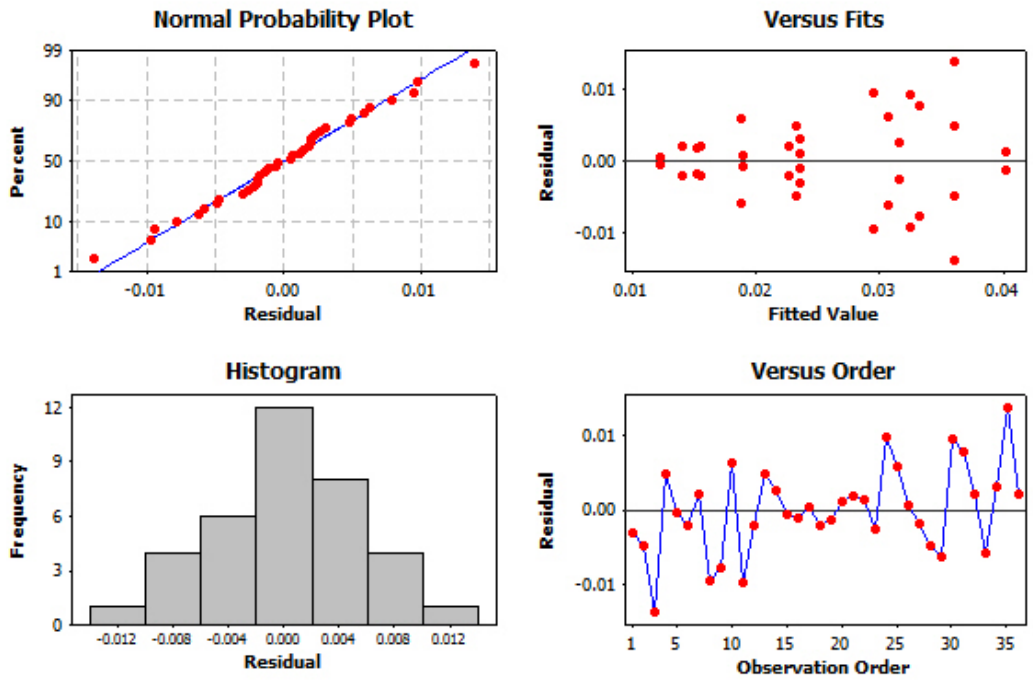

Figure G.2: Residual plots of the damping coefficient.

Appendix H

Sensitivity comparison between accelerometer and microphone on the damping coefficient

When performing vibration tests to measure the stiffness and the damping of a rectangular specimen, accelerometers are the preferred choice. They are a direct measurement of damping through the variation of acceleration. Yet, accelerometers require to be attached to the specimens using wax. Microphone on the other hand is another type of sensor that is not in contact with the specimen and the measure of the material damping is derived through the variation in air pressure.

In the present work, the damping coefficient were measured to compared the sensitivity of the 2 different types of sensor. The damping coefficient and the elastic modulus of the same set of specimens were measured using a Pico Technology accelerometer serial number 352C23 SN 105215 and a microphone THS 130P10 SN6156 from National instrument. The results indicated that the microphone sensitivity was up to 5 times higher than than the accelerometer (Figure H.1). As a results of this comparison, a microphone was used in the resonance test instead of an accelerometer.

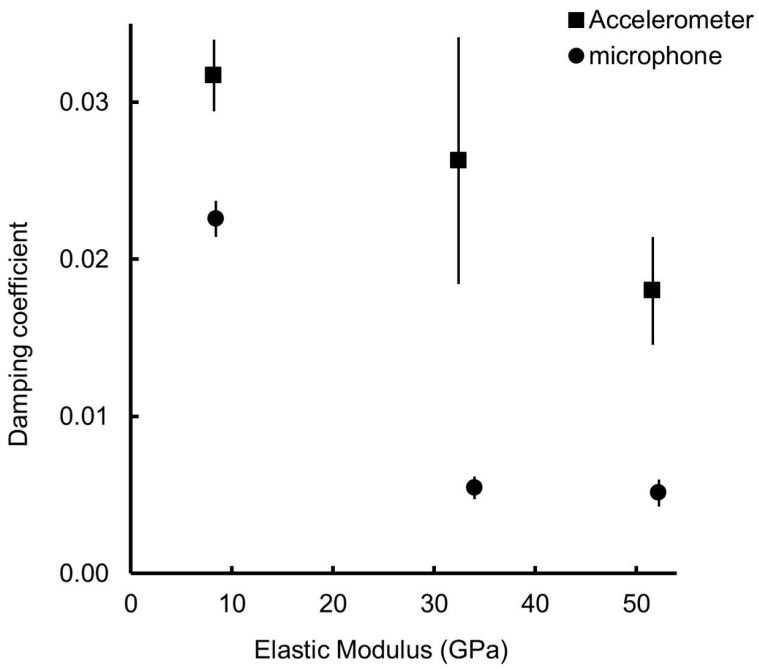

Figure H.1: Comparison of damping coefficients and elastic moduli for flax hybrid laminates at the first resonant frequency in flexural mode measured with a microphone or an accelerometer. The error bar represents 1 standard deviation for 3 specimens.

Appendix I

Comparison of different experimental methods to measure stiffness

The elastic modulus can be evaluated using different methods: acoustic, DMTA and quasi-static test. The results indicated that acoustic test are the most reproducible and the DMTA the least, but overall all measurements are comparable (Table I.1, Figure I.1).

Table I.1: Elastic modulus measured by quasi static 3-point bending, dynamic 3-point bending and free-resonance in bending mode for the same flax fibre composite. The error bars represent the 95% CI.

Method	Elastic modulus (GPa)	CI 95
3-point bending	6.37	0.49
Acoustics	6.28	0.03
DMA	6.43	0.67

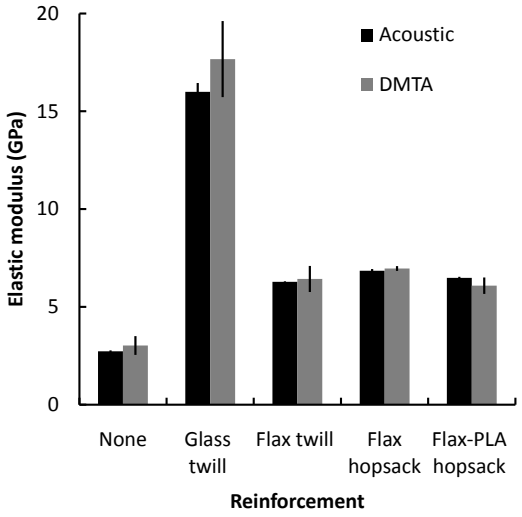

Figure I.1: Elastic modulus measured by dynamic 3-point bending and free-resonance in bending mode for different fibre reinforced composites.

Appendix J

Time and temperature superposition validation

Temperature and time were shown to have equivalent effects on the molecular and kinetic mechanisms occurring in polymers [Ferry, 1980].

The most popular model to determine the equivalence of the time and temperature effect is the Williams-Landel and Ferry (WLF) equation presented below:

$$log(a_T) = -\frac{c_1^0\ (T - T_0)}{c_2^0 + (T - T_0)} \tag{J.1}$$

where a_T is the shift factor, c_1^0 and c_2^0 are empirical constants, T and T_0 are the working temperature and reference temperature, respectively. Equation J.1 is applicable for working temperature between the T_g and 100°C above.

When the working temperatures are below the T_g of the polymer, the Arrhenius equation presented below is then preferred:

$$log(a_T) = \frac{E_a}{R}\ (\frac{1}{T} - \frac{1}{T_0}) \tag{J.2}$$

where E_a is the apparent activation energy.

However, to apply these equations, the system must be considered thermo-rheologically simple, which implies the absence of crystallinity or cross linking effects, phase segregation or composites structures (Guideline to TTS TA instrument).

In this study, the specimens of interest were composite laminates studied below the T_g of the resin. Even though, from a theoretical stand point, TTS should not be used on composite materials, the purpose of this study was only to extend the range of frequencies.

The validity of the superposition can be seen by plotting the log (a_T) against 1/T. If the empiric plot is a linear curve, the TTS can be considered applicable as the shift factor is constant over the studied temperature and frequency range. Such plots are presented in the Figures below:

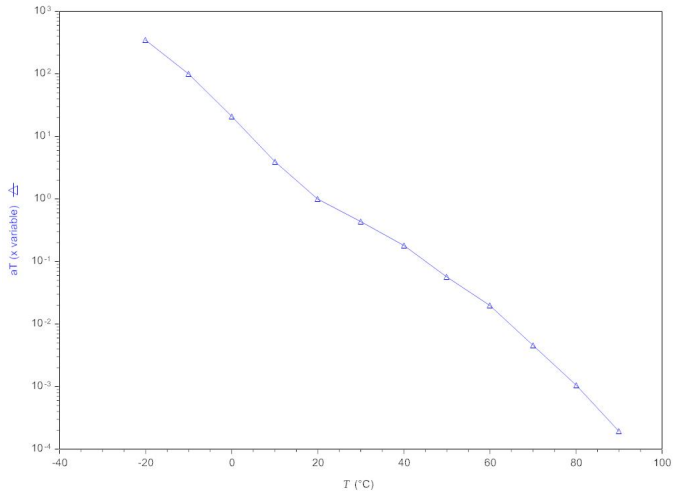

Figure J.1: Semi-log plot of the shift factors a_T as a function of temperature for Flax (No polyol) composites.

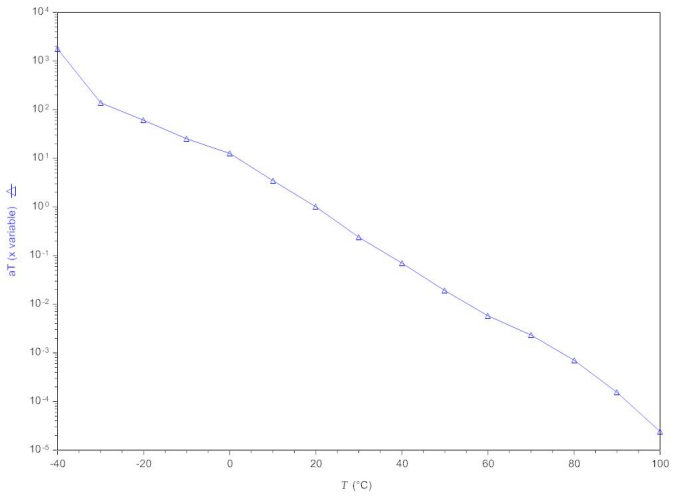

Figure J.2: Semi-log plot of the shift factors a_T as a function of temperature for Flax (Glycerol) composite.

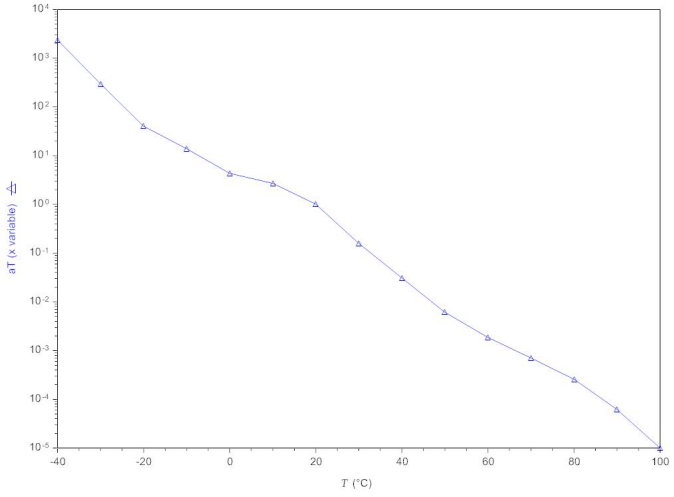

Figure J.3: Semi-log plot of the shift factors a_T as a function of temperature for Flax (PG3) composite.

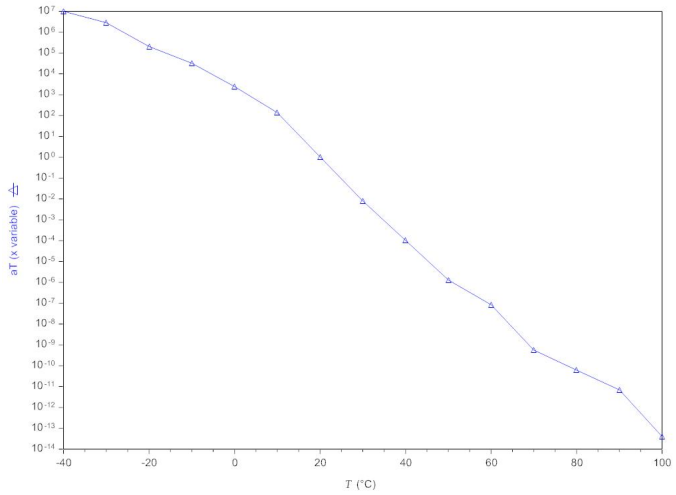

Figure J.4: Semi-log plot of the shift factors a_T as a function of temperature for carbon composite.

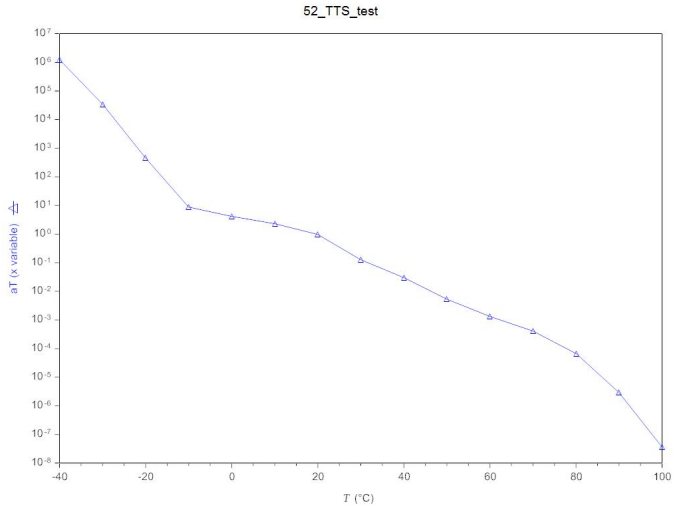

Figure J.5: Semi-log plot of the shift factors a_T as a function of temperature for aramid composite.

References

D. Akash, N. Thyagaraj, and L. Sudev. Experimental study of dynamic behavior of hybrid jute-sisal reinforced polyester composite. *International Journal of Science and Engineering Applications*, 2, 2013. 131

L. Akerholm, M. Salmen. Interactions between wood polymers studied by dynamic ft-ir spectroscopy. *Polymer*, 42(3):963 – 969, 2001. 18, 39, 40

H. Akitsu, M. Norimoto, T. Morooka, and R. Rowell. Effect of humidity on vibrational properties of chemically modified wood. *Wood and Fiber Science*, 25: 250–260, 1993. 74

C. C. Angrizani, M. O. H. Cioffi, A. J. Zattera, and S. C. Amico. Analysis of curaua glass hybrid interlayer laminates. *Journal of Reinforced Plastics and Composites*, 2014. 115

O. M. Astley and A. M. Donald. A small-angle x-ray scattering study of the effect of hydration on the microstructure of flax fibers. *Biomacromolecules*, 2 (3):672–680, 2001. 60

ASTM D3039/D3039M-14. Standard Test Method for Tensile Properties of Polymer Matrix Composite Materials. 118

ASTM D5023-07. Standard Test Method for Plastics: Dynamic Mechanical Properties: In Flexure (Three-Point Bending). 88

ASTM D790-10. Standard Test Methods for Flexural Properties of Unreinforced and Reinforced Plastics and Electrical Insulating Materials. 118

ASTM E1875-13. Standard Test Method for Dynamic Young's Modulus, Shear Modulus, and Poisson's Ratio by Sonic Resonance. 7

ASTM E1876-09. Standard Test Method for Dynamic Young's Modulus, Shear Modulus, and Poisson's Ratio by Impulse Excitation of Vibration. 7, 89

K. E. Atkinson and C. Jones. A study of the interphase region in carbon fibre/epoxy composites using dynamic mechanical thermal analysis. *The Journal of Adhesion*, 56(1-4):247–260, 1996. 102, 105

B. S. Bains. Technical review on the state-of-the-art of dimensional stabilization of wood products using chemical impregnation. Technical report, Canadian Forestry Service, 1986. 64

C. Baley. Analysis of the flax fibres tensile behaviour and analysis of the tensile stiffness increase. *Composites Part A: Applied Science and Manufacturing*, 33 (7):939 – 948, 2002. 19, 55, 58, 59, 78

C. Baley. Influence of kink bands on the tensile strength of flax fibers. *Journal of Materials Science*, 39(1):331–334, 2004. 19, 22, 173

S. Basu. Tensile deformation of fibers used in textile industry. Technical report, Agilent Technologies, 2012. 49, 58

S. L. Berry and M. L. Roderick. Plant-water relations and the fibre saturation point. *New Phytologist*, 168(1):25–37, 2005. 164

J.-M. Berthelot and Y. Sefrani. Damping analysis of unidirectional glass and kevlar fibre composites. *Composites Science and Technology*, 64(9):1261 – 1278, 2004. 8, 14, 26

J.-M. Berthelot and Y. Sefrani. Longitudinal and transverse damping of unidirectional fibre composites. *Composite Structures*, 79(3):423 – 431, 2007. 49, 120

J.-M. Berthelot, M. Assarar, Y. Sefrani, and A. E. Mahi. Damping analysis of composite materials and structures. *Composite Structures*, 85(3):189 – 204, 2008. 2

A. Bledzki and J. Gassan. Composites reinforced with cellulose based fibres. *Progress in Polymer Science*, 24(2):221 – 274, 1999. 20, 44

A. Borodulin. Plasticizers for epoxy adhesives and binders. *Polymer Science Series D*, 6(1):59–62, 2013. 71

H. Bos. *The potential of flax fibres as reinforcement for composite materials*. PhD thesis, Eindhoven University of Technology, 2004. 1, 16, 19, 22, 69

I. Bremaud. What do we know on resonance wood properties? selective review and ongoing research. In *Proceedings of the Acoustics Nantes Conference*, 2012. 30, 61

I. Bremaud, K. Minato, P. Langbour, and B. Thibault. Physico-chemical indicators of inter-specific variability in vibration damping of wood. *Ann. For.Sci*, 67:707, 2010. 60, 132, 138, 169

C. Buksnowitz, R. Adusumalli, A. Pahler, H. Sixta, and W. Gindl. Acoustical properties of lyocell, hemp, and flax composites. *Journal of Reinforced Plastics and Composites*, 2010. 1, 132, 133, 138

I. Burgert and J. W. Dunlop. *Mechanical Integration of Plant Cells and Plants*. Springer, 2011. 58

I. Cave. Theory of x-ray measurement of microfibril angle in wood. *Wood Science and Technology*, 31(3):143–152, 1997. 31, 33

A. Celino, S. Freour, F. Jacquemin, and P. Casari. The hygroscopic behavior of plant fibres a review. *Frontiers in Chemistry*, 1(43), 2014. 63

A. C. Chakravarty and J. W. Hearle. Observations on the tensile properties of ultimate cells of some plant fibres. *Journal of the Textile Institute*, 58(12):651–656, 1967. 29

R. Chandra, S. Singh, and K. Gupta. Damping studies in fiber-reinforced composites - a review. *Composite Structures*, 46:41 – 51, 1999. 13, 14

K. Charlet, S. Eve, J. Jernot, M. Gomina, and J. Breard. Tensile deformation of a flax fiber. *Procedia Engineering*, 1(1):233 – 236, 2009. Mesomechanics 2009. 31

S. Chauhan. *Primary Wood Processing: Principles and Practice Second edition*. Springer, 2006. 30

D. Chung. Structural composite materials tailored for damping. *Journal of Alloys and Compounds*, 355(1):216–223, 2003. 12, 14

R. W. Clough and J. Penzien. *Dynamique des structures translated from Dynamics of structures by JL. Claudon*. Pluralis, 1980. 143

L. Cremer, M. Heckl, and B. A. T. Petersson. *Structure-Borne Sound: Structural Vibrations and Sound Radiation at Audio Frequencies*. Springer, 3rd edition edition, 2005. 84, 89, 90, 118

T. Czigany. *Polymer composites: From nano to macro scale*, chapter 17, page 316. Springer, 2005. 119

I. M. De Rosa, J. M. Kenny, D. Puglia, C. Santulli, and F. Sarasini. Tensile behavior of new zealand flax (phormium tenax) fibers. *Journal of Reinforced Plastics and Composites*, 2010. 19

H. Dhakal, Z. Zhang, M. Richardson, and O. Errajhi. The low velocity impact response of non-woven hemp fibre reinforced unsaturated polyester composites. *Composite Structures*, 81(4):559 – 567, 2007. 12, 115

H. Dhakal, Z. Zhang, R. Guthrie, J. MacMullen, and N. Bennett. Development of flax/carbon fibre hybrid composites for enhanced properties. *Carbohydrate Polymers*, 96(1):1 – 8, 2013. 115

I. Diddens, B. Murphy, M. Krisch, and M. Muller. Anisotropic elastic properties of cellulose measured using inelastic x-ray scattering. *Macromolecules*, 41(24): 9755–9759, 2008. 32

F. Divos and T. Tanaka. Effects of creep on modulus of elasticity determination of wood. *Journal of Vibration and Acoustics*, 122(1):90–92, 2000. 98, 125

L. Donaldson. Microfibril angle: measurement, variation and relationships: a review. *IAWA Journal*, 29:345–386, 2008. 31, 174

A. Dorigato and A. Pegoretti. Fatigue resistance of basalt fibers-reinforced laminates. *Journal of Composite Materials*, 46(15):1773–1785, 2012. 131, 134

F. Duc, P. Bourban, C. Plummer, and J.-A. Manson. Damping of thermoset and thermoplastic flax fibre composites. *Composites Part A: Applied Science and Manufacturing*, (0):–, 2014. 1, 11, 12, 98, 111, 115

A. L. Duigou, C. Baley, Y. Grohens, P. Davies, J.-Y. Cognard, R. C. Cadec, and L. Sohier. A multi-scale study of the interface between natural fibres and a biopolymer. *Composites Part A: Applied Science and Manufacturing*, (0):–, 2014. 12

S. Dumitriu, editor. *Polysaccharides: Structural Diversity and Functional Versatility, Second Edition*. Marcel Dekker, 2005. 18, 30

P. Ebrahimzadeh and H. Bertilsson. Effect of impregnation on mechanosorption in wood and paper studied by dynamic mechanical analysis. *Wood Science and Technology*, 32(2):101–118, 1998. 26, 60, 61, 63, 169, 170

R. Elenga, G. Dirras, J. G. Maniongui, P. Djemia, and M. Biget. On the microstructure and physical properties of untreated raffia textilis fiber. *Composites Part A: Applied Science and Manufacturing*, 40(4):418 – 422, 2009. 20

K. M. Entwistle. *The hemicelluloses workshop 2005*, chapter The reaction of hemicelluloses to applied stresses with emphasis on the effect of changes of water concentration, pages 137–146. The Wood Technology Research Centre, University of Canterbury, Christchurch, New Zealand, 2005. 26, 30, 58, 59, 60, 61, 63, 169, 170

R. Evans. *A Variance Approach to the X-ray Diffractometric Estimation of Microfibril Angle in Wood*. Research report (Cooperative Research Centre for Hardwood Fibre and Paper Science (Australia). CRC Publications, 1999. 33

J. D. Ferry. *Viscoelastic properties of polymers*. Wiley, 1980. 183

M. E. A. Fidelis, T. V. C. Pereira, O. da Fonseca Martins Gomes, F. de Andrade Silva, and R. D. T. Filho. The effect of fiber morphology on the tensile strength of natural fibers. *Journal of Materials Research and Technology*, 2(2): 149 – 157, 2013. 20

V. Fiore, A. Valenza, and G. Di Bella. Mechanical behavior of carbon flax hybrid composites for structural applications. *Journal of Composite Materials*, 46(17): 2089–2096, 2012. 115

K. Freudenberg. Biosynthesis and constitution of lignin. *Nature*, 183:1152–1155, 1959. 18

J. Gassan. A study of fibre and interface parameters affecting the fatigue behaviour of natural fibre composites. *Composites Part A: Applied Science and Manufacturing*, 33(3):369 – 374, 2002. 12, 14, 19

J. Gassan and A. K. Bledzki. Possibilities for improving the mechanical properties of jute/epoxy composites by alkali treatment of fibres. *Composites Science and Technology*, 59(9):1303 – 1309, 1999. 25, 30

J. Gassan, A. Chate, and A. Bledzki. Calculation of elastic properties of natural fibers. *Journal of Materials Science*, 36(15):3715–3720, 2001. 29

V. Geethamma, G. Kalaprasad, G. Groeninckx, and S. Thomas. Dynamic mechanical behavior of short coir fiber reinforced natural rubber composites. *Composites Part A: Applied Science and Manufacturing*, 36(11):1499 – 1506, 2005. 102, 105

A. K. Ghosh, I. D. Baere, J. V. Walleghem, J. D. Thaeye, W. V. paepegem, and J. Degrieck. Effect of flax fibre reinforcement on the riding comfort of composite racing bicycle frames. *Procedia Engineering*, 2(2):3435 –, 2010. 1, 11

R. F. Gibson and R. Plunkett. Dynamic mechanical behavior of fiber-reinforced composites: Measurement and analysis. *Journal of Composite Materials*, 10(4): 325–341, 1976. 96

N. Gierlinger, M. Schwanninger, A. Reinecke, and I. Burgert. Molecular changes during tensile deformation of single wood fibers followed by raman microscopy. *Biomacromolecules*, 7(7):2077–2081, 2006. 45, 58

W. Goertzen and M. Kessler. Dynamic mechanical analysis of carbon/epoxy composites for structural pipeline repair. *Composites Part B: Engineering*, 38(1):1 – 9, 2007. 85

M. Gomina. Flax & hemp composite applications. *Reux F, Verpoest I, editors: Flax and Hemp fibres: a Natural Solution for the Composite Industry, JEC Composites*, Chapt. 8:141–162, 2012. 1, 11, 115, 138

R. Greenspan, Frank Light. Thermoset epoxy resin plasticized with a glycol ether-ester, January 1963. US Patent 3,073,793. 71

Y. Haddad and J. Feng. On the trade-off between damping and stiffness in the design of discontinuous fibre-reinforced composites. *Composites Part B: Engineering*, 34(1):11 – 20, 2003. 12

J. Handcock. *Fatigue of Composite Materials*. American Society for Testing & Materials, 1975. 6

B. Harris, editor. *Engineering Composite Materials Second Edition*. Institute of Materials, London, 1999. 14

C. A. S. Hill. *Wood modification*. Wiley, 2006. 63, 64

S. J. Hill. *Water in Pinus radiata wood secondary cell walls: An investigation using Nuclear Magnetic Resonance and Synchrotron X-ray Diffraction.* PhD thesis, Victoria University of Wellington, 2010. xvii, 31, 65, 70, 71, 75, 77, 78, 167

B. Hinterstoisser, M. Akerholm, and L. Salmen. Load distribution in native cellulose. *Biomacromolecules*, 4(5):1232–1237, 2003. 58

S. V. Hoa and P. Ouellette. Damping of composite materials. *Polymer Composites*, 5(4):334–338, 1984. 14, 123

M. Hughes. Defects in natural fibres: their origin, characteristics and implications for natural fibre-reinforced composites. *Journal of Materials Science*, 47(2): 599–609, 2012. 13, 107

M. Hughes, C. Hill, and J. Hague. The fracture toughness of bast fibre reinforced polyester composites part 1 evaluation and analysis. *Journal of Materials Science*, 37(21):4669–4676, 2002. 11, 26, 173

M. Hughes, J. Carpenter, and C. Hill. Deformation and fracture behaviour of flax fibre reinforced thermosetting polymer matrix composites. *Journal of Materials Science*, 42(7):2499–2511, 2007. 1

M. Idicula, S. Malhotra, K. Joseph, and S. Thomas. Dynamic mechanical analysis of randomly oriented intimately mixed short banana/sisal hybrid fibre reinforced polyester composites. *Composites Science and Technology*, 65:1077 – 1087, 2005. 13

M. C. Jarvis. *The hemicelluloses workshop 2005*, chapter Cellulose structure and hemicellulose-cellulose association, pages 87–102. The Wood Technology Research Centre, University of Canterbury, Christchurch, New Zealand, 2005. 54, 60, 147

A. Jauneau, M. Quentin, and A. Driouich. Micro-heterogeneity of pectins and calcium distribution in the epidermal and cortical parenchyma cell walls of flax hypocotyl. *Protoplasma*, 198(1-2):9–19, 1997. 15, 18

M. Jawaid and H. A. Khalil. Cellulosic synthetic fibre reinforced polymer hybrid composites: A review. *Carbohydrate Polymers*, 86(1):1 – 18, 2011. 115

M. Kabir, H. Wang, K. Lau, and F. Cardona. Chemical treatments on plant-based natural fibre reinforced polymer composites: An overview. *Composites Part B: Engineering*, 43(7):2883 – 2892, 2012. 16, 64, 73

M. A. Kamal, A. M. Taha. Vibration damping behavior of fiber reinforced composites: A review. *Key Engineering Materials*, 425:179–194, 2010. 14

J. Keckes, I. Burgert, K. Fruhmann, M. Muller, K. Kolln, M. Hamilton, M. Burghammer, S. Roth, S. Stanzl-Tschegg, and P. Fratzl. Cell-wall recovery after irreversible deformation of wood. *Nature Materials*, 2:810–813, 2003. 13, 45, 56, 64, 111

V. Keryvin, M. Lan, A. Bourmaud, T. Parenteau, L. Charleux, and C. Baley. Analysis of flax fibres viscoelastic behaviour at micro and nano scales. *Composites Part A: Applied Science and Manufacturing*, 68(0):219 – 225, 2015. 58

V. K. Kinra. *Mechanics and Mechanisms of Material Damping*. American Society For Testing and Materials International, 1992. 10, 84

L. Köhler and H.-C. Spatz. Micromechanics of plant tissues beyond the linear-elastic range. *Planta*, 215(1):33–40, 2002. 45, 58

K. Kölln, I. Grotkopp, M. Burghammer, S. V. Roth, S. S. Funari, M. Dommach, and M. Müller. Mechanical properties of cellulose fibres and wood. Orientational aspects *in situ* investigated with synchrotron radiation. *Journal of Synchrotron Radiation*, 12(6):739–744, Nov 2005. 32, 49

T. Koshijima, T. Watanabe, editor. *Association Between Lignin and Carbohydrates in Wood and Other Plant Tissues*. Springer Series in Wood Science, 2003. 39

H. Kraessig. Cellulose chemistry and its applications, t. p. nevell and s. h. zeronian, eds., halsted press, john wiley, new york, 1985, 552 pp. *Journal of Polymer Science Part C: Polymer Letters*, 25(2):87–88, 1987. 16

D. Kretschmann. Velcro mechanics in wood. *Natural materials*, 2:1476–1122, 2003. 13, 64, 111

A. Kulkarni, K. Satyanarayana, K. Sukumaran, and P. Rohatgi. Mechanical behaviour of coir fibres under tensile load. *Journal of Materials Science*, 16(4): 905–914, 1981. 55

K. S. Kumar, I. Siva, P. Jeyaraj, J. W. Jappes, S. Amico, and N. Rajini. Synergy of fiber length and content on free vibration and damping behavior of natural fiber reinforced polyester composite beams. *Materials & Design*, 56(0):379 – 386, 2014. 1

R. Lakes. High damping composite materials: Effect of structural hierarchy. *Journal of Composite Materials*, 36:287–297, 2002. 26, 138

X. Li, L. Tabil, and S. Panigrahi. Chemical treatments of natural fiber for use in natural fiber-reinforced composites: A review. *Journal of Polymers and the Environment*, 15(1):25–33, 2007. 64, 73

S. Liang, P. Gning, and L. Guillaumat. A comparative study of fatigue behaviour of flax/epoxy and glass/epoxy composites. *Composites Science and Technology*, 72(5):535 – 543, 2012. 13

B. Madsen. *Properties of plant fibre yarn polymer composites*. PhD thesis, Technical University of Denmark, 2003. 22

R. E. Mark. *Cell wall mechanics of tracheids*. Yale University Press, 1967. 167

G. Marom, S. Fischer, F. Tuler, and H. Wagner. Hybrid effects in composites: conditions for positive or negative effects versus rule-of-mixtures behaviour. *Journal of Materials Science*, 13(7):1419–1426, 1978. 119

K. Martinschitz, P. Boesecke, C. Garvey, W. Gindl, and J. Keckes. Changes in microfibril angle in cyclically deformed dry coir fibers studied by in-situ synchrotron x-ray diffraction. *Journal of Materials Science*, 43(1):350–356, 2008. 33, 44, 45, 49

A. Martone, M. Giordano, V. Antonucci, and M. Zarrelli. Enhancing damping features of advanced polymer composites by micromechanical hybridization. *Composites Part A: Applied Science and Manufacturing*, 42(11):1663 – 1672, 2011. 12, 14

E. McLaughlin and R. Tait. Fracture mechanism of plant fibres. *Journal of Materials Science*, 15(1):89–95, 1980. 29

J. Meredith, R. Ebsworth, S. R. Coles, B. M. Wood, and K. Kirwan. Natural fibre composite energy absorption structures. *Composites Science and Technology*, 72 (2):211 – 217, 2012. 1, 6, 11

C. Morvan, C. Andme-Onzighi, R. Girault, D. S. Himmelsbach, A. Driouich, and D. E. Akin. Building flax fibres: more than one brick in the walls. *Plant Physiology and Biochemistry*, 41:935 – 944, 2003. 16, 18

K. Mukherjee, P.S. Satyanarayana. An empirical evaluation of structure-property relationships in natural fibres and their fracture behaviour. *Journal of materials science*, 21:4162–4168, 1986. 30

M. Müller, C. Czihak, G. Vogl, P. Fratzl, H. Schober, and C. Riekel. Direct observation of microfibril arrangement in a single native cellulose fiber by microbeam small-angle x-ray scattering. *Macromolecules*, 31(12):3953–3957, 1998. 44

M. Müller, B. Murphy, M. Burghammer, I. Snigireva, C. Riekel, J. Gunneweg, and E. Pantos. Identification of single archaeological textile fibres from the cave of letters using synchrotron radiation microbeam diffraction and microfluorescence. *Applied Physics A*, 83(2):183–188, 2006. 33

S. Munawar, K. Umemura, and S. Kawai. Characterization of the morphological, physical, and mechanical properties of seven nonwood plant fiber bundles. *Journal of Wood Science*, 53(2):108–113, 2007. 44, 55

B. Muralidhar, V. Giridev, and K. Raghunathan. Flexural and impact properties of flax woven, knitted and sequentially stacked knitted/woven preform reinforced epoxy composites. *Journal of Reinforced Plastics and Composites*, 31(6):379–388, 2012. 14

J. Müssig. *Industrial Applications of Natural Fibres Structure, Properties and Technical Applications*. Wiley Series in Renewable Resources, 2010. 1, 2, 15, 16, 17, 19, 20, 21, 22, 23, 25, 29, 39, 41, 45, 166

L. Y. Mwaikambo and M. P. Ansell. Chemical modification of hemp, sisal, jute, and kapok fibers by alkalization. *Journal of Applied Polymer Science*, 84(12): 2222–2234, 2002. 17

S. Nam and A. N. Netravali. Green composites. i. physical properties of ramie fibers for environment-friendly green composites. *Fibers and Polymers*, 7(4): 372–379, 2006. 20

A. D. Nashif, D. I. G. Jones, and J. P. Henderson. *Vibration Damping*. Wiley-Interscience, 1985. 7

R. Newman. *5. Properties and performance of natural-fibre composites*, chapter Development of non-wood natural-fibre composites. Woodhead Publishing, 2008. xv, 18, 19, 32

R. H. Newman. Effects of finite preparation-pulse power on carbon-13 cross-polarization nmr spectra of heterogeneous samples. *Journal of Magnetic Resonance (1969)*, 72(2):337 – 340, 1987. 71

R. H. Newman. *The hemicelluloses workshop 2005*, chapter Solid-state NMR as a tool for studying dancing molecules, pages 77–86. The Wood Technology Research Centre, University of Canterbury, Christchurch, New Zealand, 2005. 39, 60, 65

R. H. Newman, E. C. Clauss, J. E. Carpenter, and A. Thumm. Epoxy composites reinforced with deacetylated phormium tenax leaf fibres. *Composites Part A: Applied Science and Manufacturing*, 38(10):2164 – 2170, 2007. 69, 73

R. H. Newman, M. A. Battley, J. E. Carpenter, and M. J. Le Guen. Energy loss in a unidirectional flax-polyester composite subjected to multiple tensile load-unload cycles. *Journal of Materials Science*, 47(3):1164–1170, 2012. 1, 26

T. Nishino, H. Naito, K. Nakamura, and K. Nakamae. X-ray diffraction studies on the stress transfer of transversely loaded carbon fibre reinforced composite. *Composites Part A: Applied Science and Manufacturing*, 31(11):1225 – 1230, 2000. 86

S. Nunna, P. R. Chandra, S. Shrivastava, and A. Jalan. A review on mechanical behavior of natural fiber based hybrid composites. *Journal of Reinforced Plastics and Composites*, 31(11):759–769, 2012. 11, 115

E. Obataya, M. Norimoto, and J. Gril. The effects of adsorbed water on dynamic mechanical properties of wood. *Polymer*, 39(14):3059 – 3064, 1998. 95

T. Ono and M. Norimoto. Study on young's modulus and internal friction of wood in relation to the evaluation of wood for musical instruments. *Japanese Journal of Applied Physics*, 22:611, 1983. 131, 132

D. Ouis. On the frequency dependence of the modulus of elasticity of wood. *Wood Science and Technology*, 36(4):335–346, 2002. 98

C. Pavithran, P. Mukherjee, M. Brahmakumar, and A. Damodaran. Impact properties of natural fibre composites. *Journal of Materials Science Letters*, 6(8): 882–884, 1987. 12, 13, 26, 30, 44

R. C. Pettersen. Wood sugar analysis by anion chromatography. *Journal of Wood Chemistry and Technology*, 11(4):495–501, 1991. 31, 36

P. E. Pfeffer and W. V. Gerasimowicz. *Nuclear Magnetic Resonance in Agriculture*. CRC Press, 1989. 69

V. Placet, O. Cisse, and M. Boubakar. Influence of environmental relative humidity on the tensile and rotational behaviour of hemp fibres. *Journal of Materials Science*, 47(7):3435–3446, 2012. 26, 58, 59, 60, 61, 78, 95

V. Placet, O. Cisse, and M. L. Boubakar. Nonlinear tensile behaviour of elementary hemp fibres. part i: Investigation of the possible origins using repeated progressive loading with in situ microscopic observations. *Composites Part A: Applied Science and Manufacturing*, 56(0):319 – 327, 2014. 37, 45

L. A. Pothan, Z. Oommen, and S. Thomas. Dynamic mechanical analysis of banana fiber reinforced polyester composites. *Composites Science and Technology*, 63 (2):283 – 293, 2003. 14, 85, 120

G. Ramtekkar, Y. Desai, and A. Shah. Natural vibrations of laminated composite beams by using mixed finite element modelling. *Journal of Sound and Vibration*, 257(4):635 – 651, 2002. 98

A. Reiterer, H. Lichtenegger, P. Fratzl, and S. Stanzl-Tschegg. Deformation and energy absorption of wood cell walls with different nanostructure under tensile loading. *Journal of Materials Science*, 36(19):4681–4686, 2001. 30, 57

S. Richter, J. Müssig, and N. Gierlinger. Functional plant cell wall design revealed by the raman imaging approach. *Planta*, 233(4):763–772, 2011. 17, 20, 31, 39, 43, 44, 45, 73, 147

D. N. Saheb and J. P. Jog. Natural fiber polymer composites: A review. *Advances in Polymer Technology*, 18(4):351–363, 1999. 1

L. Salmen. Micromechanical understanding of the cell-wall structure. *Comptes Rendus Biologies*, 327:873 – 880, 2004. 54

K. Satyanarayana, C. Pillai, K. Sukumaran, S. Pillai, P. Rohatgi, and K. Vijayan. Structure property studies of fibres from various parts of the coconut tree. *Journal of Materials Science*, 17(8):2453–2462, 1982. 30

H. V. Scheller and P. Ulvskov. Hemicelluloses. *Annual Review of Plant Biology*, 61:263–289, 2010. 16

L. Schmitz and K. Smith. *Mechanical Vibrations: Modeling and Measurement*. Springer, 2011. 89, 118

R. J. Scott and A. D. Stead, editors. *Molecular and Cellular Aspects of Plant Reproduction*. Cambridge University Press, 1994. 18

E. Segerman. Some aspects of wood structure and function. Technical note, 2001. 59

D. Shah. Developing plant fibre composites for structural applications by optimising composite parameters: a critical review. *Journal of Materials Science*, 48 (18):6083–6107, 2013. 11, 13

D. U. Shah, P. J. Schubel, and M. J. Clifford. Modelling the effect of yarn twist on the tensile strength of unidirectional plant fibre yarn composites. *Journal of Composite Materials*, 2012a. 14

D. U. Shah, P. J. Schubel, M. J. Clifford, and P. Licence. The tensile behavior of off-axis loaded plant fiber composites: An insight on the nonlinear stress strain response. *Polymer Composites*, 33(9):1494–1504, 2012b. 25

D. U. Shah, P. J. Schubel, and M. J. Clifford. Can flax replace e-glass in structural composites? a small wind turbine blade case study. *Composites Part B: Engineering*, 52(0):172 – 181, 2013. 11

A. Shahzad. Comparison of tensile properties and impact damage tolerance of hemp and glass fiber composites. *Journal of Reinforced Plastics and Composites*, 30(22):1877–1893, 2011. 11

W. A. Sisson. X-ray studies of crystallite orientation in cellulose fibers natural fibers. *Industrial & Engineering Chemistry*, 27(1):51–56, 1935. 33

K. Song, Y. Yin, L. Salmen, F. Xiao, and X. Jiang. Changes in the properties of wood cell walls during the transformation from sapwood to heartwood. *Journal of Materials Science*, 49(4):1734–1742, 2014. 64

M. Stevanovic and T. Stecenko. Mechanical behaviour of carbon and glass hybrid fibre reinforced polyester composites. *Journal of Materials Science*, 27(4):941–946, 1992. 134

W. F. Stockey. *Vibration of systems having distributed mass and elasticity*, chapter 7, pages 1–50. McGraw-Hill, 2002. xvii, 84

S. Suarez, R. Gibson, C. Sun, and S. Chaturvedi. The influence of fiber length and fiber orientation on damping and stiffness of polymer composite materials. *Experimental Mechanics*, 26(2):175–184, 1986. 14

I. Subagia and Y. Kim. A study on flexural properties of carbon-basalt epoxy hybrid composites. *Journal of Mechanical Science and Technology*, 27(4):987–992, 2013. 129, 134

J. Sugiyama, R. Vuong, and H. Chanzy. Electron diffraction study on the two crystalline phases occurring in native cellulose from an algal cell wall. *Macromolecules*, 24(14):4168–4175, 1991. 32

J. Summerscales, N. Dissanayake, A. Virk, and W. Hall. A review of bast fibres and their composites. part 2 composites. *Composites Part A: Applied Science and Manufacturing*, 41:1336 – 1344, 2010. 1, 11, 115

S. P. Sutton, F. Principe, and M. Gentile. Vibration damping composite material, 1999. 85

M. C. Symington, W. Banks, O. D. West, and R. Pethrick. Tensile testing of cellulose based natural fibers for structural composite applications. *Journal of Composite Materials*, 43(9):1083–1108, 2009. 166, 167

T. Thamae and C. Baillie. Influence of fibre extraction method, alkali and silane treatment on the interface of agave americana waste hdpe composites as possible roof ceilings in lesotho. *Composite Interfaces*, 14(7-9):821–836, 2007. 73

A. Thuault, S. Eve, D. Blond, J. Brard, and M. Gomina. Effects of the hygrothermal environment on the mechanical properties of flax fibres. *Journal of Composite Materials*, 48(14):1699–1707, 2014. 63

F. Thuvander, L. Wallström, L. A. Berglund, and K. Lindberg. Effects of an impregnation procedure for prevention of wood cell wall damage due to drying. *Wood Science and Technology*, 34(6):473–480, 2001. 64, 99

L. Thygesen, M. Eder, and I. Burgert. Dislocations in single hemp fibres: investigations into the relationship of structural distortions and tensile properties at the cell wall level. *Journal of Materials Science*, 42:558–564, 2007. 22, 26, 58, 173, 176

A. N. Towo and M. P. Ansell. Fatigue of sisal fibre reinforced composites: Constant-life diagrams and hysteresis loop capture. *Composites Science and Technology*, 68:915 – 924, 2008. 6

S. W. Tsai and H. T. Hahn. *Introduction to Composite Materials*. Technomic, 1980. 122, 131

E. Ungar and E. Kerwin. Loss factors of viscoelastic systems in terms of energy concepts. *Journal of the Acoustical Society of America*, 34(7):954–957, 1962. 120, 121

J. Van Raemdonck. Method for preparing thermosetting or thermoplastic polymer or elastomer composites that are reinforced with natural fibers, and their multiple applications as construction material, 2008. 115

B. van Voorn, H. Smit, R. Sinke, and B. de Klerk. Natural fibre reinforced sheet moulding compound. *Composites Part A: Applied Science and Manufacturing*, 32(9):1271 – 1279, 2001. 95

J. Vantomme. A parametric study of material damping in fibre-reinforced plastics. *Composites*, 26(2):147–153, 1995. 120

J. Vanwalleghem. Study of the damping and vibration behaviour of flax-carbon composite bicycle racing frames. Master's thesis, University of Gent, 2010. 11, 13, 138

N. Venkateshwaran, A. Elayaperumal, and G. Sathiya. Prediction of tensile properties of hybrid-natural fiber composites. *Composites Part B: Engineering*, 43 (2):793 – 796, 2012. 119

L. Wallstrom. *Cell wall bulking and distribution of different chemicals in pine, Pinus Sylvestris*. PhD thesis, Lulea tekniska universitet, 1998. 64

P. Wambua, J. Ivens, and I. Verpoest. Natural fibres: can they replace glass in fibre reinforced plastics? *Composites Science and Technology*, 63(9):1259–1264, 2003. 1, 14, 115

W. M. Wang, Z. S. Cai, J. Y. Yu, and Z. P. Xia. Changes in composition, structure, and properties of jute fibers after chemical treatments. *Fibers and Polymers*, 10 (6):776–780, 2009. 17

D. C. Wehi, P. M. Bruce. Biological flora of new zealand 10. phormium tenax, harakeke, new zealand flax,. *New Zealand Journal of Botany*, 45:4:521–544, 2007. 147

C. Wei and S. Kukureka. Evaluation of damping and elastic properties of composites and composite structures by the resonance technique. *Journal of Materials Science*, 35(15):3785–3792, 2000. 89

L. Yan. Effect of alkali treatment on vibration characteristics and mechanical properties of natural fabric reinforced composites. *Journal of Reinforced Plastics and Composites*, 31(13):887–896, 2012. 12

S. Zabler, O. Paris, I. Burgert, and P. Fratzl. Moisture changes in the plant cell wall force cellulose crystallites to deform. *Journal of Structural Biology*, 171(2): 133 – 141, 2010. 59

S. Zhai, Y. Horikawa, T. Imai, and J. Sugiyama. Cell wall characterization of windmill palm () fibers and its functional implications. *IAWA Journal*, 34(1): 20–33, 2013. 20, 41, 43, 44

S. H. Zhang and H. L. Chen. A study on the damping characteristics of laminated composites with integral viscoelastic layers. *Composite Structures*, 74(1):63 – 69, 2006. 120

Y. Zhang, Y. Li, H. Ma, and T. Yu. Tensile and interfacial properties of unidirectional flax/glass fiber reinforced hybrid composites. *Composites Science and Technology*, 88(0):172 – 177, 2013. 119, 125, 126, 134